Epigenetics in regulation of oesophageal cancer stromal myofibroblasts

Thesis submitted in accordance with the requirements of the University of Liverpool for the degree of Doctor in Philosophy by

Olivier Thierry Giger

January 2017

Disclaimer

This thesis is the result of my own work. The material contained in the thesis has not been presented, nor is currently being presented, either wholly or in part for any other degree or other qualification. The research was performed in the Department of Cellular and Molecular Physiology, Institute of Translational Medicine, University of Liverpool, United Kingdom. All other parties involved in the research presented here, and the nature of their contribution, are listed in the 'Acknowledgements' section of this thesis.

Acknowledgements

I would like to express my sincere gratitude to my supervisors and advisors:

Dr Triantafillos Liloglou, for his continuous support, technical advice, intellectual input and reflective discussions.

Professor Graham Dockray for his continuous support throughout my PhD study, for his wisdom and immense knowledge. His guidance consistently helped me with research and the writing of this thesis.

My primary supervisor Professor Andrea Varro for her continuous support right from the beginning and throughout my PhD study: without her political engagement and her networking skills this work could not have been realised. I would also thank her for the freedom she granted me to experiment, for her patience, her drive and her guidance.

Special thanks go to Dr Jithesh Puthen and Dr Hannah Najgebauer for the methylation array data analysis and Dr Dinesh J Kumar for his contribution with the 3D culture assay and xenografts.

I thank my fellow lab mates for the stimulating discussions, for the sleepless nights we were working together before deadlines, and for all the fun we have had in the last four years.

I would like to thank the Swiss National Foundation (SNF) which supported me with a research award to pursue my research abroad. I would like to thank the Guggenberg foundation for financial support. Special gratitude to CRUK which was the funding body for this PhD and all the people who support this great charity supporting the research helping to beat cancer sooner.

I would like to thank my family: my parents Antoinette and Max and my sisters Mélanie and Annette for all their support; my in-laws Shaho and Anwar and my sisters in-law Sairan (with Iain and Lara) and Jawan and Sairan for all their support.

My sincere thanks also to Dr Michael Kurrer as a friend and mentor.

The running section of Mossley Hill AC, specifically Martin and Diane, Colin, Tony, Iain & Michelle, Paul and Dominic who turned me into a Scouser.

Dr Simon Oliver, Alison Beckett and Scarlett for their friendship and hospitality.

Most importantly to my wife Roshan for her endless support throughout the PhD studies and the writing process.

1 Table of contents

2 Abstract

Cancer is the 2nd most common cause of death in our society and is associated with high morbidity and costs. The word 'cancer' amalgamates the complex interplay between cells which have acquired genetic alterations leading to uncontrolled proliferation, i.e. the malignant cells, and genetically 'normal' host cells, i.e. stromal cells, vascular cells and inflammatory cells which all acquire modified biological phenotypes in the presence of malignant cells. This community of cells and their secreted proteins defines the tumour microenvironment. Stromal cells in the tumour microenvironment display characteristic biological changes which promote cancer growth. Little is known on the underlying regulatory mechanisms defining this phenotype.

Epigenetics describes inheritable changes not encoded by the nucleic acid sequence. Epigenetic regulation has been described to occur in stromal cells in the tumour microenvironment, but little is known about its role on myofibroblasts.

In this work I describe how oesophageal cancer derived stromal cells, i.e. cancer associated myofibroblasts (CAMs) accelerate tumour growth in vivo. I observed that CAMs not only affect the local tumour microenvironment but might also accelerate tumour growth at a distant site. I also show how myofibroblasts play an important role in early tumour niche formation in xenograft models and describe their disappearance and replacement by murine stromal cells during tumour progression.

Oesophageal CAMs were shown to be epigenetically distinct from matched adjacent tissue myofibroblasts (ATMs). They exhibited a global DNA hypo-methylation compared to ATMs. We identified distinct DNA methylation signatures between oesophageal cancer CAMs and ATMs with the use of the Illumina 450k bead chip methylation array. The methylation array data showed altered methylation signatures of genes implicated Wnt/β-catenin signalling pathway. The transcription factor *paired like homeodomain* (PITX) 2 and the regulatory protein *secreted frizzled like protein* (SFRP) 2 both showed

altered methylation signatures and expression patterns between oesophageal cancer CAMs and ATMs. I found that upregulation of SFRP2 in myofibroblasts induces angiogenesis and I hypothesise that epigenetic modification regulates myofibroblasts-derived SFRP2 expression which may play an important role in tumour neovascularisation. Based on these findings I conclude that ATMs and CAMs are epigenetically distinct and altered protein expression is at least partially regulated by altered DNA methylation.

This work also presents a model for epigenetic modification of tumour stroma cells: exposure of myofibroblasts to the DNA methyl transferase inhibitor 5'Aza-3'deoxy cytosine (DAC) lead to a mild decrease of global DNA methylation and induced persistent biological changes in myofibroblasts. These epigenetically modified myofibroblasts induced an accelerated xenograft growth when injected together with oesophageal cancer cells. Based on these experiments I conclude that DAC epigenetically modifies myofibroblasts which induces an activation of normally silenced genes leading to a biologically more active cell.

3 Hypothesis

The work described in this thesis addresses the hypothesis that oesophageal cancer associated myofibroblasts are epigenetically distinct from tumour adjacent tissue myofibroblasts and that some biological differences between the two are epigenetically defined.

4 Introduction

4.1 History of Cancer in Medicine(1)

Tumours have captured the attention of scientists and doctors since ancient times. Medical scripts originating from the five ancient high cultures (China, India, Persia, Babylonia and Egypt) contain descriptions and treatment plans for cancer. The first known historic documentation of tumours comes from ancient Egypt and originated from ancient papyri transcripts originally written around 2650 BC, the time of Imhotep who was a high priest, doctor and architect of the first pyramid and vizier to King Djoser. A transcript dated to 1950-1550 BC is the so called Edwin Smith, Ebers and Kahoun medical papyri, named after its 19th century discoverers (2). Also in the ancient Sanskrit epic *Ramayana* originating from the period around 1200-1000 BC and written in 400-200 BC there are descriptions of cancers and their treatment. The first documentation and explanation for the origin of cancers is attributed to the Greek doctor Hippocrates born on the isle of Kos 460 BC. Hippocrates revolutionised medicine, abolishing mystic explanations, and based his ideas on those of the Greek philosopher Empedocles who lived in the 5th century BC. Hippocrates thought that the body consisted of the four elements, i.e. earth, air, fire and water. He hypothesised that diseases are the result of a disequilibrium of the four elements of blood, phlegm, black bile and yellow bile. He postulated that cancer was the result of too much of black bile. Hippocrates introduced the term 'carcinos' which means 'crab' in Greek believed to be related to the prominent static blood vessels that surround tumours. Later the Roman aristocrat Aurelius Cornelius Celsus (ca 30 BC – AD 38) documented tumours in his books entitled '*de medicina*'. Another important exponent of Roman medical history was undoubtedly Claudius Galenus, a surgeon who was born in AD 130. Galenus took over Hippocrates' ideas and further developed them. He believed that the deposition of black bile in certain parts of the body led to the development of tumours which he called 'cancer'. During medieval times medical progress stalled in the West, whereas it thrived in the Chinese empire. In the Chinese Tang dynasty (618-907) Sun Simiao (581-627) divided tumours into bony, fatty, stony and

suppurating tumours as well as tumours of muscles and blood vessels. In Europe, only with the beginning of the Renaissance, the dogma of black bile as the origin for malignancies was slowly rejected. The Parisian surgeon Henri François le Duran (1685-1770) published a theory stating that cancer is a local complaint, at least in its early stages, based on observations on post mortems. He also described the dissemination of breast cancer via the lymph ducts to the lymph nodes in various parts of the body and stressed the likelihood of relapses (3). Major advances in the understanding of cancer were gained through studies of pathological anatomy, for example as expounded by Giovanni Battista Morgagni (1682-1771) who was professor of theoretical medicine and anatomy at the University of Padua. Morgagni published the monumental work '*De sedibus et causis morborum et anatomen indagatis'* (About the location and causes of disease) in five books (4). Further advances on the understanding of cancer were closely related to the invention of microscopy by the Dutch spectacle-maker Hans Janssen from Middelburth and his son Zacharias (ca. 1580-1638) which allowed the study of disease at cellular level. This lead to the development of the cell theory in 1838 by the German physiologist Theodor Schwann (1810-1882) who together with the botanist Matthias Jakob Schleiden (1804-1881) declared that all plants and animals were made up of cells and cellular products. Everard Home (1756-1832) was the first to study cancer with a microscope, and described his findings in his book 'A short tract on the formation of tumours, and the peculiarities that are met within the structure of those who have become cancerous, with their mode of treatment' in 1830 (5). This was followed by the publication of the German pathologist Johannes Müller (1801-1858) who described in this work '*Ueber den feinen Bau und die Formen der krankhaften Geschwülste*' (On the delicate built and the different forms of morbid tumours) published in 1838 (6). He distinguished different types of tumours on the basis of their microscopic structure, supporting the macroscopic descriptions by René Théophile Hyacinthe Laënnec (1781-1826) (7). It was the Danish pathologist Adolph Hannover who published in 1843 his book '*Das Epithelioma*' (the epithelioma), a description of cancer cells and

their normal counterparts (8). The basic characteristics of malignant tumours were then defined with the publication of '*die Cellularpathologie*' (cellular pathology) (9) published by the founder of histopathology and former Professor of Anatomy at the Charitée in Berlin, Rudolf Ludwig Karl Virchow (1821-1901). He established the medical dogma '*omnis cellula e cellula*' (every cell derives from another cell) and also that each tumour originates from the cells of the organ in which it develops. Johannes Müller and Rudolf Virchow concluded that a cancer was made up from two components the malignant parenchyma and the benign stroma that consists of fibrous connective tissue and blood vessels. Langenbeck postulated that every single cancer cell must be regarded as an organism, alive and capable of development. It was Stephen Paget who in 1889 described the relation between primary tumour and site of metastasis in his 'seed and soil' theory based on a post mortem study of breast cancer patients(10).

Further advances in understanding malignant tumours went in parallel with technological progress. Probably, the first experimental approaches with the intention to treat cancer go back to the mid-19th century when Joseph Leidy grafted fragments of breast tumours into frogs. He observed that capillaries from the frog penetrated the transplanted tissue. Arthur Nathan Hanau, a German-Swiss pathologist successfully induced peritoneal metastasis after transplanting solid carcinoma fragments between rats in 1888 (11). Techniques which allowed the culture of cells outside the body were developed in the early 20th century initially by MT Burrows and Alexis Carrel.

The basis of modern molecular techniques was set with the discovery of deoxyribose nucleic acid (DNA) by Friedrich Miescher in Tübingen in 1869 even though its significance remained unclear until the genetic code was deciphered by James Watson and Francis Crick in 1953 (12) on the basis of x-ray crystallography by Rosalind Franklin.

The idea of a genetic basis of cancer emerged with the publication of chormosomal aberation by Theodor Boveri (1862-1915) in 1914 where he stated that mutations in somatic cells lead to uncontrolled cell proliferation

(13). Its involvement in cell fate became evident with the realisation that human cells consists of 46 chromosomes in 1956 by Joe Hin Tjio and Albert Levan (14). This was followed by the description of chromosomal aberrations and a description of the first malignancy-related chromosomal aberration in 1960 by the two pathologists Peter Carey Nowell and David Hungerford in Philadelphia (15). They observed the translocation between chromosomes 9 and 22 t(9;22)(q34;q11), the so called Philadelphia chromosome, which leads to constitutive activation of the Abl tyrosine kinase (16, 17). Techniques allowing the identification of DNA by Southern blotting in 1975(18), of ribonucleic acid (RNA) by northern blotting in 1977 (19) and proteins by western blotting (20) took the field of anti-cancer research further.

The characterisation of cells using antibodies first emerged in the 1930s, but it was only in 1941 that Albert Coons described the first fluorescent immunohistological studies which he subsequently developed further (21). The linking of antibodies to enzymatic visualisation reactions (immune peroxidase reactions (22) and alkaline phosphatase (23)) allowed their use in routine clinical diagnostic methods.

Knowledge gained on DNA manipulation by cloning into vectors and the establishment of the polymerase chain reaction (PCR) (24-26) and dideoxy sequencing as first described by Frederick Sanger in 1977 (27) were further technical milestones which led in the end to the sequencing of the complete first human chromosome in 2006 (28). Visualisation of individual genes by fluorescence *in situ* hybridisation was first published in 1982 (29) and has since then become a standard procedure in routine tumour diagnosis with prognostic and predictive value. Sequencing based technologies have now become part of routine tumour diagnostics not only of prognostic but more importantly of predictive value. The field continues to develop rapidly in parallel with technology (30, 31). Tumour monitoring based on circulating tumour cells (32) and circulating tumour DNA and miRNA in micro vesicles (33, 34) are the latest techniques offered to cancer patients.

Manipulation of cells at the protein level using antibodies became possible after the development of monoclonal antibodies in the late 1970s (35). Manipulation of transcription by RNA interference was discovered by Andrew Fire and Craig Mello in 1998 (36, 37) and its latest tool CRISPR/Cas9 (38).

4.2 Anticancer therapy

Treatment of cancer was restricted to surgery until 1896 when the first successful anti-cancer radiotherapy cases were described by A. Voigt and later also by Emil Grubbe (39). Leukaemias were treated with the so called Fowler's solution (potassium arsenic) by the Stafford doctor Fowler in 1786. The word chemotherapy is attributed to Paul Ehrlich's (1854-1915) treatment of infectious disease in rodents. Ehrlich's idea was taken to the next level by George Clowes (1877-1958) who started to test chemical compounds on inbred rodents in order to screen for potential anticancer drugs. The American pathologists E. B. and Helen D. Krumbhaar observed in post mortem studies of soldiers who had been exposed to mustard gas in World War I an atrophy of the lymphatic and testicular tissue as well as damage to the bone marrow (40). The significance of this remained unclear until the discovery of nitrogen mustard cytostatics and the first application of such in 1942 on a patient with radiation resistant non-Hodgkin lymphoma by Albert Gilman (41). In 1948 Sidney Farber published the first successful chemotherapy using folic acid analogues in acute lymphatic leukaemia (42). Various toxic chemical compounds have followed since then.

The idea of a hormonal dimension to cancer control originates in empirical case studies described by George Thomas Beatson (1848-1933) in 1896(43). Beatson performed bilateral oophorectomies in advanced breast cancer patients and observed remarkable remission of disease. The underlying mechanism of hormone deprivation became a corner stone in ablative hormone therapy in breast cancer first described by W. M. Biden in 1943 and published as a clinical trial by Alexander Haddow (1907-1976) (44).

In the late 1990s the field of anticancer therapy was revolutionised with the introduction of the first monoclonal antibody therapy targeting the BCR-ABL

fusion protein (45-47). Numerous other antibodies have followed and so called small molecule drugs interfering with single proteins have followed since then.

In the last decade agents targeting epigenetic changes have been successfully tested as anti cancer therapies. Agents which target DNA methylation (48, 49) were developed and as an example 5'Aza-3'deoxy cytosine has been approved for the treatment of myelodysplastic syndrome in 2006. Epigenetic inhibitors, known as EpiDrugs have recently been introduced for anti-tumour therapy (50).

4.3 Morphology of malignant tumours

Recognising the abnormal requires deep knowledge of the normal. Understanding of normal anatomy, histology and molecular characteristics and their physiological state has therefore been a prerequisite for the differentiation between malignant and benign. Already in ancient Egyptian, Greek and Roman times studies of anatomy were documented, but progress was slow. Only in the Renaissance the study of the human anatomy was launched by pioneers such as Leonardo Da Vinci and Andreas Vesalius. Vesalius is regarded as the father of modern anatomy as a consequence of his work '*De humani corporis fabrica*' (On the building of the human body) published in 1543 (51). The first macroscopic description of tumours '*The Morbid Anatomy of Some of the Most Important Parts of the Human Body',* was published by Matthew Baillie in 1793 (52). As mentioned above technical developments such as the invention of the microscope led to further understanding of cancers and up to date histological characteristics are still the main criteria to classify cancers. They are revised on a regular basis by the World Health Organisation (WHO) in their series of WHO classification of Tumours, published by the International Agency for Research on Cancer (IARC).

4.4 The concept of neoplasia

Neoplasias can be regarded as de-novo proliferative diseases and are subdivided based on the behaviour of tumours as benign, semi-malignant and

malignant. The latter are defined by their malignant growth pattern and their ability to metastasise. Malignant tumours can be sub-classified as epithelial-derived neoplasias, i.e. carcinomas; proliferative disease of the hematopoietic system, i.e. lymphomas and leukaemias; tumours of soft tissues and articulation, i.e. sarcomas and of mesothelial origin, i.e. mesotheliomas. Tumours of the central nervous system and the meninges are classified as gliomas and tumours of the meninges. Malignant tumours are classified, staged and graded according to the WHO/IARC guidelines and TNM classification. These days many malignant tumours are defined based on their molecular/genetic alterations (for example loss of heterozygocity, gene rearrangements, gene copy number alterations, mutations and many more) with not only prognostic but also predictive relevance. The mechanism leading to malignant tumours (i.e. tumour or carcinogenesis) can be regarded as an accumulation of genetic errors in a normal cell leading to an uncontrolled proliferation, change of behaviour in the tissue and migration within the body. Douglas Hanahan and Robert Weinberg have summarised cancer in their two milestone reviews 'the hallmark of cancer' (53, 54). They describe cancers as being able to thrive independently of proliferative signalling and to evade growth suppression. Cancer cells possess the enablement of replicative immortality, induction of angiogenesis, resistance to cell death and lastly the ability to invade and metastasise. Cancer is the 2nd most common cause of death in industrialised countries (around 20-25 % in the UK (55)). Big current questions are how to overcome the drive of malignant cells to escape current therapies. One small part of this main goal to control of cancer is the understanding of the tumour stroma. Since Paget's 'seed and soil' paradigm has been established (10), the tumour stroma has been known to play a pivotal role in metastasis. We know now that the tumour stroma in some cases directly interacts with malignant cells and plays an important role in progression.

4.5 Tumour microenvironment

The tumour microenvironment is a complex mixture of cancer cells and non-malignant cells of the host tissue (i.e. inflammatory, stromal and vascular

cells). These cells interact at different levels, supporting growth advantage, invasion, intravasation and metastasis of cancer cells, but also homing of inflammatory cells, mesenchymal stem cells, stomal cells and neovascularisation (for review see Hanahan & Weinberg (53, 54)).

4.6 Cancer cells

Cancer cells are the consequence of many genetic and epigenetic aberrations leading to loss of tumour suppressor genes and activation of oncogenes which in turn leads to independent growth with the ability to infiltrate and destroy the adjacent tissue and to metastasise.

4.7 Myofibroblasts

Myofibroblasts can be regarded as a subtype of stromal fibroblasts which show myogenic differentiation (56, 57). In various organs myofibroblasts evolve from mesoderm during embryogenesis. In the tumour microenvironment however, many myofibroblasts are recruited from the local environment (58). For example, cancer cells secrete a variety of growth factors such as transforming growth factor (TGF) β (59, 60) and platelet-derived growth factor (PDGF) (61, 62) which have been shown to induce CAMs. In the case of squamous cell carcinoma in the oral cavity, the cancer cells induce an 'activated' myofibroblasts phenotype via TGFβ-1 signalling (63). Upper gastrointestinal cancer cells can increase cancer associated stromal cell proliferation which in turn promotes epithelial to mesenchymal transition (EMT) in cancer cells (64).

In addition, already over two decades ago a subtype of circulating cells in peripheral blood was identified as being adherent on plastic and were showed to exhibit a mesenchymal expression signature (vimentin, collagen and CD34): they were called fibrocytes (65). Fibrocytes were described to have the propensity to home towards scar tissue. Similarly a portion of myofibroblasts within the tumour bulk may derive from primary local cells such as resident mesenchymal stem cells (MSC) or can originate from bone marrow-MSCs (66, 67). Fibrocytes harvested from peripheral blood have been shown to accelerate gastric MKN45 tumour growth *in vivo* (68).

Myofibroblasts have also been described to originate from malignant tumour cells which have undergone EMT (69).

A characteristic feature of myofibroblasts in conventional light microscopy is the so-called desmoplastic stroma reaction which features activated myofibroblastic cells surrounding cancer cells. Myofibroblasts can present under a similar picture in granulation tissue and wound healing. Myofibroblasts are characterised by their stromal appearance and their expression of the stromal cell markers αSMA, vimentin, fibroblast activating protein (FAP) (70) and the lack of epithelial characterisation markers such as cytokeratins 8 and 20 and E-cadherin (71). A growing body of evidence indicates that there is considerable heterogeneity in myofibroblasts populations (71). All cells designated as myofibroblasts in this thesis were previously characterised by their lack of cytokeratin and E-cadherin expression and their immunoreactivity towards αSMA and vimentin.

This thesis describes work with myofibroblasts derived from organs of tumour-free patients, i.e. normal tissue myofibroblasts (NTM) as well as myofibroblasts derived from patients with cancer. In the latter we differentiate between myofibroblasts derived from the tumour bulk, i.e. cancer associated myofibroblasts (CAMs) and myofibroblasts derived from tumour adjacent, macroscopically tumour free tissue, i.e. adjacent tissue myofibroblasts (ATMs) (72, 73) (figure 1).

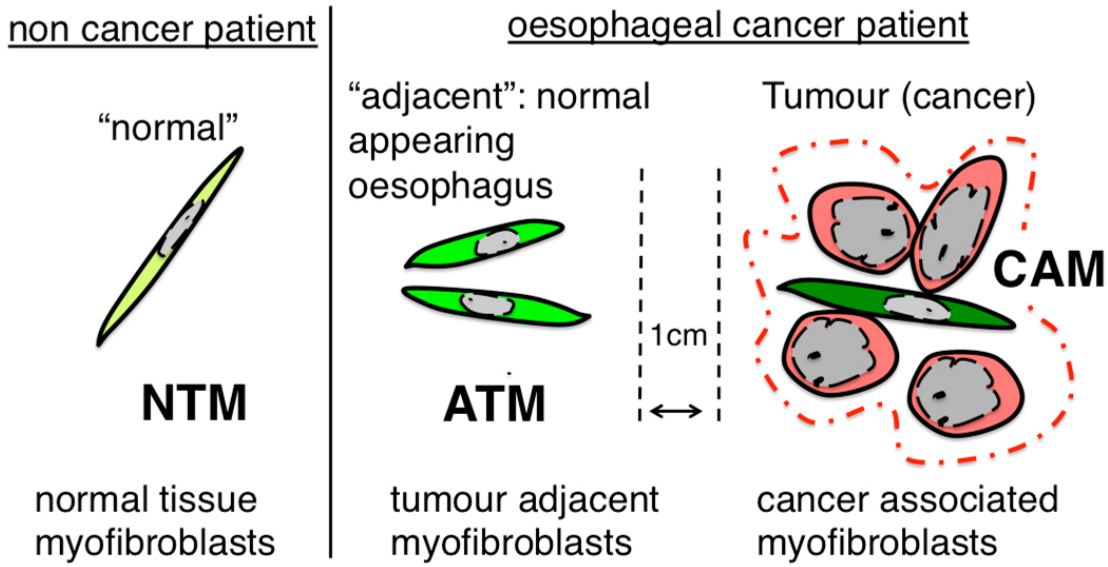

Figure 1: Abstracted figure of our conception of myofibroblasts.

It has been shown that CAMs differ from ATMs in various dimensions. They display a distinct morphological difference with increased nuclear size, altered chromatin structure and increase of rough endoplasmic reticulum (74), by their secretory and contractile phenotype together with increased expression of PAI-1(75-77), αSMA(78, 79), laminin and fibronectin (80) and differential secretion of metalloproteinases (81). Also at a transcriptional level, cancer associated stromal cells show distinct signatures in lung cancer (82), breast cancer (83), oesophageal cancer (84) and colorectal cancer (85). For review see (71).

Stromal cells show tissue specific lineage differentiation which also applies to gastrointestinal fibroblasts as described by Higuchi and his colleagues (86). Fibroblasts have distinct transcriptomes, which allows segregation between gastrointestinal and fibroblasts from other provenience. Furthermore this group described gene expression signatures differentiating between submucosal and subserosal origin and a differential homeotic gene expression pattern along the intestinal axis (oesophagus, stomach, duodenum, ileum and colon). There are also distinct miRNA signatures described in gastrointestinal myofibroblasts (87).

4.7.1 Role of stromal cells on tumour growth

Cancer stromal cells secrete a broad spectrum of cytokines and chemokines. CAMs have been shown to sustain proliferative activity by secretion of a variety of growth factors (insulin like growth factor (IGF) 2, stroma cell derived factor (SDF) 1, hepatocyte growth factor 1) which directly stimulate cancer cell proliferation (88) but have also been described to be involved in the initiation of aberrant proliferation in stem cells or tumour initiation cells (89). Conditioned medium (CM) from pancreatic stellate cells which are regarded as a source of myofibroblastic stroma have been shown to increase tumour cell proliferation with an activation of the ERK signalling cascade and to interfere with drug induced cell death in pancreatic cancer cell lines (90). Oesophageal cancer associated fibroblasts (CAFs) secrete periostin which leads to a PI3kinase-AKT pathway activation in oesophageal cancer cells. Periostin at the cellular interface between CAF and cancer cells is associated with more aggressive tumour behaviour (84).

CAMs also indirectly stimulate tumour growth through their effect on angiogenesis by the release of vascular endothelial growth factor (VEGF), fibrobast growth factor (FGF) 2 and osteopontin which increases vascular density in the tumour through their angiogenetic stimuli (91-93).

Furthermore CAMs play an important role in tissue remodelling where they exert their effect through the secretion of matrix metalloproteinases (MMPs), tissue inhibitors of metalloproteinases (TIMPs) and a variety of matrix proteins and signalling peptides (81, 94) which lead to the characteristic stiffness of tumour tissue (68). Work published by the group has shown that myofibroblasts in the tumour microenvironment play an important role in the recruitment of mesenchymal stromal cells to the tumour site (95). MSC can then differentiate themselves into CAMs (96).

Evidence of reciprocal stimuli between cancer cells and stromal cells was demonstrated by Terai and his colleagues: when gastric MKN45 cancer cells were cultured together with bone marrow derived fibrocytes (65) the cancer cells showed increased expression of SDF-1 and E-cadherin whereas the

stromal cells showed an increase in their expression of collagen type I and αSMA (68). The group further observed an accelerated tumour growth of xenografts when primary fibrocytes were co-injected together with the cancer cells and an increased αSMA positive stromal cell component in these tumours. This stands in parallel with findings described and data produced in our lab where injection of CAM together with different cancer cells accelerate tumour cell growth (97, 98).

4.8 Epigenetics

Epigenetic changes can be described as gene transcript-affecting modifications which are not defined by the four base pair code of the DNA. The field of epigenetic modification has been growing rapidly since the beginning of the 21st century and currently altered DNA methylation (99), histone modification (100), nuclear structure arrangement (101), RNA interference (102), post translational modification (103) and prions (104) are regarded as epigenetic changes. Epigenetic changes have major impact on non-expansional and proliferative (cancerous) human diseases and are related to aberrant gene expression. A particular feature of cancer cells is the loss of global DNA methylation which has been associated with chromosomal instability, activation of transposable elements and loss of genomic imprinting which all contribute to an increase in genomic entropy resulting in aberrant gene expression (105).

DNA methylation in genomic eukaryotic DNA occurs predominantly in repetitive regions, including satellite DNA, short interspersed transposable elements (SINE) and long interspersed transposable elements (LINE). DNA methylation of LINE elements can therefore be assessed as a marker for global DNA methylation (106).

Aberrant DNA methylation as a surrogate for epigenetic modification in malignant cells is regarded as a hallmark of malignancy (54, 107). Relatively little is known of such alterations in cancer associated non-neoplastic stromal cells (85, 108), even though the latter are known to be directly involved in tumour progression (73, 109). Treatment of pancreatic cancer myofibroblasts

with the demethylating agents azacyitidine (AZT) and 5-aza-2'-deoxycytidine (decitabine; DAC) leads to an induction of epigenetically silenced genes (110). DNA methyl transferases (DNMTs) play a key role in promoter hypermethylation and concomitant loss of gene expression (for review see (111)).

DNA promoter methylation is a major definer of transcriptional regulation. DNA methylation patterns are passed onto daughter cells in cell division, mainly through DNMT1. The inhibition of the DNMT1 by DAC is directly associated with increased gene transcription. Downregulation of tumour suppressor genes by promoter hypermethylation is a commonly observed epigenetic modification in cancers. Accordingly, in oncology, drugs interfering with the epigenetic regulation are in use for selected malignancies (112).

The two demethylating agents AZT and DAC are established for treatment of solid and hematopoietic neoplasias respectively. DAC is an analogue of cytosine that when incorporated into DNA irreversibly binds DNMT1 and 3B (49) and leads to a lack of methylation in the daughter strand during DNA replication and hence a loss of DNA methylation (48)(figure 2).

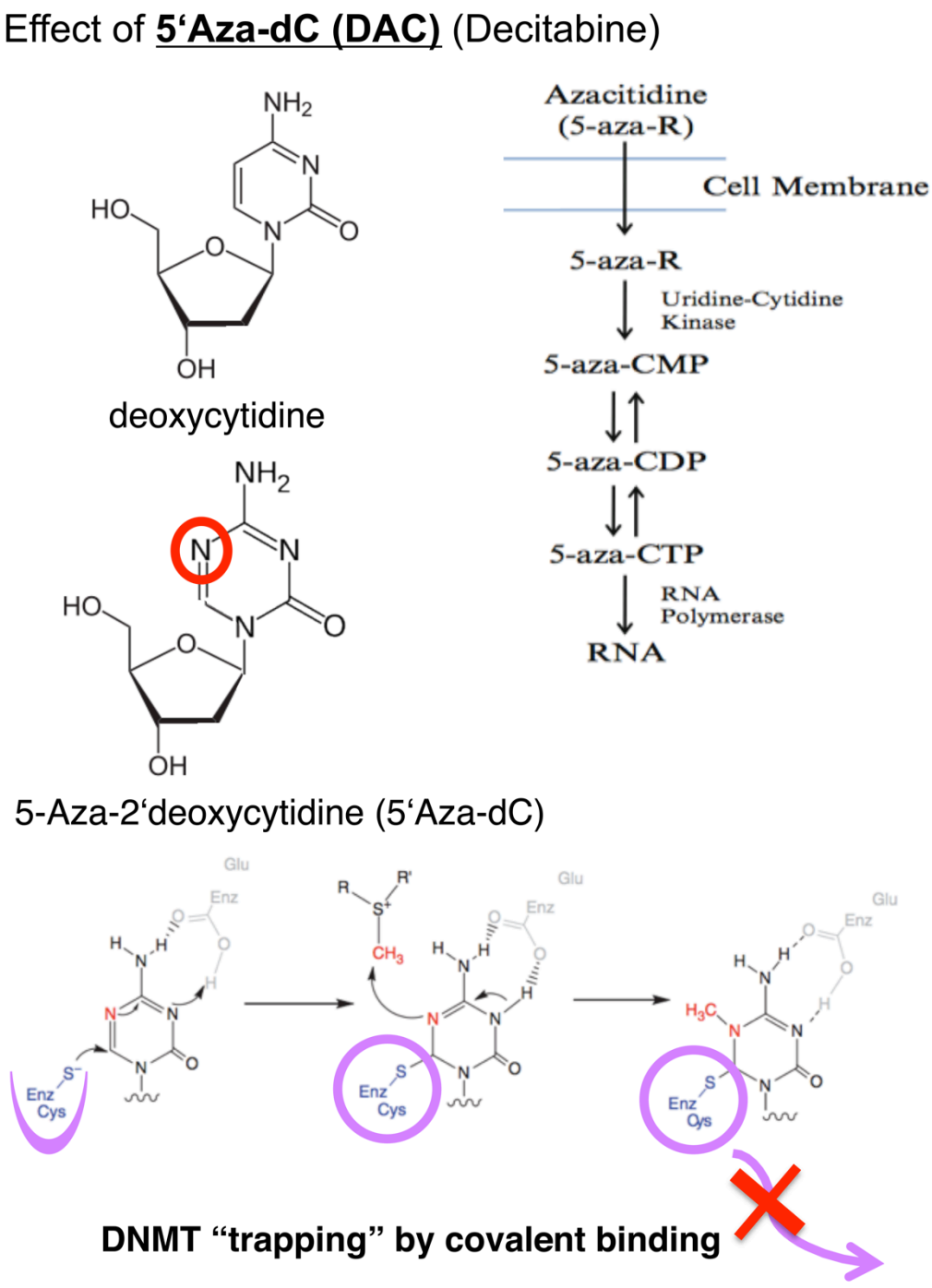

Figure 2: Mode of action of DAC. Modified form EA Griffiths and SD Gore, Advances in Experimental Medicine and Biology Volume 754, 2013, pp 253-283 (112).

Treatment of non-malignant cells with DAC leads to altered gene transcription (113) and can be used as an epigenetic modulator. It is noteworthy that DAC has also been associated with mutagenesis, i.e. point mutations and genome

rearrangements in murine fibroblasts (114).

4.8.1 Epigenetics in Cancer

The importance of epigenetics in cancers has been described for altered DNA methylation and histone modification. In cancer cells entire chromosomal segments may be densely packed as heterochromatin. Genes in these regions are inaccessible for the translation apparatus which consecutively leads to a silencing of genes encoded on these stretches of the genome. Silencing by altered packing has been described for tumour suppressor genes and their target genes (115, 116). Another mechanism of tumour suppressor gene silencing has been attributed to interfering RNA (117). Also aberrant gain of expression of oncogenes linked to promoter hypomethylation such as for *pS2* a pleiotropic factor which is implicated in the control of cell proliferation (118) or of the homeobox gene *HOX11* (119), but also loss of expression by hypermethylation of tumour suppressor genes such as p16 (120) and *MLH1*, a gene of the DNA mismatch (MMR) complex involved in the carcinogenesis of colorectal cancer (121) have been described. Epigenetic inhibitors, so called EpiDrugs have recently been introduced for anti-tumour therapy (50).

4.8.2 Epigenetics in tumour stroma

Epigenetic changes have been described in non-malignant tumour stromal cells of various cancers. Epigenetic variation at the DNA level has been documented in stromal fibroblasts of breast cancer (122), prostate cancer (123), gastric cancer (109, 124) colorectal cancer (85) and non-small cell lung cancer (NSCLC) (108). Epigenetic regulation of microRNA (miR)-200 which is regarded as an epigenetic modulator itself has been described in cancer associated fibroblasts in gastric cancer where it is involved in cancer progression (125) and work published by the group has shown that miRNA profiles differ between CAM and ATM (87).

Epigenetic activation of the TGFβ signalling through SMAD3 silencing by promoter hypermethylation leads to a hyper responsiveness to exogenous TGFβ1 stimulation and increased contractility and extra cellular matrix

deposition by CAF (108).

4.9 Gastrointestinal tumours and oesophageal cancer

The gastrointestinal (GI) tract can include the digestive organs (oral cavity, oesophagus, stomach, duodenum, jejunum, ileum, caecum with appendix, colon and rectum) and connected organs (liver & pancreas). The GI tract gives rise to a wide variety of tumours of epithelial, haematopoietic and stromal differentiation, with epithelial being the most common type. Various different risk factors such as smoking, alcohol, obesity, infections and geographical location are currently recognised by the WHO for the different organs (126).

Oesophageal tumours account for the 14th most common tumour type in the UK and oesophageal cancers are the eighth leading cause of cancer and the sixth most common cause of cancer-related death worldwide (127, 128).

The majority of the tumours are epithelial in nature and develop from precursor lesions of the mucosa (dysplasia/intraepithelial neoplasia, low and high grade) to invasive carcinomas. The majority of oesophageal cancers are squamous cell carcinomas (OeSCC). OeSCC are related to alcohol consumption and smoking (129). Alcohol decreases detoxification and promotes oxidation in the oesophageal microenvironment. Alcohol is a solvent that increases the permeability of tobacco derived toxins and promotes carcinogens. A second large group derives from metaplastic Barrett's epithelium with different grades of dysplasia dedifferentiating into invasive adenocarcinoma or Barrett's carcinoma (OeAC). Barrett's metaplasia is related to acid and bile reflux into the oesophagus known as gastro-oesophageal reflux disease (130). Barrett's adenocarcinoma of the oesophagus is distinct from its counterparts in the stomach and exhibits increased incidence in Western countries (131).

The WHO provides a more elaborate classification for tumours of the oesophagus and the oesophagogastric junction beyond OeSCC and the OeAC. The current (published in 2010) WHO list of tumours of the

oesophagus includes adenoid cystic carcinoma, adenosquamous carcinoma, basaloid squamous cell carcinoma, mucoepidermoid carcinoma, spindle cell (squamous) carcinoma, verrucous (squamous) carcinoma and undifferentiated carcinoma. The WHO further lists neuroendocrine neoplasms and mesenchymal tumours and lymphomas. Metastases from other sites are also not uncommon (126).

4.10 Investigating the tumour microenvironment

4.10.1 Addressing the tumour microenvironment in vitro

In order to investigate the tumour microenvironment, models which supposedly mimic the human disease have been generated and are widely used. For every pillar which Hanahan and Weinberg cite in their review various in vitro models addressing the same questions have been generated. Most models are based on basic cell culture systems with different nuances. Chamber systems have been developed to study migration and chemotaxis. Artificial barriers can be used in order to study invasion. The limitation of all these models are that they do not perfectly mirror the reality in vivo.

4.10.2 Addressing the tumour microenvironment in vivo

Studying tumours in live animals, i.e. *in vivo* has the advantage that all cellular components occurring in the tumour microenvironment can be observed in a four dimensional context. *In vivo* models are closer to events occurring in humans than *in vitro* conditions. Numerous models which replicate the accumulation of genetic defects in specific organs leading via dysplasia to invasive cancer exist (132). Chemically inducible models do also exist for oesophageal cancer (133). The modulation of the immune system in mice has allowed implantation of tumours notwithstanding the species barrier. The investigation of human derived cancers *in vivo* as xenografts or xenotransplants have become a pillar of drug development. These models are most useful in order to study drug related effects on tumour growth. Animal models are prone to higher biological variability and require ethical considerations. Furthermore the host immune system does not correlate with the human condition. Humanised animal models where human bone marrow

has been xenotransplanted have been established in order to better mimic reality (134).

4.11 Wnt/β-catenin signalling

Wnt/β-catenin is a key cellular regulator of gene expression. At least three pathways of Wnt signalling have been described in mammalian cells: A) the Wnt/β-catenin (also known as canonical) pathway, B) the planar polarity pathway which regulates cell polarity in the plane in developing tissues, and C) the Wnt/Ca^{2+} pathway which is involved in intracellular Ca^{2+} homeostasis. An initial binding of Wnts to receptors of the Frizzled family and it's co-receptor low-density lipoprotein receptor related protein 5 or 6 occurs in all of the three pathways which leads to a recruitment of Dishevelled to the trans membrane receptor and a consecutive binding of the Axin complex to the membrane. In the canonical Wnt/β-catenin pathway Wnt acts as a transcription activator. In the absence of Wnt signalling unbound β-catenin is phosphorylated by the Axin complex which consisting of the two protein kinases glycogen syntase kinase 3 (GSK3), a serine/threonine kinase casein kinase 1 (CK1) and the two scaffold protein Axin and Adenomatous polyposis coli (APC). Upon phosphorylation β-catenin is degraded through the ubiquitin disintegration process. Phosphorylation and ubiquitination of β-catenin through the Axin complex is supressed and β-catenin instead transported to the nucleus where it acts as a transcription activator by binding to the T cell factor/lymphoid enhancer factor (TCF/LEF) family of proteins. Nuclear accumulation of β-catenin is hence a surrogate marker for Wnt signalling pathway activation. For reviews see (135, 136).

4.12 Secreted frizzled related proteins and Wnt-signalling

Secreted frizzled related proteins (SFRP) act as soluble modulators/inhibitors of Wnt signalling pathway by competing with Wnt for the cell surface receptor Frizzled binding site (137-140). As inhibitors of the Wnt pathway SFRPs are key-players in developing organs such as oesophageal epithelia (141). Unsurprisingly loss of SFRP expression has been associated with a variety of tumours. Downregulation of SFRP expression has been related to promoter

hypermethylation in premalignant and malignant tumours of various organs. Downregulation of SFRP genes was observed as an early event in adenoma development in the colonic mucosa (142, 143). Silencing of SFRP genes has been described in urothelial carcinoma (144), renal cell carcinoma (145), squamous cell carcinoma of the oral cavity (146), gastric cancer (147), basaloid squamous cell carcinoma of the oesophagus (148), colorectal cancer (149, 150) and malignant mesothelioma (151). Altered methylation of this gene is a potential biomarker for colorectal cancer (152, 153).

Kaur et al describe in a recent study that SFRP2 expression in the tumour microenvironment is age-related. In their work on malignant melanoma they observed that stromal cells from young patients have a different effect on tumour growth and metastasis. Whereas young stromal cells lead to an accelerated tumour growth, aged fibroblasts showed a SFRP2 dependent increase in invasion, angiogenesis and metastasis (154). This data underlines the importance of stromal cells and their epigenetic modification during aging and tumourigenesis.

4.13 Paired-like homeodomain transcription factor (PITX) 2

PITX2 is located on 4q25 and belongs to the RIEG/PITX homebox family - as such it is a bicoid homeodomain protein. PITX2 acts as a transcription factor and down-stream effector of the Wnt/β-catenin signalling pathway leading to a cell type specific regulation of proliferation. It has been shown to regulate the Wnt/beta-Catenin pathway in ovarian carcinoma cell lines (155).

Several genes involved in cell migration, adhesion and motility have been identified as PITX2 targets. These include microtubule stabilization, actin cross-linking and tubulin related and intermediate filaments (156). These data suggest that myogenic cells have large single protrusions with a highly directed migration by continuous remodelling of their cytoskeleton and stabilization of their adhesion to the extracellular matrix. PITX2 can regulate myogenic cell migration by influencing their polarity and shape by restricting the microtubule growth and providing membrane and associated proteins needed for forward protrusion, fusion and muscle formation (156).

PITX2 is involved in the determination of left-right symmetry during development. It controls cell proliferation in a tissue-specific manner and is involved in morphogenesis and myogenesis by direct regulation of the expression of a number of cyclin-dependent kinases (157). It is involved in cell motility in craniofacial development (158). PITX2 has been shown to be associated with different histone H3 lysin 4 methylatransferase (HKMT) subunits and to regulate the procollagen lysyl hydroxylase gene expression (159).

Mutations of PITX2 are associated with atrial fibrillation and ocular and dental malformation such as the Axenfeld-Rieger syndrome which can involve other systemic abnormalities such as craniofacial dysmorphism with maxillary hypoplasia (160). Furthermore aberrant hypermethylation of PITX2 in adenocarcinoma of the prostate has been shown to be an independent adverse prognostic factor for recurrence (161).

4.14 Aim of this work

The specific aims of this thesis were to establish whether oesophageal CAMs can be defined by their epigenetic trait. We therefore assessed whether CAMs and ATMs differ at a global DNA methylation level. We further decided to address this question by investigating site specific altered DNA methylation using array technology. The primary objective was to identify candidate loci (CpG islands, CpG shores and differentially methylated regions (DMRs)) with altered DNA methylation that can be linked either positively or negatively to the mechanisms by which CAMs influence cancer cell function. The methylation array data were then to be validated by pyrosequencing and three differently methylated genes with correlating altered expression to be selected (ADAMTS12, PITX2 and SFRP2) for investigations on their biological role in CAMs by overexpression and knock-down studies.

A second aim was to assess whether myofibroblasts can be epigenetically modified in vitro and whether this would influence tumour growth. In order to assess whether myofibroblasts are targets of epigenetic modification at DNA methylation level, we treated myofibroblasts with DAC, a DNA methyl transferase inhibitor. We assessed whether DAC treatment would lead to a modification of DNA methylation and alter the cellular phenotype which can be passaged and hence regarded as being

epigenetically inherited. We further wanted to investigate whether epigenetic modification of the tumour stromal myofibroblasts would influence tumour growth *in vitro* and *in vivo*. We therefore studied tumour growth in a xenograft model where we co-injected epigenetically modified myofibroblasts.

A third aim was to study the fate of myofibroblasts in xenografts. To address the role of myofibroblasts co-injected in xenograft studies we investigated myofibroblasts at defined time points after injection.

5 Methods

5.1 Ethical approval

5.1.1 Human primary cell lines

The harvesting of, and work on, primary human myofibroblasts was approved by the Ethics Committee of the University of Szeged, Hungary and stands in accordance with the Human Tissue Act (162).

5.1.2 Animal work

Mice were kept, and all procedures performed, in accordance with the Animal Act 1986 (163).

5.2 Eukaryotic cell culture

5.2.1 Eukaryotic cells

Cells were cultured in filter-vented plastic flasks at 37°C in high humidity incubators with 5 % v/v CO_2. All myofibroblast cell lines and all cancer cell lines were grown in complemented myofibroblast medium (MM) which is Dulbecco's Modified Eagle's Medium, glucose (4500 mg/L), L-glutamine, and sodium bicarbonate, without sodium pyruvate, supplemented if not otherwise stated with 10 % foetal bovine serum (FBS), 2 % antibiotic antimycotic solution (A/A), 1 % penicillin/streptomycin and 1 % non-essential amino acids.

Cells were passaged at 90 % confluence in a ratio of 1:2 or 1:3 depending on their growth behaviour. For passaging, cells were washed with 1x phosphate buffered saline (PBS), followed by proteolysis with 1 x trypsin/ethylene diamine tetraacetic acid (EDTA). The activity of trypsin was subsequently quenched by the addition of MM.

5.2.2 Cancer cell lines

Oesophageal cancer cell lines (OE19, OE21, OE33 (164)) were adapted to MM.

5.2.3 Primary human myofibroblasts

Primary human myofibroblasts had previously been isolated by the out-growth method as described by Wu et al in 1999 for stromal cells of the gastric

mucosa (95, 165, 166). Most myofibroblast lines had been isolated by Professor Peter Hegyi, University of Szeged, Hungary and have been described in several publications (73, 81, 94, 95, 97, 167-170). Three types of myofibroblast were used, namely CAMs, ATMs and NTMs. CAMs were isolated from the macroscopic tumour bulk whereas ATMs derive from macroscopically normal appearing tissue 1 cm away from the tumour bulk (figure 1). NTMs derived from tumour free individuals (transplant donors). Cell counting was performed with use of a Neubauer Zählkammer.

5.2.4 Transwell migration assay

Transwell migration assays were performed using Boyden chamber (171) inserts with 8 μm pores. Cells were harvested with trypsin/EDTA and trypsin activity then quenched with 0.1 % FBS in cell culture medium. The cells were kept on ice for further processing. The appropriate number of cells was transferred into a 50 ml screw cap tube and centrifuged for 7 min (800 x G, 4°C). The supernatant was then carefully removed and the cells suspended in Dulbecco's modified Eagle's medium (DMEM) (for OE21 cells 100,000 cells, for myofibroblasts 40,000 cells per ml). Test medium (750 μl) was added to the individual wells and the cell suspension to the chamber inserts. Cells were allowed 16 h to migrate to the outer face of the Boyden chamber through the 8 μm pores in the membrane. The inserts were removed, media discarded and the inner face of the membrane wiped with a wet Q-tip to remove cells which had not migrated. Membranes were then stained using a Quick-Diff kit. In brief, cells were fixed for 8 min, followed by sequential staining with red and blue dyes for 5 and 4 min respectively. Inserts were then washed with water. Excess water was removed and the membranes dried in air. Finally, membranes were excised using a pointed scalpel blade and mounted on a glass slide using mounting medium. Migrated cells in five low power fields were counted.

5.2.5 Ibidi® chamber systems

Ibidi® silicon two chamber systems with a defined gap of 500 μm between the chambers were used for time lapse video microscopy. The self-adherent

ibidi® chambers were attached to 12 well tissue culture plates. Into one chamber 80 μl of OE21 cells (1.25 x 10^5) were plated, and myofibroblasts (2.5 – 6.25 x 10^5) were plated into the other. Cells were then allowed to adhere (18 h for cancer cells, 8 h for myofibroblasts) after which 2 ml of serum-free medium was added to the well, and the chamber carefully removed using forceps. The wells were then washed twice with serum-free media. For migration studies, fresh supplemented DMEM with 2 % FBS was added.

5.2.6 Cell proliferation assay by EdU incorporation

Visualisation of integrated 5-ethynyl-2'-deoxyuridine (EdU) into DNA during the S-phase of the cell cycle by the "click" reaction (172) was used to assess proliferation rates (173). Click-iT® EdU Alexa Fluor® 488 or 594 imaging kit were used. In brief, cells 1 – 2 x 10^4 myofibroblasts or 2 – 4 x 10^4 cancer cells were plated on glass cover slips in a 24 well plate. Cells were incubated with 10 μM EdU in MM (60 min for cancer cells and 24 h for myofibroblasts), rinsed thereafter with PBS and fixed for 30 min in 10 % formalin. The cells were then permeabilised with TBS with 0.5 % Triton X-100 for 10 min and washed thereafter twice with PBS. Cells were then incubated with freshly prepared Click-iT ™ reaction mix consisting of 1 x Click-iT™ reaction buffer, 4 % copper sulphate and 1 x reaction buffer for 30 min. The samples were washed twice for 5 min with PBS and either mounted on glass slides with Vectashield® plus 4,6-Diamidin-2-phenylindol (DAPI) or further processed according to the immunofluorescence protocol sparing the permeabilisation and the BSA blocking step. The number of nuclei labelled with DAPI and proliferating cells tagged with Alexafluoracids linked to EdU were assessed by fluorescent microscopy and the total number of cells were counted in a 400x magnification field.

5.2.7 Cell expansion assay

Upon DAC treatment in 75 cm^2 flasks myofibroblasts were harvested and 5000 plated on glass cover slips in triplicates on 24 well plates. Myofibroblasts were then grown in 10 % MM until confluence was reached in one of the samples. Cells were then stained using the Quick Diff staining

system and mounted on glass cover slips. Slides were then scanned with a conventional high definition (HD) scanner.

5.2.8 Gel contraction assay

Gels were set up on ice. Samples were prepared as triplicates of gel-cell mixes. For each sample 800 µl of collagen I (3.5 – 4.5 mg/ml), 100 µl 10 x DMEM, 80 µl of water, 20 µl of 1 M NaOH and 1.0 ml of cell suspension (80,000 cells per ml in DMEM) were mixed by pipetting. Into wells of a 24 well plate 500 µl of the liquid gel-cell mixture were added and left in the incubator for the gel to solidify. Thereafter gels were detached with a pipette tip and 500 µl of DMEM were added to each well. Macroscopic pictures were taken at different time points and area change as an indirect measure for cell contraction was assessed in imageJ. The decrease of contraction area over time was used as an indicator for cell contractibility.

5.2.9 Organotypic culture (experiment performed by Dr Kumar)

Organotypic cultures were grown as described previously (174, 175). In brief, OE21 cells (1×10^6) were seeded on top of 1 : 1 Matrigel/collagen-I with or without myofibroblasts (0.5×10^6) suspended in the gel. On day 3, the culture was raised on wire gauze and maintained at an air medium interface for 15 days, changing medium every 48 h. Cultures were fixed in 10 % neutral-buffered formalin and paraffin-embedded sections were stained with H&E. Invasion was determined by measuring the depth of invading cancer cells into the Matrigel. A total of eight measurements were taken per field and 18 fields were captured per group at 100x magnification.

5.2.10 5'Aza - 2'deoxy cytidine toxicity assays

DAC was suspended in DMSO to a stock concentration of 10 mM and kept at -80° C. DAC stock solution was diluted in MM for treatment. Treatment of myofibroblasts with DAC was performed as follows: 0.5×10^6 cells were plated in a 75 cm^2 tissue culture flask and allowed to adhere overnight and the medium then exchanged. One day later cells were treated every 24 h for three consecutive days with DAC diluted in MM, and diluted DMSO as

controls. The cells were then washed with PBS and incubated for another 24 hours with MM before further use (figure 3).

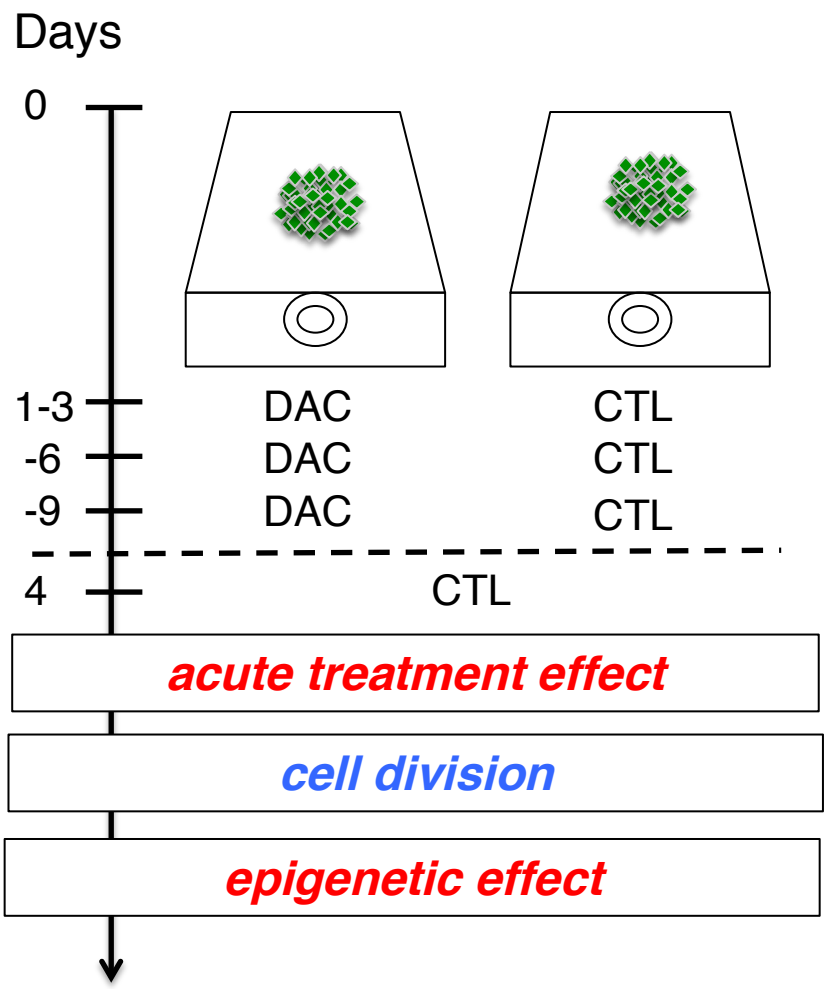

Figure 3: 5'Aza-dC treatment scheme. Myofibroblasts were seeded and treated on three, six or nine consecutive days. Thereafter all cells were grown in control media.

Demethylation treatment was performed with DAC concentrations varying from 0.001 μM to 10 μM in MM, every 24 h after initial seeding for 3, 6 or 9 days. Upon the last treatment cells were washed with serum free medium twice and then kept in culture in MM.

5.2.11 Fluorescent cell labelling

Myofibroblasts and cancer cells were labelled using a hydrophobic cell linker technique. In brief PKH26 Red-, PKH67- and CellVue® Clarent Far

Fluorescent Cell Linker (176, 177) were used. Briefly, 2 x 10^7 cells harvested as described above, were centrifuged (6 min 600 x G at 20°C) and the supernatant removed. The cell pellet was then suspended in 10 ml of DMEM and centrifuged a second time (400 x G for 5 min at 20°C). The supernatant was then entirely removed and the pellet suspended by gentle pipetting in 1 ml of Diluent C of the kit. Thereafter 1 ml of 40 μM of the fluorescent dye diluted in Diluent C was added to the cell suspension and mixed by pipetting. The cell/dye suspension was then incubated at room temperature for 2 min before 2 ml of 10 % MM were added in order to bind excess dye. Cells were then centrifuged at 400 x G for 10 min at 20°C, the supernatant discarded and the pellet resuspended in 10 ml of 10 % MM. Excess dye was removed by two consecutive steps of pelleting by centrifugation (400 x G for 5 min at 20°C) and resuspension in 10 % MM. Cells were then plated in 75 cm cell culture flasks and used for experiments or cryopreserved two days after labelling.

5.2.12 Endothelial tube formation assay

Endothelial tube formation/sprouting angiogenesis assays (178-180) were performed according to the protocol from Life Technologies (http://www.lifetechnologies.com /uk /en /home /references /protocols /cell-and-tissue-analysis/ cell-profilteration-assay-protocols/ angiogenesis-protocols/ endothelial-cell-tube-formation-assay.html).

Briefly, human umbilical vein endothelial cells (HUVEC) were grown in supplemented endothelial basal medium (EBM) until 80 % confluent. Matrigel (Geltrex™) was thawed at 4°C overnight and kept on ice before plated into on ice pre-chilled 24 or 96 well plates (50 μl/cm^2 for 24 well plates, i.e. 95-100 μl per well and 100 μl/cm^2 for 96 well plate, i.e. 30-40 μl per well). The gels were then incubated at 37°C for 30 min to solidify. In the meantime HUVECs were harvested as described (5.2.1) and resuspended in serum free MM. The number of cells needed were pipetted into a 1.5 ml Eppendorf® tube and pelleted by centrifugation (6 min at 600 x G). The pellet was then re-suspended in CM (harvested as described; 8 x 10^4 cells per ml) and 200 μl

HUVEC suspension were plated per cm^2. Cells were then allowed to sediment and adhere in the humidified incubator at 37°C. After one hour, which was defined as time point zero (t_0), photomicrographs were taken at defined intervals (every 20 min for time lapse microscopy, t_0 +1, +2, +3, +4, +6). Images were analysed using ImageJ software 1.50 with the use of the Angiogenesis Analyser plugin (181).

5.2.13 Conditioned medium

CM was harvested as described previously (95). Briefly, for CM from myofibroblasts and OE21 cells, 0.5×10^6 or 3×10^6 cells respectively, were plated in MM in a $75cm^2$ TTP tissue culture flask (i.e. 6,666 cells/cm^2 for myofibroblasts and 4×10^4 /cm^2 for OE21 cells). After 24h, cells were washed three times with PBS. Thereafter 10 ml of DMEM was added (133 μl/cm^2). After 24 h in culture, media were collected and centrifuged for 7 min at 800 x G at 4°C. The supernatant was then carefully removed, aliquoted and stored at -80°C.

5.2.14 Transfection of myofibroblasts by electroporation

Myofibroblasts were transfected by electroporation (182) using the Nucleofector™ system from Lonza. Briefly, myofibroblasts were harvested as described and 5.5×10^5 cells pelleted by centrifugation at 4°C for 6 min at 800 x G. Cells were then suspended in 100 μl Amaxa™ *Fibroblast Nucleofector* medium together with 3 μg of DNA or siRNA. The cell suspension was electroporated using program U-23 on the Amaxa® Nucleofector instrument. After electroporation, 500 μl of MM was added to the cuvette and the suspension transferred into a tissue culture flask containing pre-warmed MM.

5.3 Prokaryotic cells

5.3.1 Transfection of bacteria

Competent bacteria (NEB Turbo Competent *E. coli*) were thawed on ice for 20 min and 10 ng of plasmid DNA in 5 μl of TE buffer (10 mM Tris 0.1 mM EDTA) was added and the tube mixed. Bacteria were then left for 30 min on

ice, heat shocked for 30 sec at 42°C and chilled immediately on ice for 5 min. Ambient temperature super optimal broth with cataboite repression (SOC) medium (950 µl) was added and incubated at 37°C under vigorous shaking (250 rpm) for 60 min. Serial dilutions of the primary bacterial culture were spread on antibiotic containing agar plates. After 16 h single colonies were picked and expanded for 16 h in 6 ml antibiotic containing LB medium.

5.3.2 Bacteria culture

Bacteria were cultured on 10 cm Petri dishes with agar or in lysogeny broth (LB) medium (on a shaker) containing kanamycin (25µg/ml) or ampicillin (100µg/ml) at 37°C.

5.3.3 Glycerol Stocks

Glycerol stocks of all *E. coli* cultures were generated by adding 200 µl of glycerol to 800 µl of cultured bacteria and mixed gently by pipetting. Cells were stored at -80°C.

5.3.4 Screening for plasmid

Expanded primary bacteria cultures (200 µl) were incubated for 5 min at 95°C and centrifuged for 2 min at > 9000 x G. The supernatant (5 µl) was used for Q-PCR amplification (for Q-PCR see 3.5.10). Bacterial cultures providing a positive Q-PCR result were used for mini-prep plasmid extraction.

5.3.5 Plasmid extraction

MiniPrep: For screening, plasmid DNA was isolated using the Zyppy™ Plasmid miniprep kit from Zymo Research according to the manufacturers instructions. Briefly, 600 µl of bacteria cultures grown in LB medium were lysed with 100 µl of 7x Lysis Buffer and mixed by inverting the tubes. The reaction was neutralized by admixing of 350 µl of neutralization buffer and the denatured proteins/lipids pelleted by centrifugation at 12,000 x G for 2 min. The supernatant was transferred into Zymo-Spin™ columns and then centrifuged for 15 sec at 12,000 x G. The samples were then washed with 200 µl of endo-wash buffer followed by a 30 sec centrifugation and 400 µl of Zyppy™ wash buffer for 1 min. Flow troughs were discarded in between

centrifugation steps. After the final wash step the sample was centrifuged for an additional 4 mins at 12,000 x G. Plasmid DNA was eluted with 30 μl of Zyppy™ elution buffer.

MaxiPrep: ZymoPURE™ Kit from Cambridge Biosciences was used for plasmid extraction according to manufacturers protocol. Briefly, bacteria were pelleted by centrifugation for 10 min at 3000 x G and resuspended in 15 ml of P1 buffer. Cells were then lysed for 1 min by admixing 15 ml P2 lysis buffer. The process was stopped by the addition and incubation of 20 ml P3 Neutralisation buffer for 5 min. The mixture was then added onto Zymo-Maxi Filter™/Zymo-Spin™ VI columns and assembled on a vacuum manifold. After the precipitate was left to float to the top vacuum was then applied and all liquid left to pass completely through both columns. The upper filter was removed and the filter on the lower column washed with 10 ml of endo wash buffer and then additionally centrifuged with 3,400 x G for 5 min before elution of the plasmid DNA with 2 ml of Zyppy™ elution buffer by centrifugation at 3,400 x G for 1 min. Plasmid DNA quality and concentrations were assessed by spectrophotometry as described. DNA was concentrated with a vacuum spin manifold in order to reach concentration above 500 ng per μl.

5.4 Animal work

5.4.1 Housing

All animals were purchased and kept in the Biomedical Service Unit at the University of Liverpool in specific pathogen-free conditions. All animals used in the experiments were immunocompromised athymic Balb/C nu/nu mice (183). Animals were kept in groups of four per cage. In each experiment same gender animals were used. All animals had reached the age of 7 weeks and were acclimatised to the facility for 10 days before the start of an experiment. The work was approved by the University of Liverpool Animal Welfare Committee, and was conducted in compliance with relevant UK legislation.

5.4.2 Xenografts

Human cells were xenografted as previously described (94). Briefly, cells were harvested as described, and processed on ice. Cells were washed twice (pelleting by centrifugation at 600 x G for 6 min at 4°C) with PBS, and then diluted in PBS. Depending on the experiment, cancer cells and myofibroblasts were mixed to a final concentrations between 10^5 – 10^7 cells per ml. Cell suspensions were then injected subcutaneously (100 μl per site) using 25 gauge needles. Before injection the cell suspension was mixed in order to maintain equal cell numbers. After injection tumour diameters were assessed regularly by calliper and tumour volumes calculated. Tumour volume was estimated by using the equation $v = (ab^2)/2$, in which 'v' is volume, 'a' is the length of the major axis, and 'b' is the length of the minor axis (68).

5.4.3 Gavage

Mice were treated by gavage (100 μl) with 400 μmol.kg^{-1} omeprazole in aqueous 3 % methyl cellulose every 48 h. Gavage was started one week before xenografting. Methyl cellulose was prepared by heating water (200ml) to 90°C and adding methyl cellulose (6 g) with vigorous mixing until the powder was dispersed. The suspension was cooled to 4°C in order to allow methylcellulose to solubilise (below 60°C).

5.4.4 Blood and tissue sampling

Mice were euthanized by CO_2 inhalation followed by cervical dislocation. Blood was obtained by cardiac puncture using a heparinised needle. Blood samples were stored on ice before centrifugation (3 min, 1000 x G). The plasma supernatant was harvested and frozen at -20°C until further use.

5.5 Histological methods

5.5.1 Processing of tissue

Fresh tissue was kept on a wet gauze in a 10 ml flask on ice before being embedded in optimal cutting temperature (OCT) compound and being snap frozen with liquid N_2. Tissue samples for paraffin embedding were fixed in 10 % buffered formalin for at least 12 h before embedding. Paraffin

embedding, sectioning of paraffin blocks and staining (haematoxylin/eosin and alcian blue - periodic acidic shift) was carried out by the Histology Laboratories of the Veterinary School of the University of Liverpool.

Snap frozen tissue was cut into 5 μm sections and mounted on glass slides. Slides were air dried and kept at -80°C until further use.

5.5.2 Haematoxylin and eosin staining (H&E)

Snap frozen tissue slides were fixed in acetone and washed in alcohol before staining in haematoxylin for 5 min. The slides were then rinsed under the warm running tap until a bluish stain became apparent. The stain was differentiated by immersing three times in 1 % hydrochloric acid/70 % ethanol. Slides were counterstained with 1 % eosin for 1 min followed by rinsing under the tap and dehydration through an increasing ethanol series (70 % - 90 % - 96 % - 100 %) and then drying in air. Coverslips were mounted with mounting medium.

5.5.3 Immunofluorescence (IF)

For immunofluorescence 22 mm glass cover slips were added into individual wells of 24 well plates and sterilisd by UV irradiation. Cells were suspended in 10 % MM (5000 myofibroblasts or 10,000 cancer cells per cm^2) on 22 mm glass cover slips and allowed to adhere for 24 to 48 h. After fixation cover slips containing cells or glass slides with tissue sections were washed with PBS (phosphate buffered saline) and fixed with 10 % formalin for 30 min. Slides were then washed twice with PBS and permeabilised with PBT (for buffers see 6.8) at room temperature for 30 min followed by two washes with PBS. Non-specific binding of the secondary antibody was inhibited by 30 min blocking with 10 % serum of the species of the secondary antibody. Slides were then washed twice with PBS and the primary antibody dissolved in PBS incubated for 1 h at room temperature or overnight at 4°C (for dilutions of the primary antibody see table 1). Samples were then rinsed with PBS, followed by washing with 0.14 M NaCl, 0.5 M NaCl and PBS for 10 min each. The secondary antibody diluted in 10 mM HEPES pH 7.5 was incubated for 1 h at room temperature. Samples were then rinsed with PBS and incubated for

5 min with DAPI diluted in PBS, followed by washes with PBS, 0.14 M NaCl and PBS for 10 min each time. Cover slips were mounted on glass slides with Vectashield®.

Table 1: antibodies for immunofluorescence

Antibody	Type	Host	Dilution	Supplier
Anti-α smooth muscle actin	polyclonal	Mouse	1:100	Fitzgerald, USA
Anti-vimentin	polyclonal	Guinea pig	1:100	Fitzgerald, USA
FITC-conjugated donkey-anti mouse	polyclonal	Donkey	1:400	Jackson, USA
Texas-Red-conjugateddonkey-anti-guinea pig	polyclonal	Donkey	1:400	Jackson, USA
FITC-conjugated donkey-anti-rabbit	polyclonal	Donkey	1:400	Jackson, USA

5.5.4 Fluorescent in situ hybridisation (FISH)

FISH of human centromeres was performed according to the protocol G1 from StarFISH®. Briefly, tissue sections were fixed in 3:1 ethanol:acetic acid for 30 min and then dried. In order to remove the acid the slides were passed through a graded ethanol series (70, 90, 100 %) and air dried before baking at 65°C for 15 min. After cooling to ambient temperature slides were incubated in acetone for 10 min followed by air drying. In order to remove RNA, slides were treated for 60 min at 37°C with RNase (100 µg/ml) in 2 x SSC followed by two washes with 2 x SSC for 5 min each. The slides were then immersed in 10 mM HCl followed by a 2 min digestion with pepsin (1 mg/ml) in 10 mM HCl in a slide staining jar at room temperature. The digestion was stopped by immersing the slides in 1 x PBS followed by dehydration through an ethanol series and then air drying. In order to denature, the cellular DNA slides were immersed for 2 min in 70 % formamide in 2 x SSC. Thereafter slides were dehydrated through an ethanol series and air dried. A circle was scratched around the tissue specimen on the slide with a diamond pen.

The probe was thawed, vortexed and denatured for 10 min at 85°C and immediately chilled on ice. Probes (10 – 20 µl) were added to the section and covered with a purpose cut glass cover slip and then sealed to the glass slide with rubber glue. The hybridisation was carried out over 16 h in a humidified chamber at 37°C. Post hybridisation washing after removal of the cover slips

was carried out as follows: initial washing for 5 min at 37°C in 2x SSC, followed by two washes for 5 min in 50 % formamide / 2 x SSC at 37°C. The slides were then washed twice for 5 min in 2 x SSC. Slides were then mounted with Vectashield® with DAPI and sealed with nail varnish.

5.5.5 Combined IF and FISH (I-FISH)

After completion of the FISH test, the antibody incubation was performed on the specimen as described in the immunofluorescence labelling protocol (5.5.3), without the permeabilisation step with 0.5 % TBE. At the end the slides were mounted with Vectashield® with DAPI and sealed with nail varnish.

5.5.6 Microscopy

Bright field and fluorescent microscopy were carried out on a Zeiss Axiopan 2 microscope. Image acquisition was performed using Zeiss AxioVision 3.1 software.

5.5.7 Quantification of histology:

Histology grading was semi quantitatively assessed on H&E stained formalin-fixed and paraffin embedded (FFPE) sections for inflammation, fibrosis, nesting (engulfment of cancer cells by myofibroblasts), necrosis, keratinisation and presence of myofibroblastic cells based on a four-tiered scale (0 = absent, 1 = few, 2 = intermediate, 3 = abundant).

5.5.8 Time lapse microscopy

Time lapse microscopy was performed on a LEICA DMIRE2 microscope controlled and pictures captured with a Hamamatsu camera. Images were processed using Metamorph and imageJ software (184). The outgrowth area of cells into the empty gap space or the gap space was measured with ImageJ at 6, 18, 18 and 24 h after removal of the chamber inserts.

5.6 Nucleic acids related molecular biology techniques

5.6.1 DNA extraction

DNA was extracted using an adapted version of the QIAamp® DNA mini Kit. Briefly, cells from confluent 75 cm² tissue culture flasks (no more than $5x10^6$) were harvested and re-suspended in 200 µl PBS. After pipetting 20 µl of protease K to the bottom of a 1.5ml centrifugation tube, the cell suspension, 4 µl of RNAse (100 mg/L) and 200 µl of buffer AL were added. The sample was digested overnight at 56°C on an Eppendorf thermomixer. After digestion, tubes were centrifuged briefly, 200 µl of molecular grade ethanol (>98 %) added, the samples shaken for 15 sec and then centrifuged briefly. The lysed and digested cell suspension was then added to a QIAamp mini spin column inserted into a 2ml collection tube and centrifuged at 6000 G for 60 sec. After centrifugation, the spin column was placed in a new 2ml collection tube, 500 µl of buffer AW1 was added and the samples centrifuged at 6000 x G for 60 sec, followed by insertion into a new collection tube with a further 500 µl of buffer AW2 and centrifugation at 20,000 x G for 3 min. The spin column was then placed in a clean collection tube and centrifuged for another minute at 20,000 x G to elute ethanol remnants. The spin column was then placed in a clean 1.5ml collection tube and 80 µl of pre-warmed (42°C) buffer AE was added onto the filter. After 5 min the column was centrifuged at 6000 x G for one minute and the eluate kept on ice until further processed.

5.6.2 Assessment of DNA quality by spectrophotometry

DNA concentration and quality were assessed by measuring absorbance at 260 and 280 nm using a NanoDrop 2000c spectrophotometer. The quality was considered appropriate when the ratio A_{260}/A_{280} nm (A_{260}/A_{280}) was greater than 1.75; A_{280} of 0.1 - 1 was regarded as suitable for further processing.

5.6.3 RNA extraction

RNA was extracted using the QIAGEN® miRNeasy mini Kit according to the manufacturer's instructions. Briefly, cells were lysed with 700 µl of QIAzol Lysis Reagent or Trizole and harvested with a cell scraper. The lysate was

incubated for 5 min at ambient temperature. Thereafter 140 µl of chloroform were added and the solutions mixed by vigorous shaking for 15 s. After 3 min incubation at room temperature, the sample was centrifuged for 15 min with 12,000 x G at 4°C. The upper (aqueous) phase was then transferred into a collection tube and mixed by pipetting with 1.5 volumes of 100 % ethanol. Nucleic acids were then trapped on the filters of spin columns by centrifugation of the total aqueous phase in repeated steps. In order to remove DNA a column treatment with DNAse was performed. The sample was then purified with 700 µl of buffer RWT and twice 500 µl buffer RPE by centrifugation steps at 12,000 x G for 30 sec each. The spin columns were centrifuged one additional time at 12,000 x G for 3 min. The RNA was then eluted with 30 µl of RNase-free water by centrifugation at 8,000 x G for 1 min. RNA was stored at -80°C.

5.6.4 Assessment of RNA quality by spectrophotometry

RNA concentration and quality were assessed by absorbance at 260 and 280 nm using a NanoDrop 2000c spectrophotometer. RNA was regarded as of appropriate quality when the ratio of A_{260}/A_{280} was greater than 2.0 and the ratio of A260/A230 nm (A_{260}/A_{230}) were in the range of 2.0 to 2.2.

5.6.5 Assessment of the RNA integrity number (RIN)

The quality of RNA used for expression arrays was assessed by evaluation of the RNA integrity number (RIN) (185, 186) which is a measure of degradation of the RNA. The RIN was assessed with the Agilent 2100 Bioanalyzer and the corresponding Agilent RNA 6000 Nano kit. Firstly the electrodes of the bioanaylser were cleaned by incubation in 350 µl RNaseZAP per well for 1 min followed by a 10 sec rinsing step with RNAse free water. The chip was prepared according to the manufacturers protocol; briefly, all reagents stored at -80°C and -20°C were equilibrated to ambient temperature for 30 min, and gel matrix (550 µl) was loaded into the top receptacle of the spin filter which was then centrifuged for 10 min at 1500 x G and aliquoted (65 µl each) into 0.5 ml RNase-free microfuge tubes. Aliquots were stored at 4°C. RNA 6000 nano dye concentrate was vortexed for 10 sec, centrifuged and 1 µl pipetted

onto the filtered gel aliquot and mixed by vortexing. The tube was then centrifuged for 10 min at 13,000 x G. The gel-dye mix was allowed to equilibrate to room temperature protected from light. The chip was positioned on the chip priming station and 9 µl of the gel-dye mix were added to the bottom of the well "12" and dispensed (figure 4). The priming station was closed and the plunger of the syringe (positioned at 1ml) pressed down until held by the clip. After exactly 30 sec the plunger was released and 5 sec later slowly pulled back into the 1 ml position. Thereafter 9 µl of gel-dye mix were pipetted into wells 4 and 8. The RNA marker (5 µl each) was then added to wells 1-3, 5-8, 9-11 and 13-16. The RNA ladder was denatured for 2 min at 70°C and before adding 1 µl into well 16. Then 1 µl of each sample or buffer was added into the sample wells (1-3, 5-8, 9-11 and 13-15). The chip was then vortexed for 60 sec at 2,400 rpm on an IKA vortex mixer and placed directly into an Agilent 2100 Bioanalyzer. The analyser program was set as default RNA quality. Quality of the run was regarded as successful when at least one RNA peak was demarked and the ribosomal 26s and 28s RNA was detectable and well resolved with correct peak size assignments in the electropherogram (figure 4). RNA quality was regarded as suitable for expression array analysis when the RIN number was 7.5 or higher.

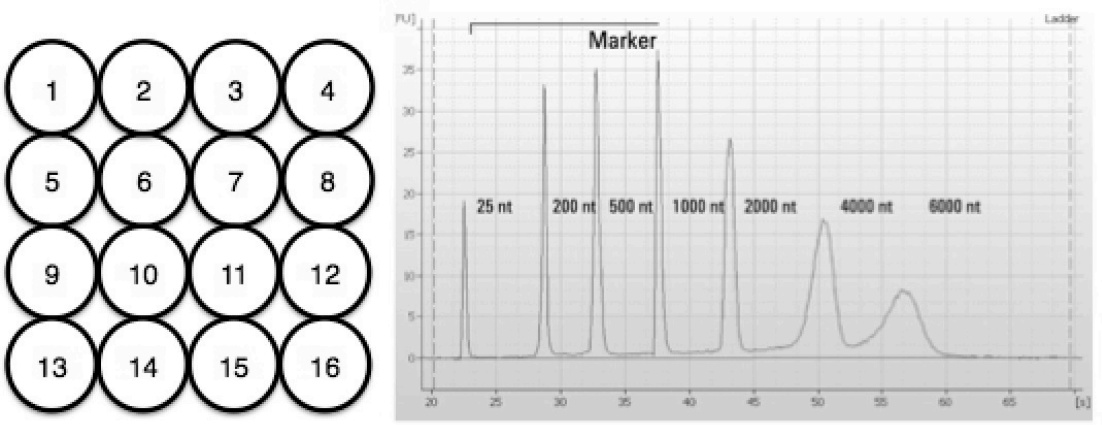

Figure 4: RIN setup and sample graph: Left: positions on chip. Right: template marker electropherogram

5.6.6 Reverse Transcription

RNA to DNA reverse transcription was performed with the High-Capacity RNA-to-cDNA™ Kit according to the manufacturer's instructions. Briefly, a 20 µl reaction mix consisted of 10 µl of 2x reaction buffer and 1 µl of 20x enzyme mix together with template RNA (1 – 2 µg) in 9 µl RNase free water. The reverse transcription was then performed on a thermo cycler by incubation at 37°C for 1 h, followed by a denaturation step at 95°C for 5 min. The sample was thereafter kept at 4°C before storage of aliquots at -20°C.

5.6.7 Bisulfite conversion of DNA

Bisulfite conversion (187) was performed using an adapted protocol of the EZ DNA Methylation-Gold™ kit. Briefly, 20 µl of DNA (50 ng/ µl) extracted according to the DNA extraction protocol was mixed with 130 µl of the CT Conversion Reagent. The bisulfite conversion was carried out in 200 µl reaction tubes on a Biorad® thermal cycler with the following steps: initial DNA denaturation (98°C, 10 min) followed by conversion (64°C, 150 min). After completion the samples were kept at 4°C for up to 16 h before mixing with 600 µl of M-binding in the Zymo-Spin™ IC columns. The columns were then centrifuged for 30 sec at >10,000 x G. M-wash buffer (100 µl) was added and the filters washed by centrifugation (30 sec at >10,000 x G). Desulphonation was carried out by incubation with M-Desulphonation buffer (200 µl, 20 min, ambient temperature) followed by centrifugation (30 sec, > 10,000 x G). The columns were then washed twice with 200 µl of M wash buffer followed by centrifugation (30 sec, > 10,000 x G). Bisulfite converted DNA was eluted with 40 µl of 42°C M-elution buffer. Samples were aliquoted and stored at -20°C.

5.6.8 Polymerase Chain Reaction

Polymerase chain reaction (PCR) (24-26) was carried out on a Bio-Rad T100 thermo cycler. Hot Star Taq PLUS® Qiagen® reagents were used for PCR. In principle: the PCR master mix contained 1x reaction buffer including corral red loading dye, dNTPs (200 µM), Taq Polymerase (2.5 U/ µl), primers (200 nM - 750 nM), additional magnesium if required (4 mM) and DNA

(10 ng/ µl) (for specific conditions see table PCR conditions). Reactions were carried out in volumes between 20 and 30 µl. PCR reactions were started with a heat activation of the polymerase at 95°C followed by 35 to 41 cycles consisting of an initial denaturation step at 95°C (30 sec), followed by annealing step (48-65°C, (30 sec) and finalised by an elongation step at 72°C (10 to 30 sec). The reaction was completed by a final elongation step for 10 minutes at 72°C. The PCR product was thereafter stored at 4°C. For PCR reactions used for pyrosequencing, DNA treated by bisulfite conversion was used as a template. A first PCR consisted of a 5' biotinylated primer and a non-modified primer on the counterstrand. For detailed PCR characteristics see Table PCR.

5.6.9 Gel electrophoresis

PCR products were separated in an electric field in 1 % agarose / 1 % TEA buffer gels containing SYBR green (188, 189) SYBR® safe DMSO stock diluted 1:10,000 for DNA labelling and visualised in ultra violet light in a BioRad Gel Doc™ reader.

5.6.10 Quantitative PCR

cDNA generated by reverse transcription as described (3 µl per reaction) was mixed with 15 µl of Q-PCR reaction mix containing primers at following SFRP2 (900 nmol), ADAMTS12 (375 nmol) and PITX2 (225 nmol) onto a 96 well plate. The plate was centrifuged for 60 sec at 1000 x G in order to avoid air bubbles at the bottom of the wells. Quantitative PCR (qPCR) was carried out on a 7500 Fast Real-Time PCR system from *Life Technologies* . Reactions were set up as follows: initial activation of the primer at 90°C for 10 min, followed by 45 cycles of 15 sec denaturation at 95°C and 60 sec annealing and elongation/detection at 60°C. As internal "house keeping" reporters beta-actin or TATA-box binding protein (TBP) were used. For data interpretations ΔCT values (value reference gene – value target gene) were assessed and duplicates averaged. ΔΔCT values were calculated as the average of ΔCT of the reference sample minus the average ΔCT of target sample. Relative expression was 2^-ΔΔCT(190).

5.6.11 Pyrosequencing

Pyrosequencing (191, 192) was performed using the Qiagen Pyrosequencer and related products according to the manufacturer's instructions. Primers for amplicons up to 200 base pairs for pryosequencing (see PCR) were designed using Qiagen Pyrodesign software. Detailed list of primer sets are listed in table 2. PCR products (25 μl) were incubated together with 50 μl of binding buffer, 2 μl of avidin coated sepharose beads and 23 μl water for 10 to 20 min in round bottom 96 well plates on a shaker at 350 rpm in order to allow the biotinylated DNA strands to bind to the beads. Beads were then washed using the Pyrosequencing wash manifold firstly with 70 % ethanol for 10 sec in order to remove unbound DNA, followed by a 20 sec denaturation step in 0.2 M NaOH followed by neutralisation in wash buffer (10 mM Tris-acetate pH 7.6 and 4 M glacial acetic acid) for 10 sec. The beads were then transferred to 96 well reaction plates containing 43 μl annealing buffer and 1.5 μl sequencing primer (10 pmol/ μl working dilution). Samples were denatured for 2 min at 80°C and thereafter cooled to room temperature on the benchtop. The plate was then mounted in the Pyrosequencer® with sample positions defined in the pyrosequencing software. The nucleotide injection sequence was determined using the *pyromark* setup program. The amount of nucleotides, enzyme mix (polymerase, ATP sulfurylase, luciferase, apyrase) as well as the substrate mix (adenosine 5'phosphosulfate, luciferin) was added into the disperser cartridge and added into the machine. After the run individual CpG methylation percentages were read and exported into a table for further processing in Excel and Prism and then plotted on the graph. The individual CpG sites in matching CAM and ATM were compared and semiquantitatively classified as gain or decrease in methylation.

Table 2: Pyrosequencing primer sets

Gene	CpG site	Biotinylated primer	Reverse primer	Sequencing Primer
c14orf23 meth1	cg15482122	5'Bio-TAGGGTATAAGTTGTTTGTTTAAT-3'	5'-CCAAACCTTTCCTATAAATAAA-3'	5'-AACCTTTCCTATAAATAAACCC-3'
TBX5 prom1a	cg16458436	5'Bio-TACATTCTTAAACCTTTCTCTC-3'	5'-AGATTTGTATAGAAATAATTATTGG-3'	5'-TGTATAGAAATAATTATTGGGT-3'
TBX5 prom1b	cg08318726	5'Bio-CCTACACAAATCATTTCAAAC-3'	5'-GTTGGAGAGAATGTTTGTAAG-3'	5'-GGAGAGAATGTTTGTAAGG-3'
ADAMTS12prom	n.a.	5'Bio-CTATCAACTAAATCACTCCCCTT-3'	5'-TAGGAAGATGTAGGGGTGTATG-3'	5'-AGATGTAGGGGTGTATGGTTA-3'
GRB2	n.a.	5'Bio-TTTCTTTAAATAATTACTTCTTAACT-3'	5'-GGATTTTAATTGGTGGAAAGG-3'	5'-TTGGTGGAAAGGAGTTTGTT-3'
PITX2	cg22717014	5'Bio-CTAAAAAATAACCTCCAACTCC-3'	5'-AAGTTAGTAGGGGAAGAATGAG-3'	5'-AAGTTAGTAGGGGAAGAATGA-3'
KCNQ1	cg13071812	5'Bio-GTGGGGGAGTTTTGTTTTAG-3'	5'-CCACTTCCTTCCCTCCTC-3'	5'-TCCTTCCCTCCTCTAC-3'
PAX9	cg26620157	5'Bio-TGTTTTAAGTATTGGTAATTGG-3'	5'-AACCACTAACCACACAAACT-3'	5'-CCACTAACCACACAAACTC-3'
TMEM51	cg25469418	5'Bio-ACTACTACCTAACTCCTTCAAAA-3'	5'-GTTTGGAAGGAAAGTAGAAA-3'	5'-GAAGGAAAGTAGAAAGAGTA-3'
MTHFD1	cg18229107	5'Bio-CCTCCCCAAAAACTAAAC-3'	5'-GGTAGTAATTTTAGTTAATTAGGGA-3'	5'-AATTTTAGTTAATTAGGGAGT-3'
GABRA5	cg16803846	5'Bio-GAAAGGGTTAGGAGTTTTG-3'	5'-AACCATAATAAAACCCCATATA-3'	5'-CATAATAAAACCCCATATAC-3'
RAMP1	cg03647559	5'Bio-AGGTGGAGATTAAGGTGTTT-3'	5'-CCAAAAAAACCTCCTAAAATA-3'	5'-AACCTCCTAAAATATTC-3'
SFRP2	cg14435644	5'Bio-GGTTTATATTTTAGTTTTTTAGAG-3'	5'-AAATAACATAACTCAATAC-3'	5'-AAATAACATAACTCAATAC-3'
LINE1	n.a.	5' Bio-TAGGGAGTGTTAGATAGTGG-3'	5' AACTCCCTAACCCCTTAC-3'	5' CAAATAAAACAATACCTC-3'

5.6.12 Dideoxy (Sanger) sequencing

Verification of plasmid sequences: Isolated plasmids were sequenced by dideoxy sequencing (27, 193). On all three constructs the primer VP1.5 (5' GGACTTTCCAAAATGTCG 3'), T_m 49°C and XL39 (5' ATTAGGACAAGGCTGGTGGG 3') Tm 58°C were used for sequencing. The sequencing PCRs were carried out in a volume of 10 µl containing 1x BigDye®, 1x Sequencing buffer, sequencing primer (0.06pM) and 500 ng of plasmid DNA. The reaction was started with a 60 sec denaturation step at 96°C, followed by 27 cycles of denaturation for 20 sec at 95°C, annealing primer dependent (see table) during 10 sec and a elongation at 60°C during 4min. The reaction was completed by a terminal elongation step of 4 min at 65°C.

5.6.13 Purification of amplification product

The amplification product of the sequencing PCR was purified using the CENTRI–SEP™ well strip columns.

In brief, after a rinsing spin of the columns for 2 min at 750 x G the sequencing PCR product was loaded onto the gel columns and then cleaned through the separation matrix by another centrifugation over 2min at 750G. The eluate was thereafter vacuum dried in a vacuum bell and resuspended in 5 µl of formamide. The sequencing process was carried out on an AbiPrism3100 capillary electrophoresis machine. Electropherograms were read on 4Peaks 1.8 software and aligned with digital sequence templates in Ape 1.17 and SnapGene® Viewer 2.7.3 software.

5.7 Methylation Array

Methylation was measured using the Illumina Infinium HumanMethylation450 BeadChip which allows to interrogate more than 485,000 methylation sites per sample at single-nucleotide resolution. Data was analysed using the Bioconductor package RnBeads (194). Differential methylation of various regions including sites, genes, promoters, CpG islands were calculated separately. Differentially methylated genes were identified using linear models and empirical Bayes algorithm and selected using the FDR corrected p-value cutoff of <0.05 and delta-beta >0.2. Data analysis was performed by Dr Jithesh Puthen, University of Liverpool.

5.8 Expression Array

Gene expression was measured using the Illumina HumanHT-12 v4 Expression BeadChip which targets more than 47,000 probes and provides genome-wide transcriptional coverage of well-characterized genes, gene candidates, and splice variants. Bioconductor package lumi (195) was used for preprocessing the array data and limma (196) for differential expression analysis. Background correction, variance stabilizing transformation and Robust Spline Normalisation (RSN) were performed as part of the preprocessing. Differentially expressed genes were identified by linear models and empirical Bayes approach and a list of genes selected using cut-off of FDR corrected p-value < 0.05 and fold change > |2|.

5.9 Statistics

Data analysis were done with Prism©. The final results were calculated as mean ± standard error of means (SEM) or as medians where appropriate. Student t-test, one-way and two-way ANOVA and correlation analysis were performed on the data as appropriate. Results were regarded as statistically significant at a $p<0.05$.

6 Animals, Cells and Materials

6.1 Animals

Athymic Balb/C nu/nu mice (BALB/c-Nude Mice CAnN.Cg-Foxn1nu/ CrlJAXTM) Mice Strain: CByJ.Cg-*Foxn1nu/J* were purchased from Charles River Laboratories, Manston Road, Margate, Kent CT9 4LT, United Kingdom.

6.2 Tissue culture

6.2.1 Cell lines

Human oesophageal myofibroblasts from cancer patients (173/1,2&5, 193/1&2, 282/1&2, 306/1&2, 360/1&2, 373/1&2, 467/1&2) were obtain from the University of Szeget, Hungary (table 3).

Table 3: Cancer patients characteristics

Patient	Age	Gender	Survival (month)	Tumour stage	Tumour grade	Tumour location	histological classification	adjacent mucosa
173	72	male	18	pT4 N1 M0	G2 + G3	oesophagus	Barrett's AC	Barrett's metaplasia
193	64	male	19	pT2 N3 M0	G3	cardia	Barrett's AC	Barrett's metaplasia
282	70	female	>25	pT3 N1 M1	G2	cardia	Barrett's AC	Barrett's metaplasia
306	56	male	34	pT3 N1 M0	G3	oesophagus	SCC	CIM, PAM (cardia)
360	52	male	31	pT3 N1 M0	G2 - G3	oesophagus	SCC	normal
373	49	male	35	pT2 N1 M0	G2	oesophagus	SCC	reflux oesophagitis
467	69	male	14	pT3 N1 M0	G2	oesophagus	SCC	PAM (cardia)

Normal tissue myofibroblasts (241/6, 246/6, 261/6, 279/6, 334/6, 351/6, 474/6) were obtained from the University of Szeget, Hungary (table 4).

Table 4: Control subjects characteristics

Patient	Age	Gender	Sample origin
241	44	female	oesophagus
246	45	male	oesophagus
261	52	female	oesophagus
279	60	male	oesophagus
334	52	female	oesophagus
351	41	male	oesophagus
494	33	male	oesophagus

Oesophageal cancer cells (OE19, OE21, OE33) (164) were purchased from the American type culture collection, ATCC, VA, USA.

Human Umbilical Vein Endothelial Cells (HUVEC) were purchased from Lonza (Cambridge, UK).

Cell labelling: PKH26 Fluorescent (red) and PKH67 Fluorescent (green) Cell Linker Kits (Sigma-Aldrich, Gillingham, UK)

Matrigel: Geltrex™ LDEV-Free Reduced Growth Factor Basement Membrane Matrix (Gibco™, no A1413202)

Omeprazole (Sigma-Aldrich, Gillingham, UK; O104-500MG)

5-Aza-2'-deoxzcztidine (Sigma-Aldrich, Gillingham, UK; No. A3656)

6.2.2 Consumables

Tissue culture flasks: TTP 75 cm^2 and 25 cm^2 (SLS TPP Flask 270 ml 75cm^2 60 ml 25 cm^2 filtered, catalogue number: TIS7016 and TIS7012).

Boyden chamber inserts: BD® Biocoat™ Corning™ with 8 μm pores (Systemic Laboratory Supplies, No. 354578).

Tissue culture plates (6, 12, 24 well plates); Fisher Scientific, Nos. 10119831, 10098870, 10604903).

6.2.3 Cell culture media and solutions

DMEM: Dulbecco's Modified Eagle's Medium - high glucose with 4500 mg/L glucose, L-glutamine, and sodium bicarbonate, without sodium pyruvate, liquid, sterile-filtered, suitable for cell culture, Sigma-Aldrich, Gillingham, UK; No. D5796.

Antibiotic/antimycotic Solution (Sigma-Aldrich, Gillingham, UK; A5955).

Penicillin/streptomycin (Sigma-Aldrich, Gillingham, UK; P0781).

Non-essential amino acids (MEM Non Essential Amino Acids (100X), Life Technologies, Catalogue number: 11140035).

Phosphate buffered saline (PBS) PBS (10x) PH7.4 W/O CAMG USA PLASTIC, Life Technologies, No 70011036.

RecoveryTM cell freezing medium Invitrogen (GIBCO®) No 12648-010.

Fetal bovine serum (FBS) was purchased from Lonza(DE14-802F).

Trypsin (0.25 % w/v)-EDTA solution: Trypsin Solution (0.5 g/l porcine trypsin and 0.2 g/l EDTA•4Na in Hank's Balanced Salt Solution with phenol red, Sigma-Aldrich, Gillingham, UK; T3924).

Matrigel (Corning, Tewksbury, MA, USA).

Collagen-I (Millipore, Watford, Hertfordshire, UK).

Ibidi® silicon two chamber inserts (Thistle Scientific Ltd, Glasgow, UK; No. 80209).

Click-iT® EdU Alexa Fluor® 488 & 594 Imaging Kit (Life Technologies, No. C10337 & C10639).

Endothelial Growth media (EGM), Lonza Transfection kits, Amaxa™.

PKH67 membrane labelling (Sigma-Aldrich, Gillingham, UK; PKH26GL).

Lysogeny broth (LB) medium (500ml): Yeast extract BP1422-500 (1g), Tryptone microbial media 1279-7099 (2g), Sodium Chloride (2g).

Agar for bacteria (500ml): Agar-Agar A/1080/53 (7.5g), Yeast extract BP1422-500 (2.5g), Tryptone microbial media 1279-7099 (5g), Sodium Chloride (5g).

6.2.4 Transfections

6.2.4.1 Eukaryotes:

Amaxa™ Fibroblasts Nucleofector™ kit and Amaxa™ Human MSC Nucleofector®, Lonza (VPD-1001).

6.2.4.2 Prokaryotes:

NEB Turbo Competent *E. coli* (High Efficiency), NEW ENGLAND BioLabs catalogue number C2984).

6.2.5 Plasmids and siRNA

Plasmids for overexpression of ADAMTS12, PITX2 and SFRP2 were purchased from Cambridge Bioscience (table 5) Lyophilised MISSION®

esiRNA esiRNA targeting human ADAMTS12, PITX2 and SFRP2 were purcheased from Sigma-Aldrich Company Ltd and resuspended in RNAse free water to a concentration of 1 μg/ μl (table 6).

Table 5: Overexpression plasmids and sequencing primers

			Vector	resistancy	primer pairs
ADAMTS12	SC126126	Homo sapiens cDNA clone MGC:61868 IMAGE:6701691, complete cds as transfection-ready DNA	pCMV6-XL5	ampicillin (100μg/ml)	VP1.5 / XL39
PITX2	RC204179	Myc-DDK-tagged ORF clone of Homo sapiens paired-like homeodomain 2 (PITX2), transcript variant 3 as transfection-ready DNA	pCMV6-Entry (C-terminal Myc and DDK tagged)	kanamycin (25μg/ml)	VP1.5 / XL39
SFRP2	RC202164	Myc-DDK-tagged ORF clone of Homo sapiens secreted frizzled- related protein 2 (SFRP2) as transfection-ready DNA	pCMV6-Entry	kanamycin (25μg/ml)	VP1.5 / XL39

Sequencing primers:
VP1.5 (5' GGACTTTCCAAAATGTCG 3') Tm 49°C
XL39 (5' ATTAGGACAAGGCTGGTGGG 3') Tm 58°C

Table 6: siRNA

ADAMTS12	SASI_Hs01_00067584	5' GUAUCAAUCCCAAGAGUGA[dT][dT]
	SASI_Hs01_00067584_AS	5' UCACUCUUGGGAUUGAUAC[dT][dT]
	SASI_Hs01_00067585	5' GAUGAACCUUGCGAUGUGA[dT][dT]
	SASI_Hs01_00067585_AS	5' UCACAUCGCAAGGUUCAUC[dT][dT]
	SASI_Hs01_00067586	5' GUCUGAUUACUGAGGGCUU[dT][dT]
	SASI_Hs01_00067586_AS	5' AAGCCCUCAGUAAUCAGAC[dT][dT]
SFRP2	SASI_Hs01_00200413	5' CAGCAUUUCCUGAGUUAUA[dT][dT]
	SASI_Hs01_00200413_AS	5' UAUAACUCAGGAAAUGCUG[dT][dT]
	SASI_Hs01_00200414	5' CAGAGAGAGUUCAAGCGCA[dT][dT]
	SASI_Hs01_00200414_AS	5' UGCGCUUGAACUCUCUCUG[dT][dT]
	SASI_Hs01_00200415	5' GUGCUAGUCCCGGCAUCCU[dT][dT]
	SASI_Hs01_00200415_AS	5' AGGAUGCCGGGACUAGCAC[dT][dT]
PITX2	SASI_Hs01_00117388	5' GCCUGAAUAACUUGAACAA[dT][dT]
	SASI_Hs01_00117388_AS	5' UUGUUCAAGUUAUUCAGGC[dT][dT]
	SASI_Hs01_00117389	5' CAGUGUCUGACAUCUUUCA[dT][dT]
	SASI_Hs01_00117389_AS	5' UGAAAGAUGUCAGACACUG[dT][dT]
	SASI_Hs01_00117390	5' CCCUUGAAAGACUGGGAAU[dT][dT]
	SASI_Hs01_00117390_AS	5' AUUCCCAGUCUUUCAAGGG[dT][dT]

6.3 Nucleic acid extraction and handling

6.3.1 RNA

- miRNeasy mini Kit (50) (Qiagen, No. 217004).
- RNase-Free DNase Set (50) (Qiagen, No. 79254).
- Agilent RNA 6000 Nano Kit (Agilent Technologies, No 5067-151).
- Agilent 2100 Bioanalyzer.

6.3.2 DNA

- QIAamp DNA mini Kit (50) (Qiagen, No. 51304).
- Bisulfite conversion: EZ DNA Methylation-Gold™ Kit, ZYMO RESEARCH, No D5005 & D5006.

6.3.3 Plasmids

- Plasmid miniprep Kit: Zyppy™ Plasmid miniprep Dit (Zymo Research, No. D4020).
- Plasmid Maxi Prep: Zyppy ™ Plasmid Maxiprep Kit (Zymo Research, No. D4028).

6.4 PCR reagents

AmpliTaq Gold (Thermo Fisher Scientific, Paisley, UK).

PyroMark Gold (Qiagen Ltd, Manchester, UK).

Taq DNA Polymerase (1000 U) 201205 (Qiagen Ltd, Manchester, UK).

Centri-Sep™ spin colums (Applied Biosystems, No 401763).

QPCR primers (ADAMTS12 Hs00229594, PITX2 Hs04183413, SFRP2 Hs00293258) Life Technologies, Pailsey, UK)

6.5 Reverse transcription

High-Capacity RNA-to-cDNA™ Kit (Life Technologies, No. 4387406)

6.6 Agarose Gel Electrophoresis

High grade agarose (Sigma-Aldrich, Gillingham, UK)

SYBR® Safe DNA Gel Stain (Life Technologies, Paisley, UK; No. S33110)

6.7 Staining & labelling

Hematoxylin: Hematoxylin Solution, Harris Modified (Sigma-Aldrich, Gillingham, UK; No. HHS32).

Eosinophil: Eosinophil Y solution (Sigma-Aldrich, Gillingham, UK; No. HT110232).

Mounting medium: DPX Mountant for histology (Fluka BioChemika, No. 44581).

FISH Probe: Ready-to-use Human Chromosome Pan-Centromeric paints; FITC (Cambio, Cambridge, UK; 1695-F-01).

Cover slips 22x50mm (Fisher Scientific, Loughborough, UK; No. 12333128).

Microscope slides, Super frost, (3 x 1 inch) (Fisher Scientific, Loughborough, UK; No. 10149870).

6.8 Solutions and Buffers

20 x Sodium chlorid Sodium Citrate buffer (SSC): In 450ml deionized water 87.6g sodium chloride and 44.1g sodium citrate were dissolved, the pH adjusted to 7.0 and then more water upped to 500 ml. The buffer was then autoclaved and stored at 4°C.

TE buffer: 0.01 M Tris, 0.1 mM EDTA, pH 7.5.

PBT: 1 x **P**BS, 5 % protease free **B**ovine serum albumin (BSA) and 0.5 % **T**riton-X.

TBS: Tris-buffered saline: 50 mM Tris, 150 mM NaCl, pH adjusted to 7.6 with 100 mM HCl.

HEPES (4-(2-hydroxyethyl)-1-piperazineethanesulfonic acid) 100 mM stock solution: 1.19 g in 40 ml of water, pH adjusted to 7.5, topped up with water to 50 ml and frozen in aliquots at -4°C.

7 Global DNA methylation in oesophageal myofibroblasts

7.1 Introduction

Epigenetic modification is a well-established event in carcinogenesis that affects not only the malignant cancer cells but also non-malignant stromal cells in the tumour microenvironment. Altered global DNA methylation is a hallmark of cancer cells characterised by a decrease of overall methylation compared to normal cells (106). A decrease of global DNA methylation has also been documented in CAMs accompanied by altered gene regulation (108, 113, 197).

DNA methylation during replication is maintained by DNMT1 and DNMT3 which can be inhibited with cytosine analogues such as DAC (49). Cytosine analogues have been well-established drugs in anticancer therapy since the late 1990s (198). The doses of DAC used to induce altered expression *in vitro* vary in the literature and direct mutagenic effects and induction of senescence upon DAC treatment have been documented. The effect of cytosine analogues on stromal cells has previously been addressed using immortalised fibroblast cell lines (113) and primary cell lines in mice (114) and humans (110); moreover the effect of DAC on the overall DNA methylation has been assessed in immortalised fibroblasts (197). However, there have been no studies in primary myofibroblasts. Thus, while there is a wealth of work on the biological effects of DAC on malignant cells, little is known about these effects on non-malignant stromal cells.

More generally, the effect of cytosine analogues on stromal cells of the oesophagus has not yet been investigated to the best of our knowledge. Generally, little is known of the implications of systemic treatment with cytosine analogues (199). The present study considered whether global DNA methylation differs between CAMs and ATMs of oesophageal cancer patients using pyro sequencing of LINE1 elements as a surrogate for global DNA

methylation. We also tried to establish a model of epigenetic modification of myofibroblasts using DAC

7.1.1 Objectives

The specific objectives were:

- To assess whether there are differences in global methylation between CAMs and ATMs.
- To assess whether epigenetic changes in primary myofibroblasts were induced by DAC.
- To characterise the biology of myofibroblasts after DAC treatment *in vitro* and *in vivo* as a model for epigenetic modification of stromal cells.

7.2 Material and Methods

Myofibroblasts (241/6 and 261/6) were expanded in MM and treated with DAC as described (5.2.10). Cell expansion was assessed as described (5.2.7).

Cell proliferation was assessed by EdU incorporation as described (5.2.6).

Contractibility of myofibroblasts was assessed with gel contraction assays as described (5.2.8) using DAC treated myofibroblasts pelleted and resuspended in 2 ml of Matrigel.

Transwell migration assays of myofibroblasts were performed as described (5.2.4). Migration was documented by photomicroscopy (5 images per chamber insert) and images processed to sequential time lapse videos as described (5.5.8).

Cellular DNA was harvested with Qiagen DNeasy kits and assessed for quality and quantity by spectrophotometry as described (5.6.2). Between 0.5 and 1 μg of DNA were then bisulfite-converted using the EZ DNA methylation Gold™ kit from ZymoResearch as described by the manufacturer. DNA methylation standards were used as controls. DNA methylation was assessed by LINE1 pyrosequencing analysis as described (5.6.11).

Myofibroblasts were treated with 0.1 μM or 0.01 μM DAC and injected into the flank of Balb/c nude mice (100 μl per mouse) as described (5.4.2).

7.3 Results

7.3.1 Assessment of global DNA methylation in myofibroblasts

Global DNA methylation was assessed by pyrosequencing of PCR amplified LINE1 elements (figure 5). In four patients (173, 282, 306 and 373) all of six CpG sites in LINE1 elements were hypomethylated in CAMs. In patient 193, three CpG sites were hypomethylated, two unchanged and one hypermethylated while in patient 467 five out of six CpG sites were hypomethylated in CAMs and one unchanged. Only in patient 360 were all CpG sites hypermethylated in CAMs compared to ATMs. When the comparison was extended to NTMs there was a trend towards lower methylation in CAMs compared to NTMs, but without reaching statistical significance. Global methylation at all sites was significantly lower in the two oesophageal cancer cell lines that were investigated in parallel (figure 6). When comparing the difference of all six CpG sites in the LINE1 amplicon investigated by pyrosequencing, a significant net decrease of global DNA methylation was detected (p=0.0008) (figure 7).

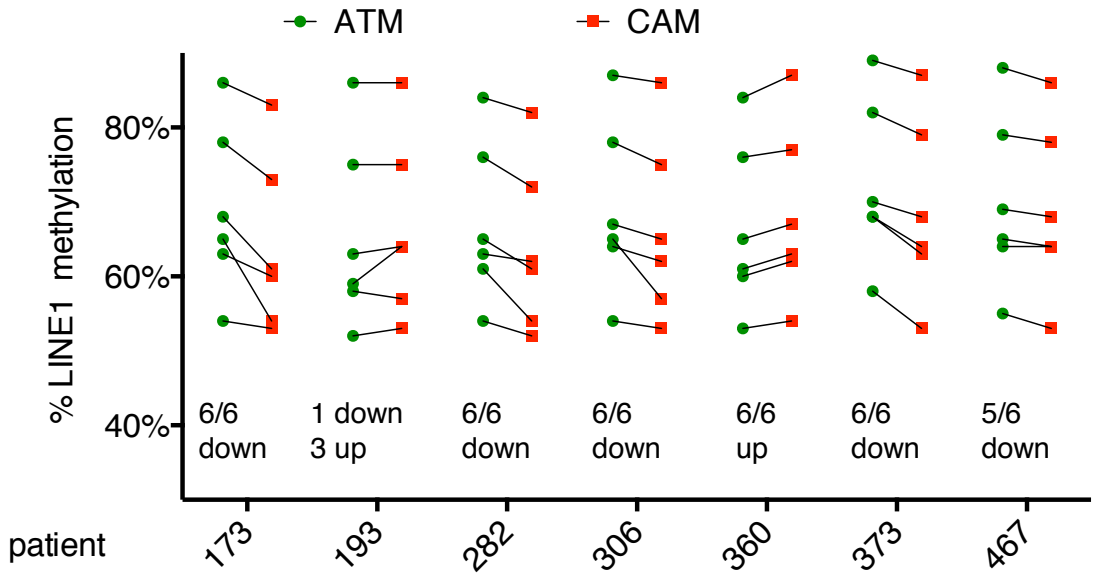

Figure 5: CpG methylation in LINE1 elements varies between CAMs and ATMs. The percentage of cysteine methylation in six LINE1 element CpG

islands varies between CAMs (red) and ATMs (green). Corresponding CpG sites are connected.

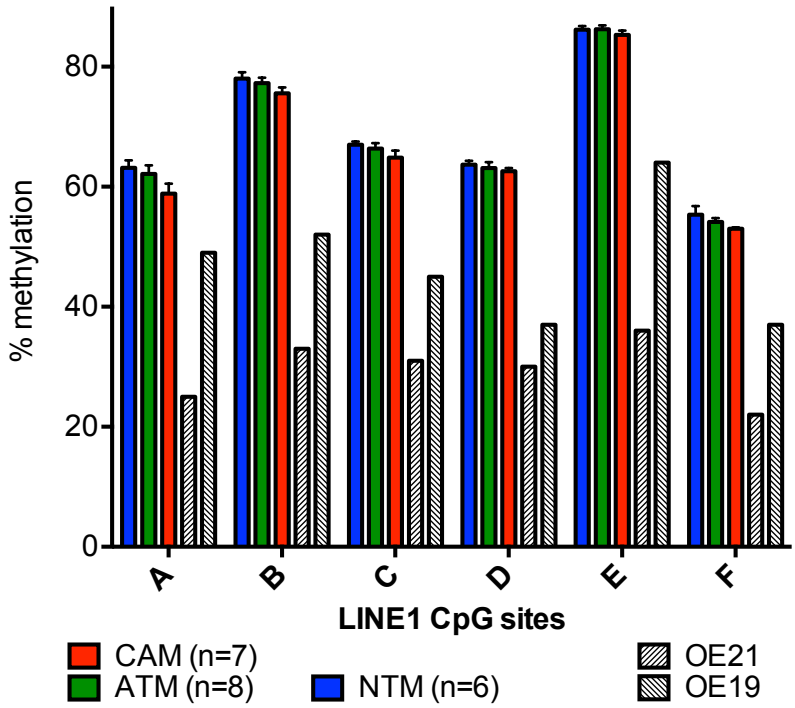

Figure 6: Global DNA methylation in NTMs is higher than in CAMs and ATMs. Percentage of methylation in LINE1 elements in six (A - F) individually amplified CpG sites in NTMs, ATMs and CAMs. Two oesophageal cancer cell lines OE19 and OE21 are included.

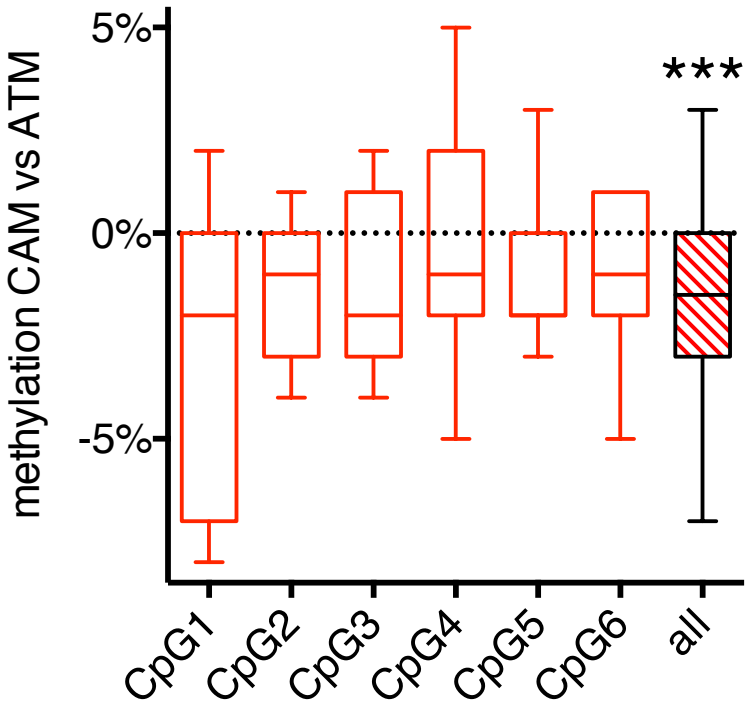

Figure 7: Global DNA methylation in NTMs is higher than in CAMs and ATMs. Box and whisker (Tukey) plot of percentage change for each individual CpG island (1-6) and the mean of all sites (all) for dinucleotide methylation in all CAMs and ATMs. Statistical analysis: one-sample t-test for column means different to the hypothetical value 'zero' indicating no change in methylation: CpG1 p=0.085, CpG2 p=0.062 and for the entire dataset p=0.0008.

7.3.2 Model for epigenetic modification of myofibroblasts

In order to modify DNA methylation, myofibroblasts were treated with different concentrations of DAC ranging from 0.001 μM to 10 μM, and global DNA methylation assessed (figure 8). The most potent effect of DAC treatment was achieved at a concentration of 0.1 μM leading to a reduction of global methylation by 10 %. Prolonged exposure of myofibroblasts to DAC did not further decrease global DNA methylation.

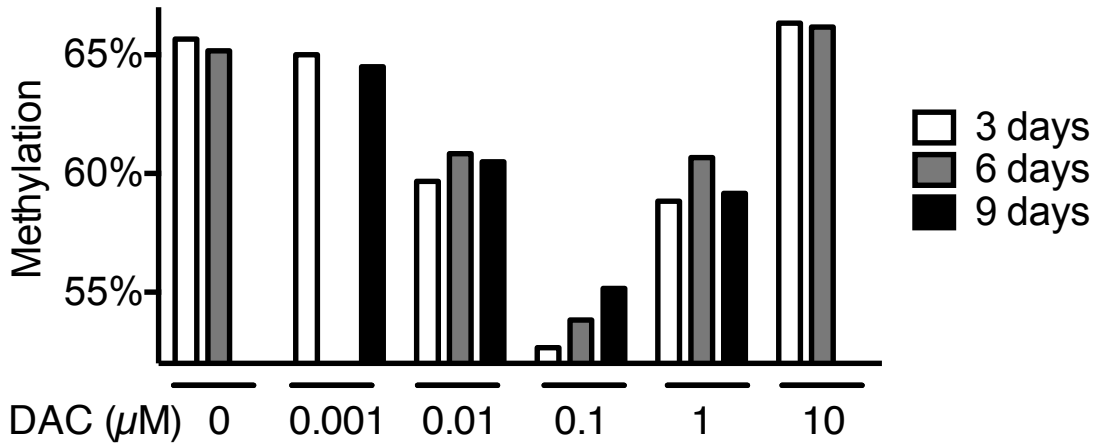

Figure 8: DAC decreases global DNA methylation in NTMs in a concentration-dependant manner. Percentage of average LINE1 methylation, assessed by pyrosequencing, in NTMs treated on 3, 6 or 9 consecutive days by different concentrations of DAC.

In studies on the long-term effect of DAC treatment on myofibroblasts, DNA methylation was assessed by pyrosequencing of LINE1 one day before (day -1), one day after (i.e. day 4), ten and 15 days after the initial treatment (i.e. day 14 and 19 of the experiment). These analyses showed a decrease of

global DNA methylation directly after the initial treatment and a relative increase two weeks after the treatment (figure 9).

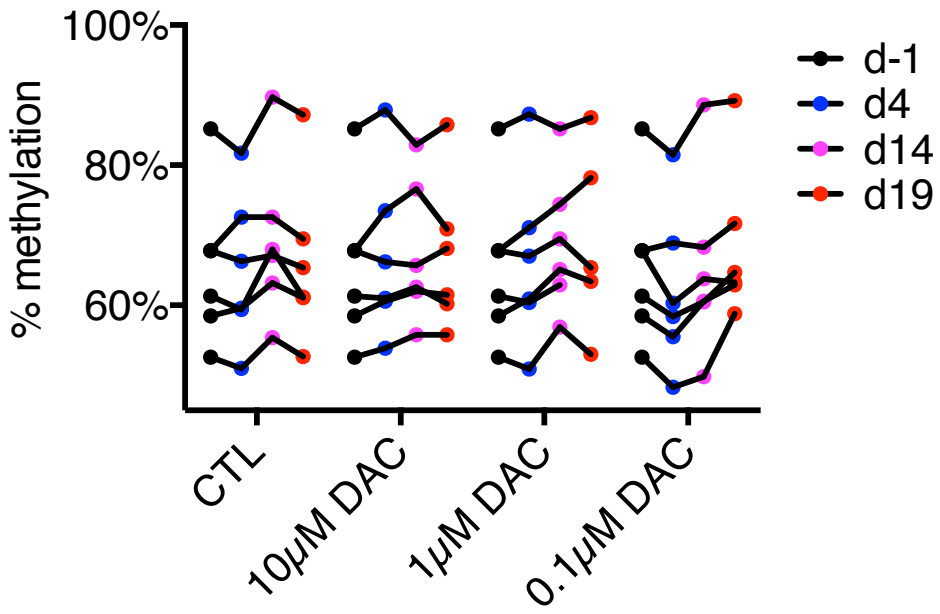

Figure 9: DAC induces a transient decrease of global LINE1 methylation. Time course experiment assessing global methylation of NTMs by LINE1 methylation in myofibroblasts one day before treatment (i.e. -1) and at days 4, 14 and 19 after initial DAC treatment with three different concentrations of DAC (0.1, 1 and 10μM) on 3 consecutive days. Matching CpG sites are connected with a line.

7.3.3 Effect of cancer cell conditioned medium on myofibroblasts proliferation

In order to provide a baseline for studies of myofibroblasts proliferation, initially we examined the effect of OE21 and OE33 cancer cell conditioned medium (CM21 and CM33 respectively) on proliferation of serum starved myofibroblasts exposed for 24 h to CM21 and CM33. Treatment led to a marked increase of EdU incorporation as compared to incubation in MM (figure 10).

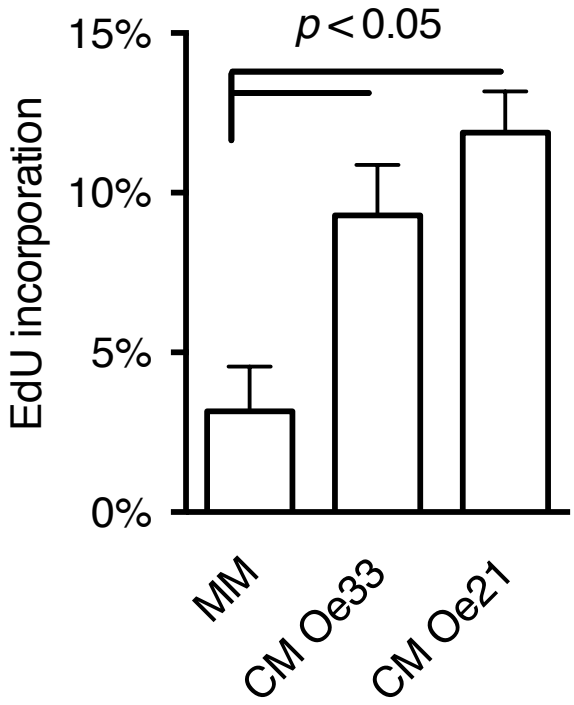

Figure 10: Effect of conditioned medium on EdU incorporation in myofibroblasts. Myofibroblasts were exposed for 24 h to conditioned medium of OE33 and OE21 cancer cells and then incubated for 2.5 h with EdU. The percentage of myofibroblasts with EdU incorporation is shown. Statistically increased EdU incorporation in student's t-test.

7.3.4 Effect of DAC treatment on myofibroblasts proliferation

DAC treatment of myofibroblasts for 3 days decreased EdU incorporation from 40 % in control cultures to less than 10 %. The inhibition was concentration-dependent at concentrations below 0.1 μM. Prolonged treatment for 6 or 9 days did not further influence EdU incorporation (figure 11). EdU incorporation remained decreased after 8 and 28 days of treatment (figure 12 A). When DAC-treated cells cultured for 28 days were exposed to CM from OE21 cells there was a trend towards increased EdU incorporation that reached statistical significance only at a concentration of 1 nM DAC (figure 12 B).

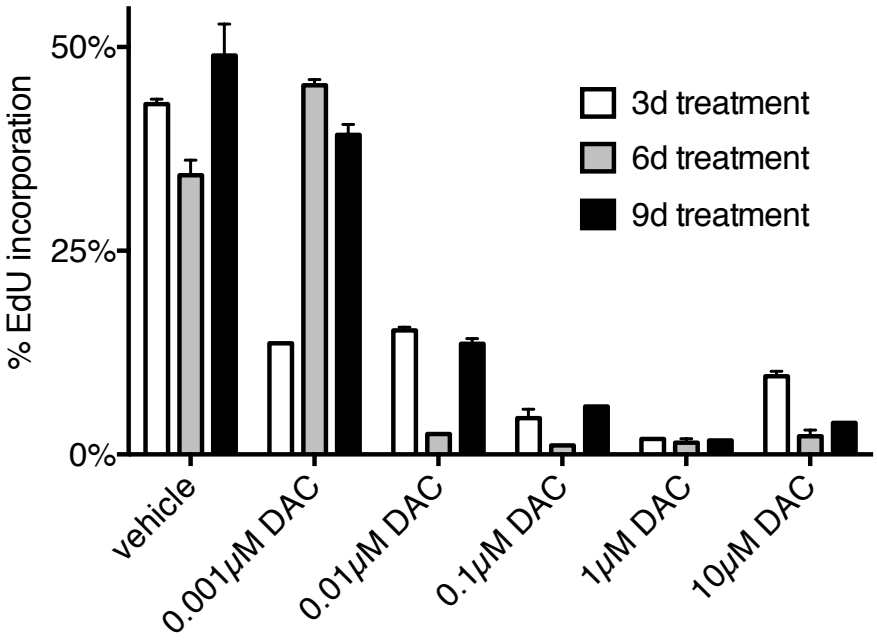

Figure 11: DAC inhibits myofibroblast proliferation in a concentration dependent manner. EdU incorporation assessed one day after 3, 6 and 9 days of treatment with different concentrations of DAC (0.001 μM – 10 μM).

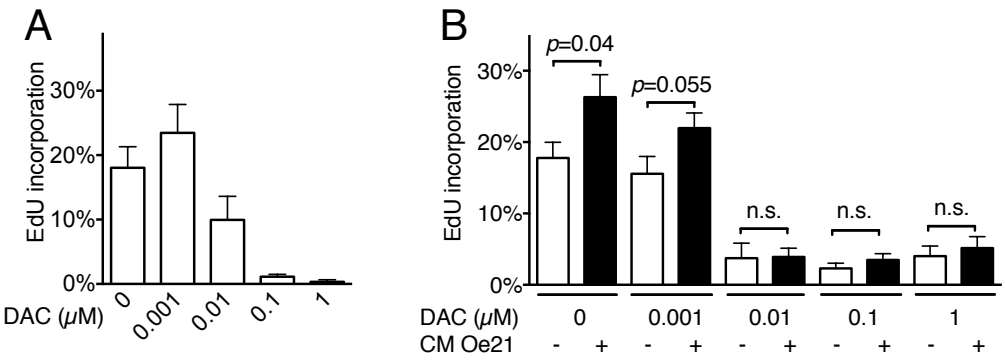

Figure 12: DAC treated myofibroblast exhibit decreased proliferation 8 days and 28 days after treatment. A) EdU incorporation 8 days after treatment with a serial dilutions of DAC ranging 0.001μM to 1μM. B) EdU incorporation 28 days after treatment with serial dilutions of DAC ranging from 0.001 μM to 1 μM. Cells additionally exposed to conditioned medium from OE21 cancer cells marked as filled bars. Statistical significance in students t-test.

Cell expansion assays demonstrated a clear suppression of cell proliferation by DAC in a concentration-dependent manner (figure 13). Treatment of myofibroblasts over 3 or 6 days decreased cell proliferation over the following 18 days in culture. Extended treatment for 6 days had a marginally stronger suppressive effect on cell expansion compared to cells treated on three consecutive days at doses of 1 and 0.1 μM DAC (figure 14).

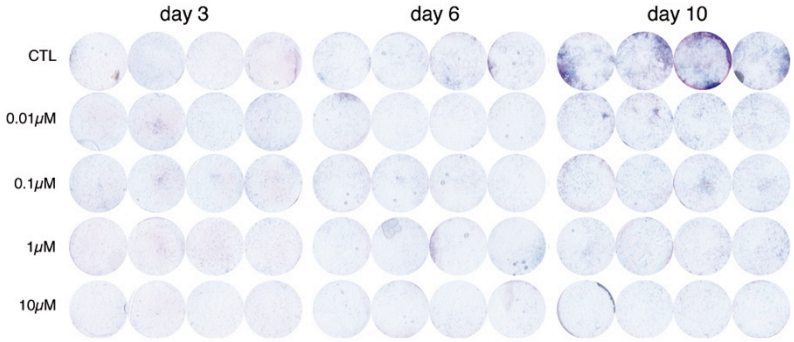

Figure 13: DAC decreases NTM expansion on glass. Haematoxylin and eosin (H&E) stained sets of four glass cover slips containing NTMs 3, 6 and 10 days after treatment with different concentrations of DAC. Note cell growth at 10 days returns after treatment with low concentrations of DAC.

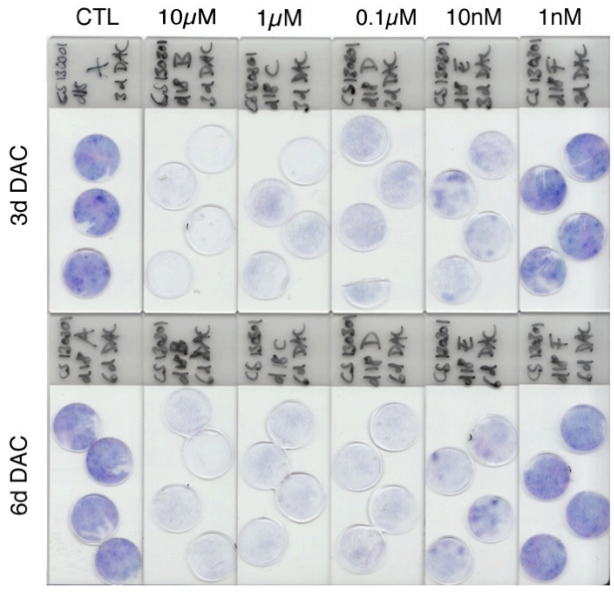

Figure 14: DAC decreases NTM expansion in a concentration-dependant manner. H&E stained glass cover slips containing NTMs 18 days after 3 or 6 days treatment with different doses of DAC. Note that 1nM DAC does not block cell growth.

7.3.5 Effect of DAC treatment on myofibroblast migration

Basal migration of myofibroblasts in Boyden chamber assays is relatively low, and so to examine the effect of DAC treatment on migration the responses to a chemotactic stimulus were examined. Thus when the effect of CM from OE21 cells on transwell migration of normal myofibroblasts (261/6) and a pair of OESCC associated myofibroblasts (373/1,/2) was assessed, CM had a strong pro-migratory effect on the myofibroblast lines. The stimulated migration was higher in ATMs compared to matched CAMs (figure 15). Myofibroblast migration in Boyden chambers was increased in a concentration-dependent manner and persisted 7 days and 28 days after DAC treatment (figure 16 A). When cells kept in culture over 28 days were exposed to full medium or CM (OE21) transwell migration was increased (figure 16 B).

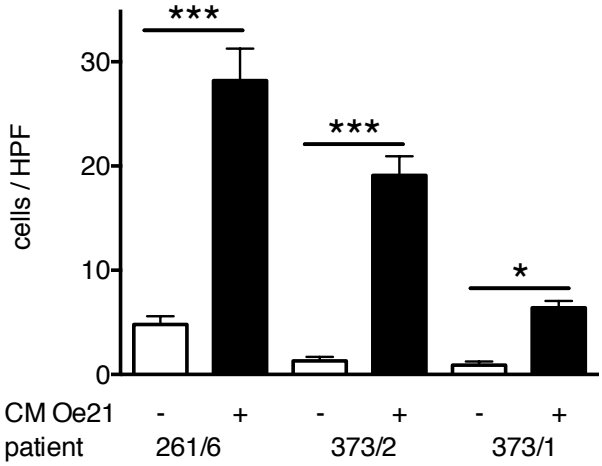

Figure 15: Cancer CM stimulates myofibroblast migration. Conditioned medium from OE21 cancer cells stimulates NTM (261/6), ATM (373/2) and CAM (373/1) migration in Boyden chamber assays. Mean increase of migration between serum-free control conditions (-) and OE21 conditioned medium (CM OE21) is 5.8x for NTM, 14.7x for ATM and 7.1x for CAM. Asterisks indicate statistical significance in t-test.

In order to study the effect of DAC treatment on myofibroblast migration, myofibroblasts treated with DAC were cultured for 1 day and transwell

migration was assessed. These assays demonstrated an increased migration of myofibroblasts upon DAC treatment (16).

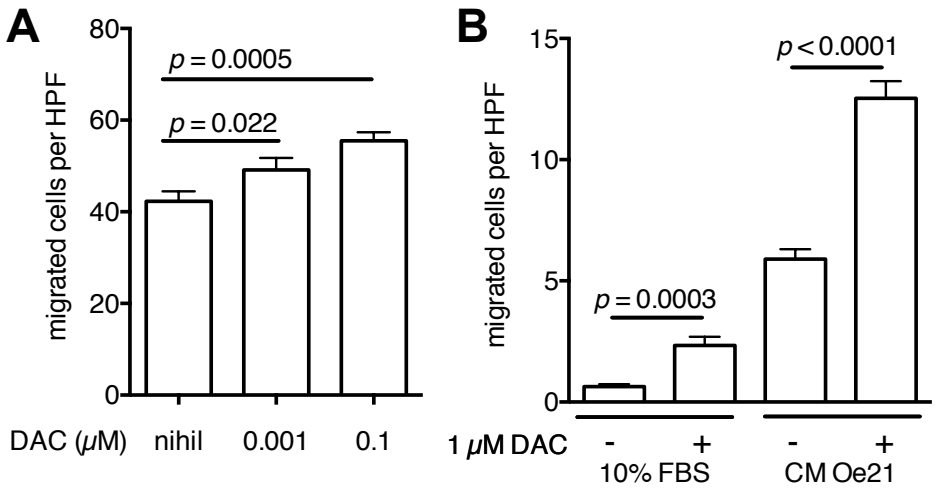

Figure 16: DAC persistently increases myofibroblast migration. Boyden chamber transwell migration of 241/6 NTMs seven days (A) and 28 days (B) after DAC treatment. NTMs display a higher migration rate 28 days after DAC treatment when exposed to conditioned medium form OE21 cancer cells (B). Statistical significance *p* between groups with student's t-test.

The effect of DAC treatment on migration towards OE21 cells was also investigated with the use of the ibidi® chamber system. Myofibroblasts treated with DAC (0.1 μM) not only exhibited increased migration towards cancer cells, but there was also increased cancer cell migration towards myofibroblasts (figure 17 & 18).

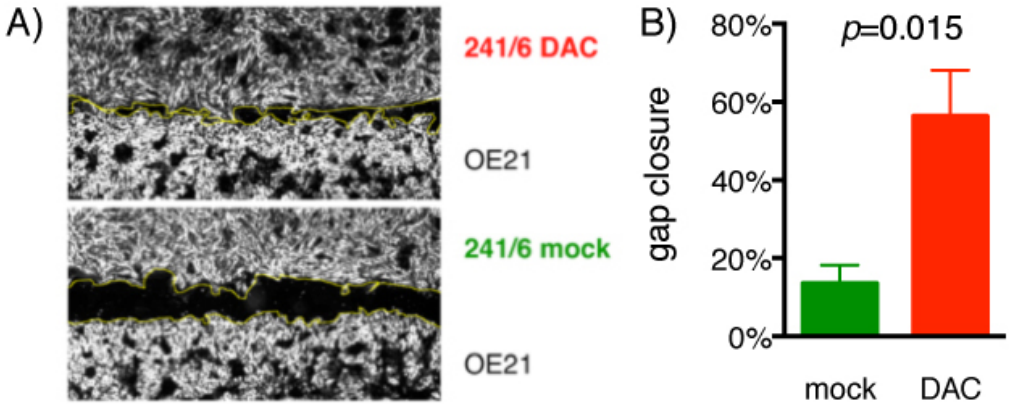

Figure 17: Ibidi migration assay. A) photomicrograph at 25 h after co-culture. B) percentage of closure of area between cells at 25 h. Red for area between DAC treated myofibroblasts and OE21 cancer cells, green for area between mock treated myofibroblasts and OE21 cancer cells. Error bars indicate standard error mean. $p < 0.01$ student t-test

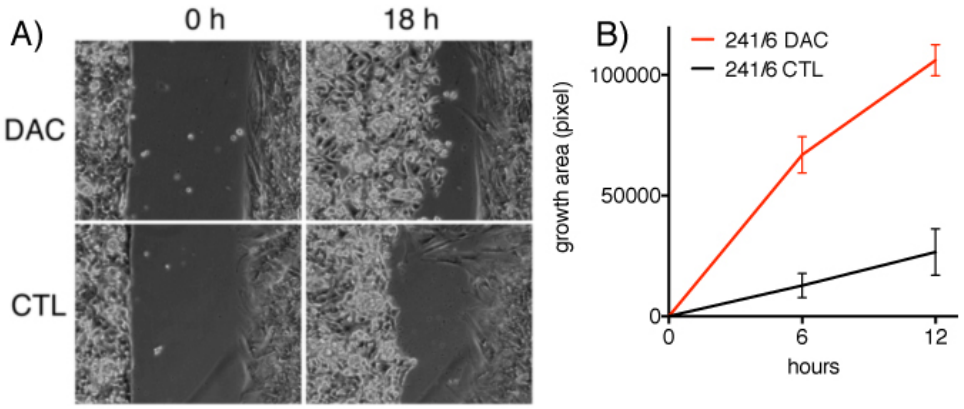

Figure 18: DAC treatment of myofibroblasts bidirectionally increases migration of myofibroblasts and cancer cells towards each other. A) photomicrograph of DAC treated myofibroblasts (upper) and sham treated myofibroblasts (lower) at time point 0 h and 18 h. OE21 cancer cells are on the left side, myofibroblasts on the right side in all cases. B) myofibroblast migration towards OE21 cells. Difference of growth area significant in two way ANOVA ($p<0.0001$)

7.3.6 Effect of DAC on myofibroblast contractility

Myofibroblasts treated with different concentrations of DAC exhibited changes in gel contraction used as a surrogate marker for cell contractility. Thus

treatment of myofibroblasts with 1 nM DAC led to a significant increase in gel contraction compared to mock-treated myofibroblasts (19). However, DAC at 0.1 μM did not significantly affect gel contraction. Myofibroblasts treated with 1 μM DAC exhibited a trend towards a reduced contractibility as compared to untreated controls.

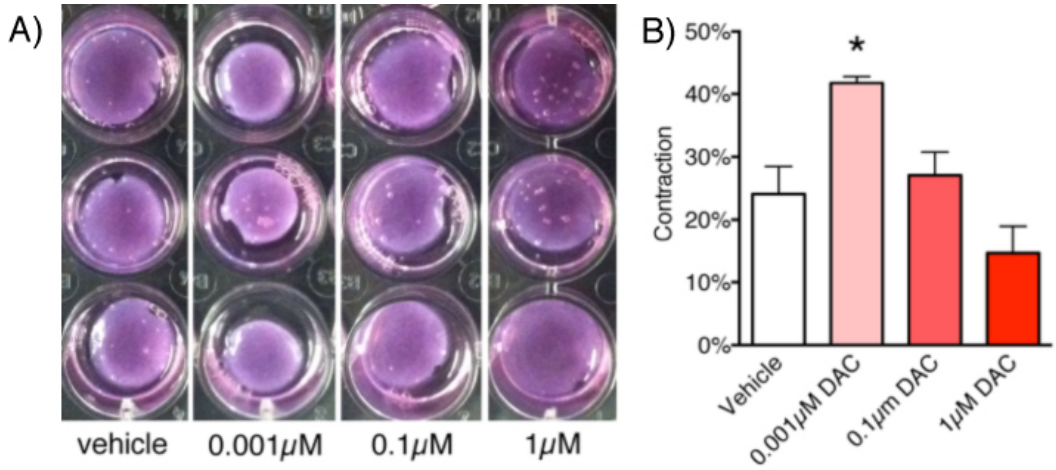

Figure 19: Gel contraction assay of NTM treated with DAC. A) gels in 24 well plate after 6 hours of contraction using myofibroblasts treated with vehicle only and 0.001, 0.1 and 1 μM DAC. B) corresponding graph depicting percentage of contraction. Value for statistical significance as compared to vehicle control in t-test p=0.02.

7.3.7 DAC treated myofibroblasts have no significant effect on OE21 cell proliferation

The effect of conditioned medium collected from DAC treated myofibroblasts (CM_{DAC}) on OE21 proliferation was not significantly different from that of conditioned medium from untreated cells (CM_{CTL}) (figure 20). In co-culture experiments, the ratio of NTM to OE21 cells affected the proliferation rate of the latter: OE21 proliferation was lower when the ratio of NTM towards OE21 was 1:1 as compared to the condition in which OE21 cell outnumbered NTM by a ratio of 2:1 (figure 21). When NTMs were pre-treated with DAC the proliferation rate of co-cultured OE21 cells was slightly decreased (mean proliferation 30.5 % vs. 32.3 %) and (24.5 % vs. 28 %). However, the differences in OE21 proliferation did not reach statistical significance (p=0.61

and *p*=0.24 respectively); the proliferation in myofibroblasts was not affected by the ratio of OE21 cells and NTMs (not shown).

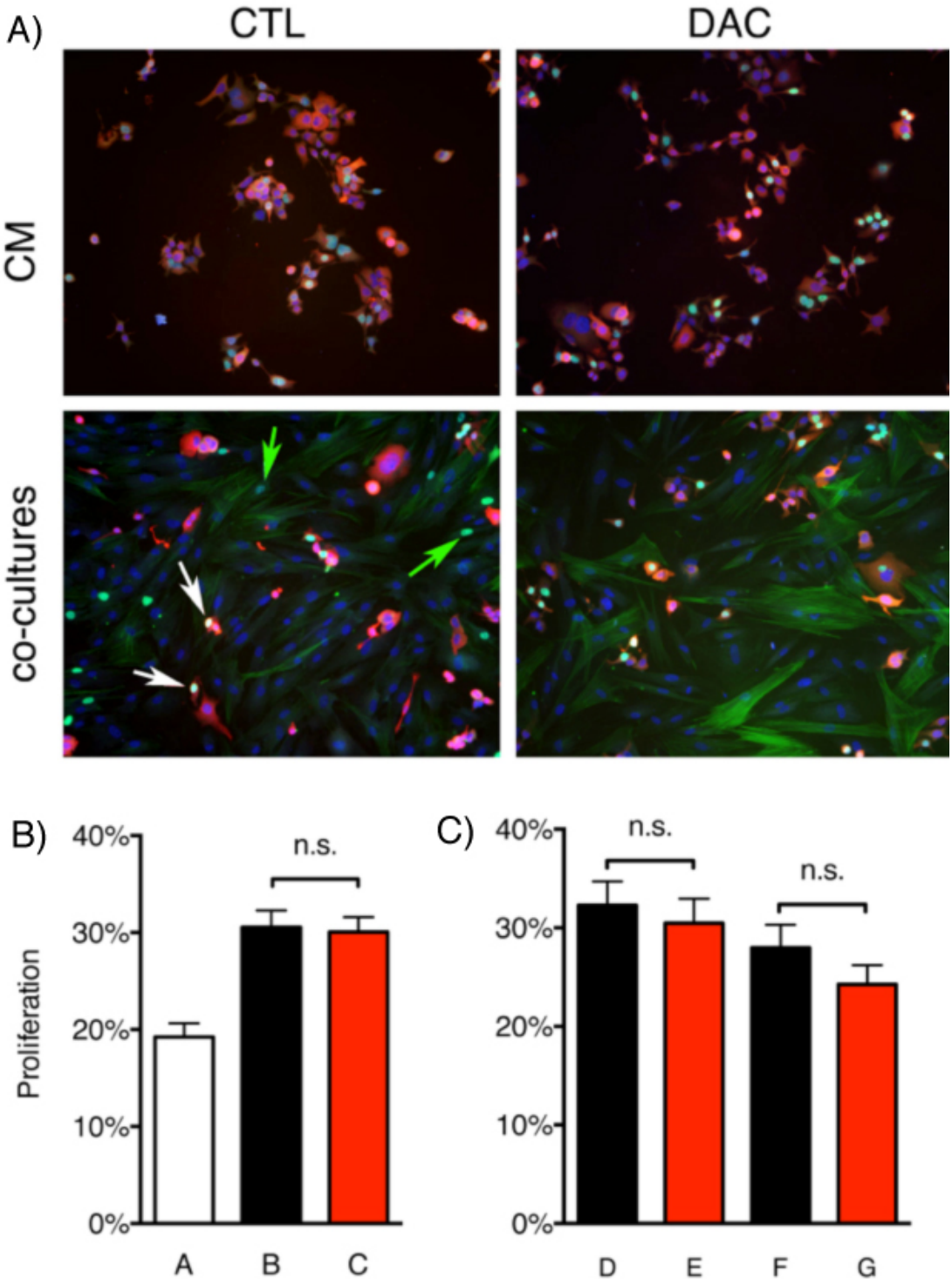

Figure 20: Effect of DAC treated NTMs on OE21 cell proliferation (conditioned medium and co-cultures. A) representative photomicrographs (100x) of pan cytokeratin (red), alpha-SMA (green) and nuclei with EdU incorporation (green). Top row: OE21 cells incubated 24h in conditioned medium (CM) from DAC pre-treated NTM and untreated NTMs (CTL), in

serum free medium. Lower row depicts co-cultures of OE21 cancer cells and either DAC pre-treated NTMs (left) or untreated NTMs (white arrows indicate proliferating OE21 cells, green arrows proliferating NTMs). B): A-C: OE21 cell proliferation after 24h incubation in CM of A, serum free medium; B, NTM CM; and C, DAC treated NTM (NTM_{DAC}). C) D: 1:2 ratio of NTMs co-cultured with OE21 cells; E: 1:2 ratio of NTM_{DAC} co-cultured with OE21 cells; F, 1:1 ratio of NTMs co-cultured with OE21 cells; G, 1:1 ratio of NTM_{DAC} co-cultured with OE21 cells. No statistically significant difference between mock treated and DAC treated groups.

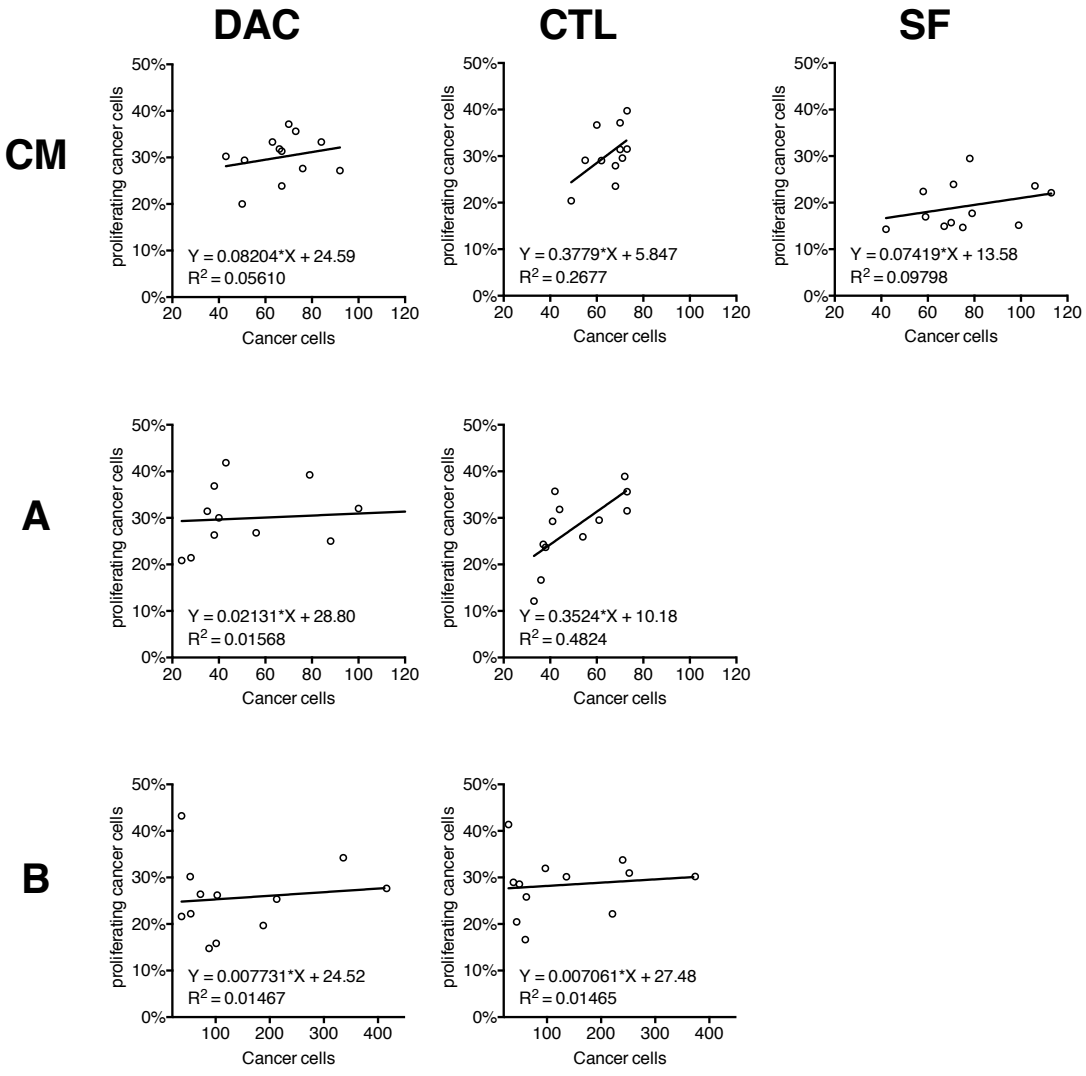

Figure 21: DAC treated myofibroblasts and their conditioned media decrease OE21 cell proliferation. Relationship between OE21 cells per field (X-axis) and percentage of proliferating OE21 cells per field (Y-axis). Top row: 50,000 OE21 cancer cells exposed 24h to conditioned medium from DAC treated, control treated and serum-free medium. Row A) ratio of plated NTM to OE21 cells 1:2; row B) ratio of plated NTM to OE21 cells 1:1

7.3.8 Conditioned media from DAC treated myofibroblasts accelerate OE21 migration

Conditioned medium harvested from DAC treated myofibroblasts increased OE21 migration in a transwell migration assay (figure 21).

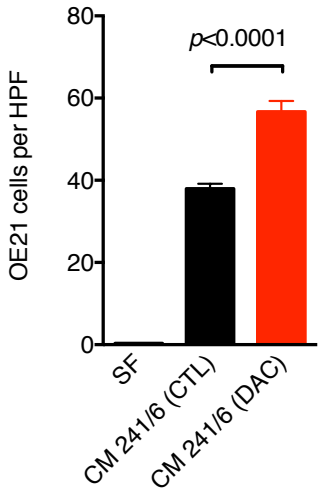

Figure 21: Conditioned media from DAC treated myofibroblasts increases OE21 cell migration. Assessment of OE21 cancer cell migration towards conditioned medium from vehicle (black) or DAC (red) treated NTM. Statistical significance in t-test, $p<0.0001$.

7.3.9 DAC treated myofibroblasts accelerate OE21 invasion in a 3D assay.

DAC treated myofibroblasts embedded in matrigel promoted OE21 invasion (figure 22).

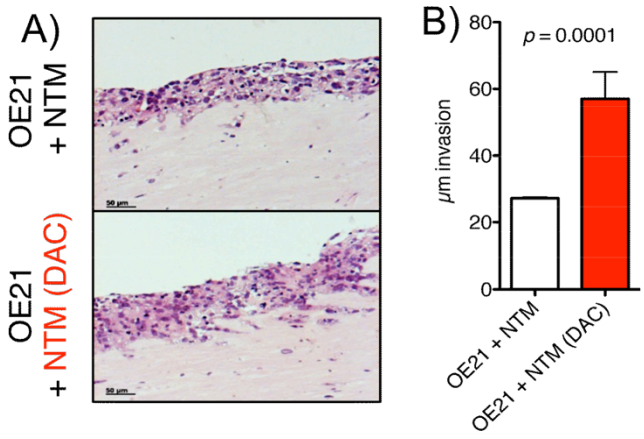

Figure 22: DAC treated myofibroblasts accelerate OE21 invasion in a 3D assay. Invasion of OE21 cancer cells into underlying matrigel containing untreated myofibroblasts (OE21 + NTM) and DAC treated myofibroblasts (OE21 + NTM (DAC)). A) representative photomicrographs, B) average depth of invasion on the right +/- SEM, p=0.009 (student t-test).

7.3.10 Influence of DAC treated myofibroblasts on xenograft tumour growth

In mouse xenografts, DAC treated myofibroblasts injected together with OE21 cancer cells significantly accelerated tumour growth (figure 23). Histologically there was no gross difference between end stage tumours of xenografts containing DAC- or sham-treated myofibroblasts.

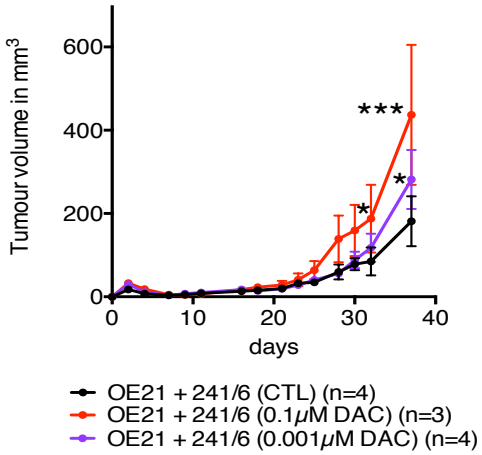

Figure 23: DAC treated myofibroblasts stimulate tumour growth in an oesophageal cancer xenograft model. Statistical significance for increased tumour size at day 32 p=0.045 and p<0.0001 at day 37 for xenografts with myofibroblasts treated with 0.1μM DAC and p=0.0008 at day 37 for myofibroblasts treated with 0.001μM DAC. Statistical significance in 2-way ANOVA.

7.4 Discussion

Altered global DNA methylation is a key feature of malignant cells. In particular, methylation of gene promoters regulates transcription (200). In malignant tumours altered gene promoter methylation is frequently observed in tumour suppressor genes such as PTEN (201), MLH1 in colorectal (202) and endometrial cancer (203, 204) and CDKN2/p16^{INKa4} in various tumours but also in Barrett's oesophagus (205). For many tumours it is known that altered gene expression due to promoter methylation is of predictive value (as for example MGMT in glioblastoma multiforme, MLH1 in colorectal and gastric cancer (206, 207)). *In vitro* and *in vivo* modification of promoter methylation in cancer cells has been targeted in order to reactivate epigenetically silenced tumour suppressor genes (208). Furthermore cancer cells typically show a decrease in their global DNA methylation (209) and in repetitive elements such as LINE1 and Alu (106).

Different global DNA methylation levels between normal stroma and tumour adjacent stroma has been described for cancers of the stomach (109), non-small cell lung cancer (108) and ductal adenocarcinoma of the pancreas (210). Whether DNA methylation differs between CAMs and ATMs in oesophageal tumours and the biological impact of chemically altered DNA methylation in oesophageal myofibroblasts has, to our knowledge, not yet been addressed. Indeed, in general little is known of the functional significance of epigenetic modification of stromal cells.

We first assessed global DNA methylation in oesophageal myofibroblasts by analysing the DNA methylation of LINE1 elements. We found that CAMs show a relative global hypomethylation in comparison to ATMs. These findings stand in accordance with other data published by Jiang et al (109) on global DNA methylation of tumour associated myofibroblasts of the upper gastrointestinal tract. They showed in their work using a methylation-sensitive single nucleotide polymorphism array (MSNP), [3H]dCTP incorporation assay and an antibody approach that DNA methylation in gastric cancer myofibroblasts was decreased as compared to their tumour adjacent

counterpart. Jiang and his colleagues also observed a decrease of DNA methylation in precancerous/dysplastic epithelia and tumours of a transgenic gastric cancer-developing mouse model.

In order to mimic a hypomethylated state in myofibroblasts we successfully established a model for a reduced global DNA methylation in NTM with the use of the demethylating chemotherapeutic DAC, as successfully shown by others in fibroblasts and cancer cells (113). In previous studies, global DNA methylation in myofibroblasts had not been assessed on the basis of LINE1 element methylation. Nevertheless, our results overlap with data obtained from HPLC analysis (113). Liang et al also observed in an expression array approach, that cells treated with a DNMT inhibitor exhibited persistently altered gene expression. This phenomenon was more prominent in cancer cell than in non-malignant stromal cells. I demonstrate here that myofibroblasts treated with DAC show an immediate but also long-term response, i.e. decreased proliferation, increased migration in two *in vitro* models (Boyden chamber assay and ibidi® chamber system), increased contractibility (gel contraction assay) and an accelerated tumour growth *in vivo*.

At this stage, the aim of our study was not to investigate the molecular mechanisms responsible for the biological effects of altered methylation, but rather to assess whether functionally relevant epigenetic modification per se can be achieved in stromal cells. In a second step we wanted to evaluate whether the modified myofibroblasts could then be used as a model for epigenetic modification in vitro. The persistence of altered migration, contractility, proliferation and interaction with cancer cells upon treatment suggest that these changes are not cytotoxic effects of DAC but rather the result of altered DNA methylation which is passed onto daughter cells. We cannot, however, exclude the possibility that a portion of the cells exposed to DAC acquired germ line mutations or entered senescence. Nevertheless, the observed biological effects are best explained as consequence of loss of promoter methylation under the DAC treatment.

In order to elicit the most effective concentration of DAC for our purpose, i.e. altered DNA methylation and persistent viability of the cells, we performed dose response experiments for DNA methylation and proliferation. From data gained in studies on immortalised fibroblasts we knew, that DAC transiently reduces proliferation which recovers, but persistently modifies cell fate leading to a reduction of the cell doubling number (211).

We have shown that conditioned medium from cancer cells increased myofibroblast migration in a transwell migration assay. This finding stands in agreement with a report that conditioned media from OESCC cells induced αSMA expression in fibroblasts (170). We did not assess whether αSMA expression was increased in NTMs exposed to CM from cancer cells, but the increased migration can be regarded the result of increased expression of proteins of the contractile apparatus.

We were able to confirm that conditioned medium from cancer cells increased stromal cell (in our case myofibroblasts) proliferation. This phenomenon was consistent for OE21 squamous cell carcinoma and the OE33 Barrett's carcinoma cell lines. This mitogenic effect of cancer cell conditioned medium was reduced when NTMs were treated beforehand with a DAC. This is an interesting finding, since we observed that the potential to increase proliferation in CAMs was markedly reduced upon cancer conditioned medium exposure as compared to matched ATMs. This further outlines the difference between CAMs and ATMs and shows that DAC treatment shifts NTMs closer to a CAM phenotype. Our findings are also comparable to the observation on altered behaviour of normal transformed keratinocytes and HaCaT cells which show increased proliferation and migration in scratch wound assay after exposure to conditioned medium from "nemotic" myofibroblasts (212-214).

The tumour promoting ability of stromal cells is thought to be mediated via angiogenic, anti-apoptotic, immunosuppressive effects as well as extra cellular matrix production. Whereas various chemotherapeutic approaches interfering with angiogenesis and immune response are currently in use, a

validated therapy against the tumourigenic effects of stromal cells is still lacking. The tumour stroma not only promotes tumour growth, but is also believed to prevent chemotherapeutic agents reaching their targets. The so called desmoplastic stromal reaction, a reactive hyperplasia of stromal cells to cancer cell stimulus is observed in various cancers and is particularly prominent in pancreatic ductal adenocarcinoma (PDAC)(215). In a model of a stroma-rich PDAC DAC treatment of myofibroblasts prior to co-injection with cancer cells into nude mice delayed tumour progression (210). Our data on the effect of DAC treated myofibroblasts in mice point in the opposite direction to the data of Shakya et al. Thus, in our hands DAC treated NTMs accelerated OE21 tumour growth while Shakya et al observed that pretreatment of murine PDCA derived CAFs reduced tumour growth. Interestingly, they reported persistent proliferation of CAFs at treatment doses of 2 μM DAC, whereas we observed that proliferation of myofibroblasts was suppressed at a dose of 0.1 μM DAC. This comparison has to be carried out with caution, since Shakya investigated murine CAFs derived from cancer producing transgenic mice in severe combined immunodeficiency (SCID) recipient mice whereas we used primary human myofibroblasts and oesophageal cancer cell lines in BALB/c nude mice.

Our observation is that treatment of myofibroblasts with DAC *in vitro* persistently decreases proliferation comparable to “nemotic” myofibroblasts. The DAC induced CAM-like phenotype with a stimulating effect on migration and proliferation in cancer cells *in vitro* and the accelerated tumour growth *in vivo* indicates that epigenetic modulation of stromal cells may have an unexpected adverse effect on tumour outcome. The use of deacetylating drugs may contribute to the development synchronous and metachronous tumours. To date there are no data available on long term effects of demethylating agents in respect to secondary tumours.

Conclusion

- Oesophageal CAMs are relatively hypomethylated compared to matched ATMs

- DAC induces a transient hypomethylation in NTMs and persistent biological effects.
- DAC treatment of myofibroblasts can be used as a model for epigenetic cell modification
- DAC treated myofibroblasts accelerate the growth of subcutaneous xenografts.

8 Myofibroblasts promote tumour growth of oesophageal squamous cell and adenocarcinoma in xenografts

8.1 Introduction

Tumour stroma cells can be isolated by outgrowth methods in a form that is suitable for in vitro culture (216, 217). Importantly, cancer associated stromal cells have been reported to play an important role in the maintenance of a provisional tumour stroma (218). However, a comprehensive understanding of tumour biology also depends on the ability to study the interactions between the different cellular components. Various *in vitro* and *in vivo* models exist in order to address these questions and more elaborate models continue to be developed. Murine xenograft models have been employed since the late 1960s (183) and are still widely used. It has been noted that when human stromal cells are injected together with cancer cells into recipient mice the stromal cells disappear (219). Even so, little is known of the fate of these cells and their role at early time points in xenografts.

Data generated in our group show that myofibroblasts derived from gastric tumours promote tumour growth when injected together with MKN45 gastric cancer cells in immune compromised nude mice (97). Kandola also observed a tumour growth inhibitor effect of myofibroblasts on distant MKN45 reporter tumours (97). Myofibroblasts isolated from the tumour bulk have been shown to exert a stronger tumour growth promoting effect than matched

myofibroblasts isolated from adjacent tissue. Moreover, in Barrett's adenocarcinomas CAFs have been associated with adverse outcome (84).

Myofibroblasts promote cancer growth in vitro mimicking early tumour growth, but their role in early in-vivo models remains relatively unexplored. In order to address this question we established xenograft models for oesophageal cancer growth using an oesophageal squamous cell carcinoma cell line (OE21) and a Barrett's adenocarcinoma cell line (OE33) (164) in combination with primary oesophageal myofibroblast lines, i.e. NTM, CAM and ATM generated and previously characterised by the group (table 3 & 4).

In addition, we examined the possible role of gastrin in oesophageal adenocarcinoma xenografts. It had previously been shown that gastrin has complex actions both accelerating and inhibiting tumour cell growth in gastric adenocarcinoma cells expressing the cholecystokinin receptor (CCK) 2 (AGS-GR) (184, 220) via ERK signalling (221). Kumar et al have shown that gastrin stimulates migration of AGS-GR cells in a MMP1 dependent manner (169, 170). It remains unclear whether hypergastrinaemia accelerates tumour growth in vivo through CCK-2 receptor signalling pathway. We investigated whether CCK-2 receptor expression in a Barrett's carcinoma cell line would also accelerate tumour growth and whether the latter was influenced by myofibroblasts with the use of the established xenograft models.

8.2 Objectives

The specific objectives were:

- To establish mouse xenograft models in order to study the role of primary human oesophageal myofibroblasts on tumour growth.
- To investigate the role and fate of primary human myofibroblasts in xenografts.
- To study whether human myofibroblasts have a systemic effect on cancer growth.
- To determine whether hypergastrinaemia accelerates tumour growth in a Barrett's carcinoma cell line expressing the CCK-2 receptor.

8.3 Material and Methods

For these experiments we used an established oesophageal squamous cell carcinoma cell line (OE21) and a Barrett's adenocarcinoma cell line (OE33) (164) in combination with primary myofibroblast lines generated by the group in collaboration with the University of Szeget. The NTM line 241/6, which in our hands is typical NTM line, was also used. For CAMs, we used line 373/1 and 467/1 which have been shown in previous work of the group (87, 95) to be a phenotypically typical CAMs and different from their matched ATMs.

Single cell suspensions (cancer cells alone or in combination with myofibroblasts) were injected into nude mice. Tumour volumes were assessed on a regular basis and animals sacrificed at defined time points for histology as described (5.4.2).

Fluorescence *in situ* hybridisation against human centromeres and immune fluorescence histology were performed on snap frozen tissue (5.4.4).

Systemic hypergastrinaemia in mice was induced with omeprazole (5.4.3).

8.4 Results

8.4.1 Establishment of a mouse model for oesophageal Barrett's carcinoma in combination with primary human myofibroblasts

Initially I established the lowest number of cancer cells needed to form tumours in nude mice. Groups of nude mice (n = 3) were injected with $0.3x10^6$, $0.6x10^6$ and $1.2x10^6$ OE33 cancer cells alone or in combination with $3x10^5$ normal tissue myofibroblasts (NTM line 241/6). In the $0.3x10^6$ group (figure 24 A) one animal in the OE33 alone and two in the combined OE33/NTM group started to grow tumours with a latency of 45 days. In the $0.6x10^6$ OE33 cell group (figure 24 B) all animals receiving NTMs developed prominent initial tumours significantly discriminating them from the OE33 cell only group. The tumour size difference peaked after 2 days ($p<0.0005$) of injection and slowly diminished over the following three weeks. Only one tumour in the combined group started to grow after 65 days, reaching $80mm^3$ after 74 days. In the $1.2x10^6$ OE33 cancer cell group (figure 24 C) again, all NTM containing

xenografts developed initial tumours significantly larger (p<0.005 at day 2) than their OE33 cancer cell alone counterparts. In both groups tumours started to grow after 42 days. Histologically there was no gross difference between the end stage xenografts (figure 24 D).

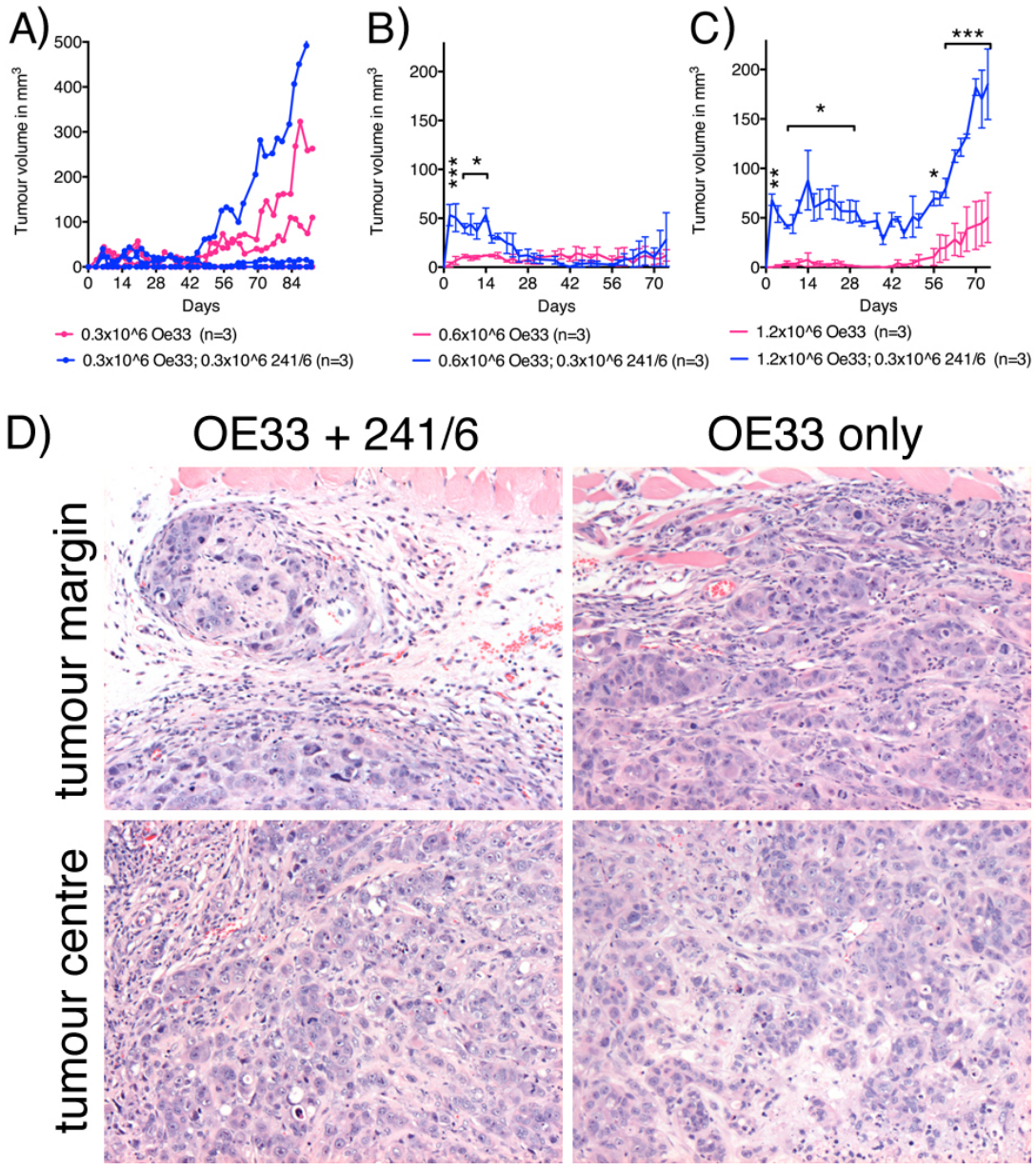

Figure 24: Optimisation of Barrett's cell carcinoma cell line (OE33) xenografts in nude mice. A) xenograft tumour volumes of individual mice injected with 0.3x10^6 OE33 alone (pink) or co-injected with 0.3x10^6 NTMs (241/6: blue). B) 0.6x10^6 OE33 alone (pink) and co-injected with 0.3x10^6 NTMs (blue). C) 1.2x10^6 OE33 alone (pink) and co-injected with 0.3x10^6 NTMs (blue). Statistical significance *: p<0.05, **: p<0.005, ***: p<0.0001, repeated measure two-way ANOVA). D) No gross histological difference between tumours consisting of injected myofibroblasts and cancer cells.

8.4.2 Investigation of the early tumour formation in xenografts consisting of OE33 cancer cells and myofibroblasts

In order to address the observation of an early tumour formation in mice when NTMs were co-injected with tumour cells, I injected 3 groups of mice (n = 4 per group) with $6x10^5$ OE33 cells alone, $3x10^5$ NTM (241/6) alone or $6x10^5$ OE33 combined with $3x10^5$ NTM (figure 25). There was a significantly increased tumour formation when NTM were injected together with OE33 cells ($p<0.0005$) on day 1 and day 2 after injection. A similar effect was observed when I injected NTMs alone 1 day after injection ($p<0.05$) on day 1 after injection. Animals were sacrificed after two days and the tumours histologically examined. In the OE33 alone group the cancer cells were dispersed as small groups of cells in oedematous and serous empty spaces, whereas in the combined OE33/NTM group the cancer cells were found surrounded by myofibroblasts and the latter seemed firmly attached to the adjacent murine host tissue (figure 25 B and D). When NTMs were injected alone, an early tumour formation was observed and the injected myofibroblasts were identifiable on H&E stained slides (figure 25 A and F, 26 G). After 28 days these early tumours in NTM-only grafted mice macroscopically disappeared (figure 26 G) and were also not detectable on serial 50μm sections of subcutaneous tissue from the injection site.

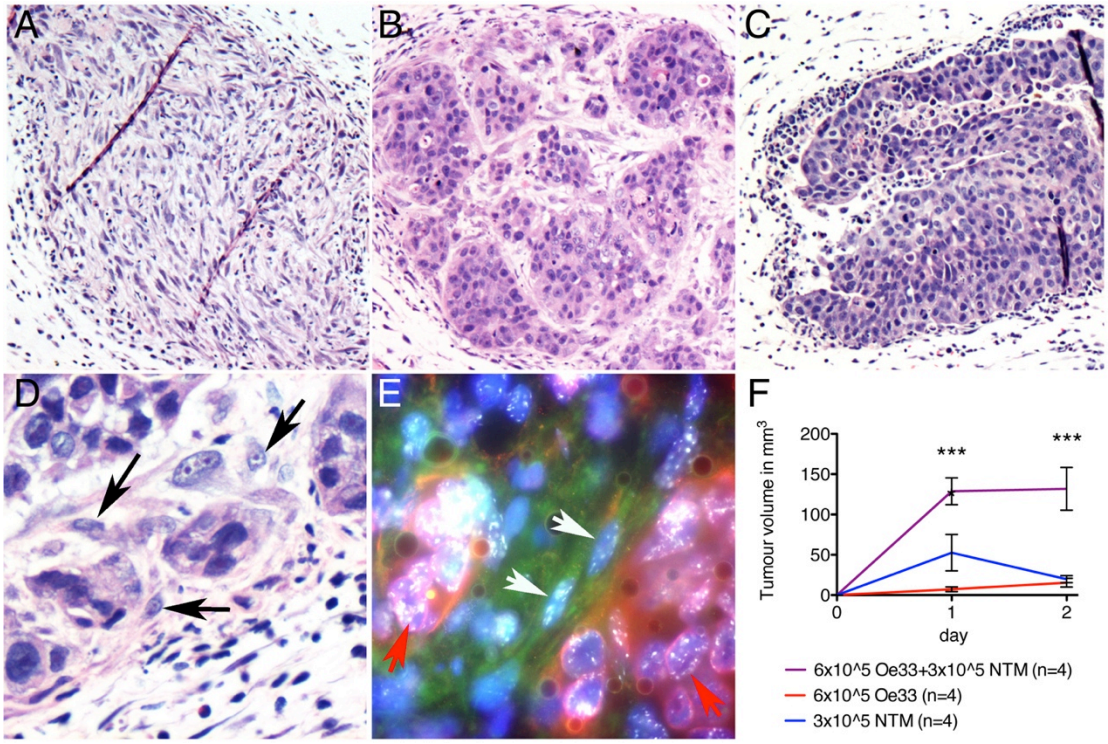

Figure 25. Myofibroblasts induce early stroma-type reaction in OE33 cell xenografts by generating a niche for cancer cells. Day two xenografts of A) NTMs, B) OE33 cells combined with NTMs and C) OE33 cells alone (100x magnification;. 400x magnification of combined OE33 and NTM day two xenografts); D) haematoxylin and eosin stain, black arrows indicate NTMs; E) immune FISH (anti pan-cytokeratin: red; anti-vimentin: green; pan-human centromere: white), red arrow head indicates OE33 cells, white arrow heads NTMs. F) Xenograft median tumour volumes; $6x10^5$ OE33+$3x10^5$ NTMs vs $6x10^5$ OE33 p=0.0005; $6x10^5$ OE33+$3x10^5$ NTMs vs $3x10^5$ NTMs p=0.0036; $6x10^5$ OE33 vs $3x10^5$ NTMs p=0.075 (repeated measure two way ANOVA)(* p<0.05, * p<0.001; Bonoferri post test vs OE33 alone)

8.4.3 Establishment of a mouse model for oesophageal squamous cell cancer with primary human myofibroblasts

In the case of OE21 cells, I again established the lowest number of cancer cells needed to be injected in order to grow tumours in nude mice using 10^5, $3x10^5$ and 10^6 OE21 cancer cells alone or in combination with $3x10^5$ normal tissue myofibroblasts in nude mice (n = 3 per group) (figure 26 A, B, C). In the $1x10^5$ group only one mouse grew a tumour. When $3x10^5$ OE21 cells were injected, all animals grew tumours and tumour growth was significantly accelerated when NTMs were co-injected with the cancer cells (figure 26 B &

D). This growth advantage disappeared when $6x10^5$ or more OE21 were injected (figure 26 C, E, F) even when the ratio of OE21 to cancer cells was kept constant (figure 26 E, F). When myofibroblasts alone were injected only a small tumour formation was observed soon after injection (figure 26 G). The initial tumour appeared in all groups in which myofibroblasts were injected but was present to a lesser extent when OE21 cells alone were injected. Tumour growth in the NTM containing xenografts was also increased when $5x10^5$ NTM were injected together with 10^6 OE21 cancer cells (figure 26 H). $5x10^5$ CAMs 373/1 had a stronger tumour promoting effect than when the same number of ATMs 373/2 were injected together with 10^6 OE21 cancer cells (figure 26 I).

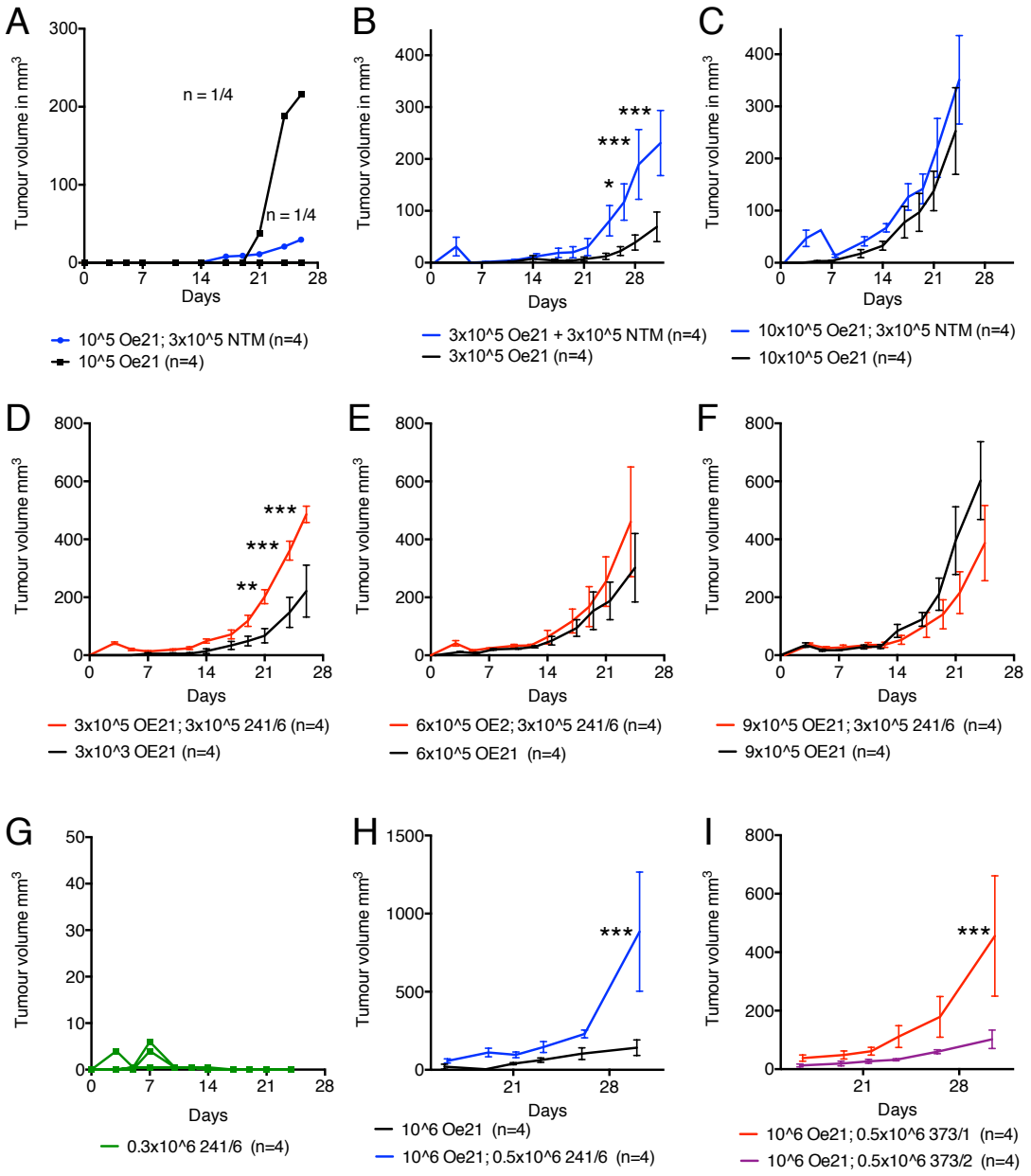

Figure 26. Optimisation of OE21 cancer cell number for xenografts. Xenograft tumour volumes; upper row optimisation of OE21 cancer cells; A) 10^5 OE21 with or without $3x10^5$ NTMs, individual tumours, B) $3x10^5$ OE21 with or without $3x10^5$ NTMs, mean +/- SEM; p=0.062, and C) $10x10^5$ OE21 with or without $3x10^5$ NTMs, mean +/- SEM. D) $3x10^5$ OE21 with or without $3x10^5$ NTMs; p=0.0088; E) $6x10^5$ OE21 with or without $3x10^5$ NTMs, mean +/- SEM and F) $9x10^5$ OE21 with or without $3x10^5$ NTMs, mean +/- SEM, G) $3x10^5$ NTMs alone, individual animals. H) tumour volumes of OE21 cancer cells alone (black) and co-injected with NTMs (241/6) (red), $p = 0.0043$; I), OE21 cells co-injected with CAMs (373/1; red) and ATMs (373/2; purple) and OE21 cells co-injected with ATMs (blue). $p < 0.001$; two-way ANOVA. Statistics: repeated measure two-way ANOVA. *: p <0.05; ***: p <0.001.

Histologically there was no gross difference between the two xenograft groups when tumours reached maximal, ethically-approved, size (figure 27). In both groups pushing border but also infiltrating tumour borders were observed together with peri-tumoural fibrosis and mild chronic inflammatory infiltrate.

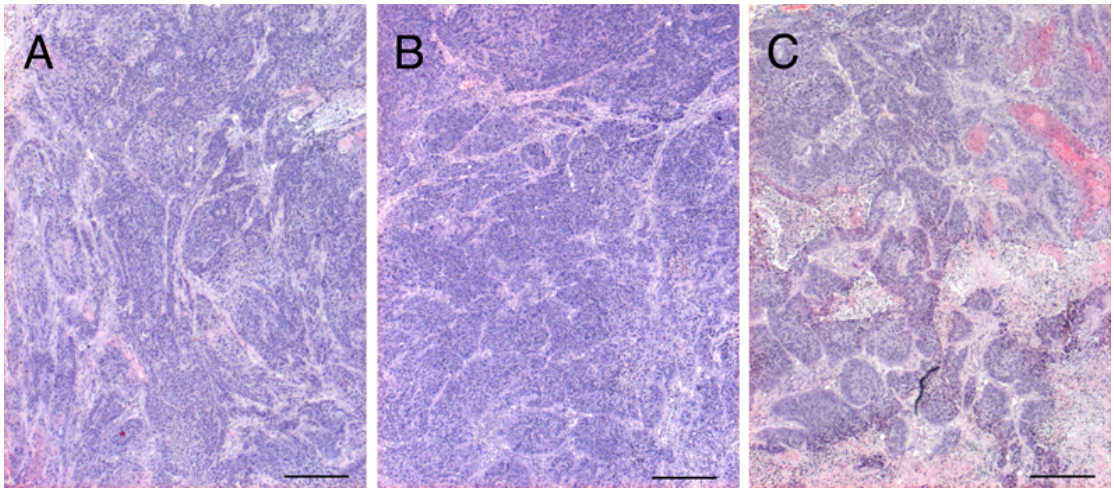

Figure 27 A): Representative photomicrographs of end stage tumours of xenografts. Xenografts consistent of A) OE21 + 373/1 (CAMs), B) OE21 + 373/2 (ATMs) and C) OE21 alone; scale bar 500 μm.

8.4.4 The role of co-injection of myofibroblasts in early xenografts

The phenomenon of early tumour formation and the fate of myofibroblasts was then examined in a time course experiment in which those animals with the largest tumours on days 2, 7 and 28 were sacrificed for histology (figure 28). The groups consisted of OE21 cells alone (figure 28 A), OE21 cells together with CAMs (373/1) (figure 28 B), OE21 together with NTMs (241/6) (figure 28 C) and OE21 cells together with PKH26 labelled NTMs (figure 28 D). The average tumour diameters in the groups containing CAM or NTM were significantly larger at day 2, 7 and 28 compared to the OE21 cancer cell alone group.

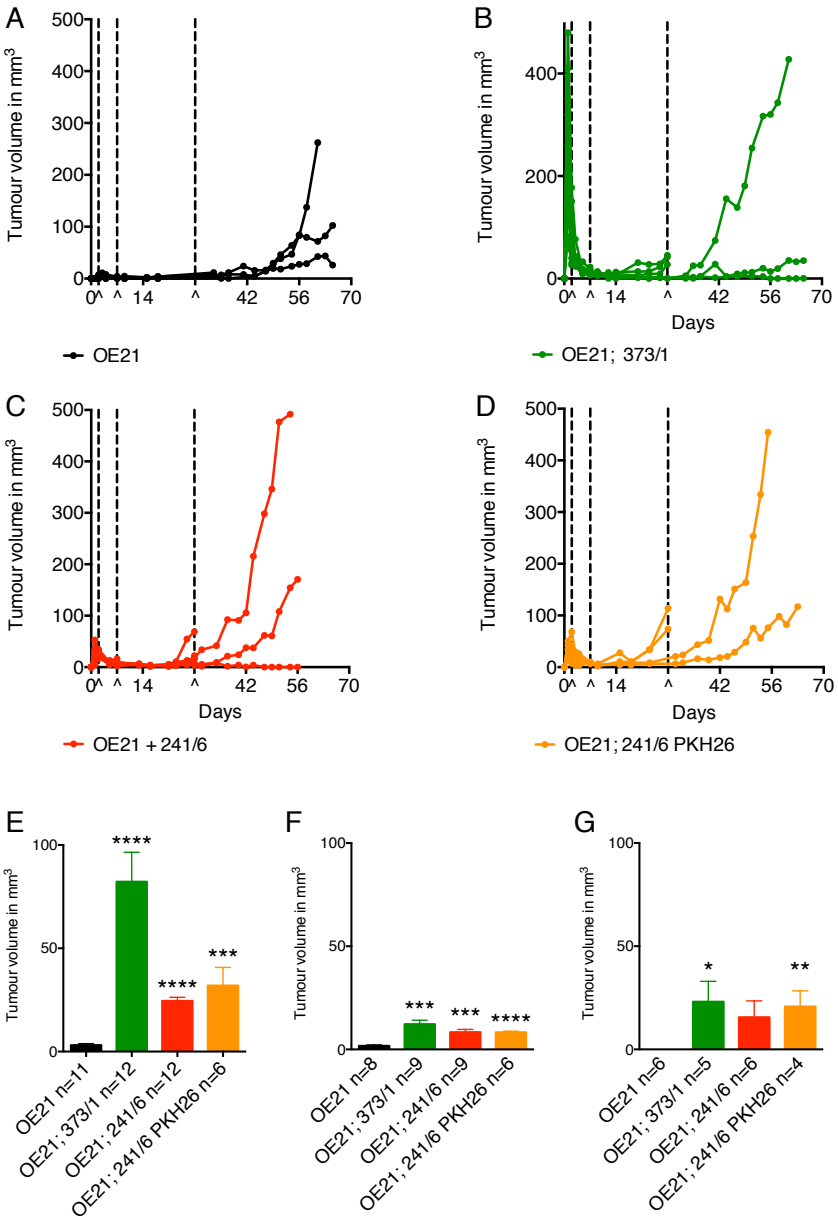

Figure 28: Time course of individual oesophageal squamous cell carcinoma xenograft growth. A - D) xenograft volumes after injection. Interceptions indicate time points when the animals with the largest tumours in each group were taken for analysis (day 2, 7 and 28). A) $3x10^5$ OE21 cells alone or co-injected with $3x10^5$ myofibroblasts: 373/1 CAMs in B), 241/6 NTMs in C) and PKH26 labelled 241/6 NTMs in D). Statistically significant difference in tumour size at day 2 (E), 7 (F) and 28 (G) after xenografting in t-test. * for $p<0.05$, ** for $p<0.01$, *** for $p<0.001$ and **** for $p<0.0001$.

Two days after injection tumours showed a significantly increased inflammatory component, a prominent nesting pattern and the presence of

myofibroblastic cells in mixed OE21 + CAM or NTM tumours. The extent of necrosis at day two was more prominent in the OE21 + CAM group. Day seven tumours showed an increased inflammation, more prominent necrosis and persistence of myofibroblastic cells in the OE21 + CAM group. Keratinisation of cancer cells was more prominent in the OE21 + NTM group. The variance between tumours of independent xenograft experiments (28 days and 2 month tumours) was little (figure 29).

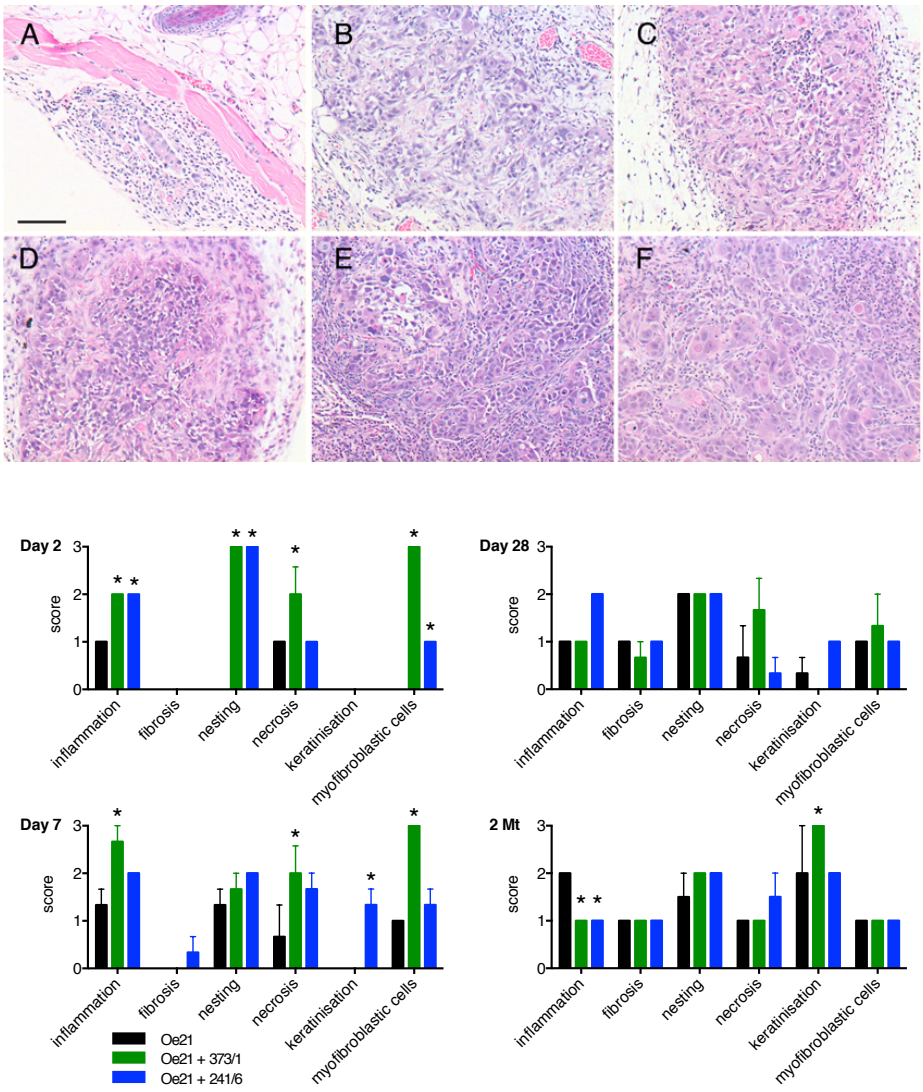

Figure 29: Histology of early xenografts. Upper panel: representative photomicrographs of tumours at day 2 (A-C) and 7 days (E-F) after xenograft injection. A & D OE21 cells alone, B & E OE21 cells + CAMs, C & F OE21 cells + NTMs. Scale bar 200 μm. Lower panel semi quantitative histological scoring of tumours after 2, 7, 28 days and 2 month for inflammation, peritumoral fibrosis, nesting, necrosis, keratinisation and presence of cells

with activated myofibroblastic features. Statistical significance in two-way ANOVA $p<0.05$ marked with asterisk.

8.4.5 Fate of co-injected myofibroblasts in oesophageal OE21 and OE33 xenografts

In order to study the fate of myofibroblasts injected into xenografts we labelled NTMs prior to injection with PKH26 a membrane-integrating dye. Already seven days after injection the dye was detectable in cells other than myofibroblasts (figure 30). The fluorescence intensity of the dye breached through different filters and diagnostic IF could not be produced. At late tumour stages, fluorescence was only detected focally in stromal cells and macrophages in the tumour bulk, predominantly in the peri-tumoural fibrotic tissue.

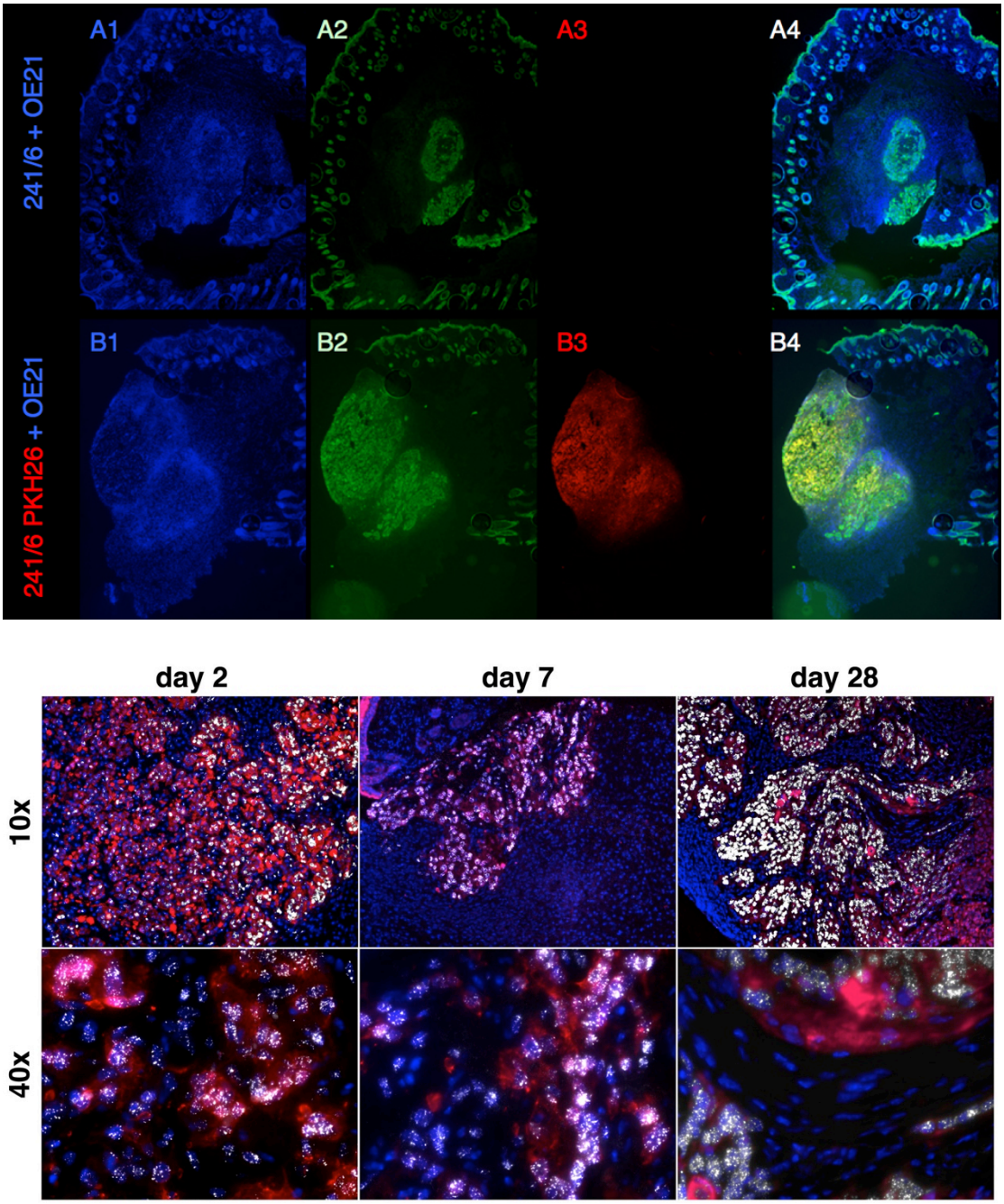

Figure 30: fluorescent microscopy pictures of xenografts. Upper panel representative image of PKH-labelled tumours at day 7. Photomicrographs of mixed myofibroblasts/OE21 cancer cells 7 days after injection. The tumour depicted in the upper row (A) contains unlabelled myofibroblasts, whereas the tumour in the lower row (B) contains PKH26 labelled myofibroblasts. 1: nuclear stain with DAPI, 2: Pan cytokeratin (FITC), 3: PKH26 (red spectrum filter). **Lower panel I-FISH of xenografts**: human myofibroblasts disappear in xenografts between 1 week and 4 weeks after injection. I-FISH of xenografts consisting of myfibroblasts and OE21 cancer cells. Upper row, low power magnification; lower row, high power magnification of combined xenografts 2, 7 and 28 days after injection. Pseudo colours: pan-cytokeratin: red, DAPI: blue, human centromeres: white.

To further define cells of human origin in mice hosts, we employed FISH using a human pan-centromeric probe. The probe displayed 100 % positivity in human primary myofibroblasts and OE21 cancer cells. A positive signal was never detected in murine tissues. When human centromere FISH was performed on tumours derived from animals with PKH26 labelled myofibroblasts a nuclear localisation of the FISH signal was not detected in PKH26 positive stromal cells (n=3 mice; 28, 54 and 56 days after xenograft injection). Immunofluorescence plus *in situ* hybridisation (I-FISH)-labelled cancer cells were identifiable by their epithelial characteristic pan-cytokeratin immunoreactivity. I-FISH performed on early tumours (figure 30) consisting of OE21 or OE33 combined with myofibroblasts (day 2 and day 7) revealed FISH positive cells with nuclear features of myofibroblasts in between FISH and CK positive cancer cells (n=6). FISH positive nuclei in stromal cells of tumours aged 28d or older were never identified (n=14). Furthermore when I-FISH was performed combining pan-cytokeratin with an anti-murine centromere probe, all stromal cells but not the cytokeratin positive cells were FISH positive (figure not shown).

8.4.6 CAM cell line 467/1 accelerate distant tumour growth

In order to study whether myofibroblasts might exert a systemic effect on tumour growth, animals were injected on one side with cancer cells and myofibroblasts and on the other side with a “reporter” tumour consisting of cancer cells only. Tumour volumes were measured on both sides (figure 31). When CAMs (467/1) were injected together with OE21 in one flank, the contralateral OE21-only tumours showed a significantly increased tumour growth (C) as compared to tumours where no myofibroblasts were injected (B). When NTM_{DAC} (see figure 3) were injected together with OE21 cells no difference regarding contralateral tumour growth was observed as compared to OE21 only or OE21 injected together with untreated myofibroblasts (D, E).

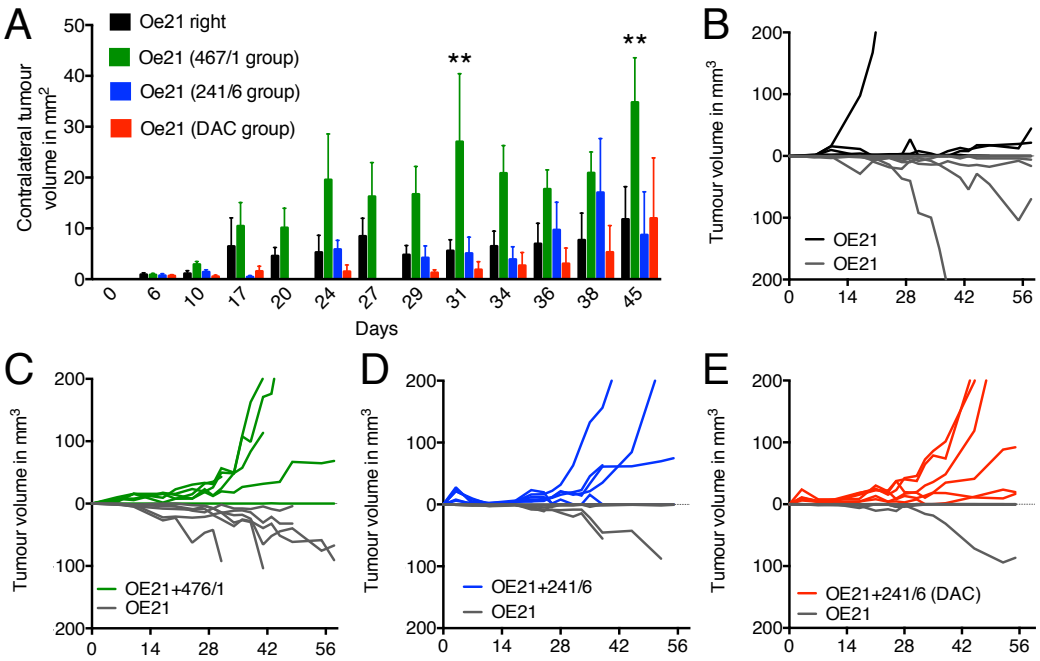

Figure 31: CAMs 467/1 systemically stimulates tumour growth. Animals (groups of six) were injected bilaterally with tumours consisting on one side of OE21 cells and myofibroblasts and on the contralateral side with OE21 cells only. Figure A depicts contralateral tumour growth. Statistical significance $p<0.001$. B-E individual bilateral tumour growth on the myofibroblast bearing side (in colours) upwards, for the indicator tumours (in gray) downwards.

8.4.7 Effect of gastrin on growth of Barrett's carcinoma xenografts

In order to study the influence of elevated systemic gastrin concentrations on Barrett's carcinoma growth we used a Barrett's carcinoma cell line (OE33) overexpressing CCK-2R (OE33-GR). Hypergastrinaemia was induced by treating mice with omeprazole (400 μmol.kg^{-1}), a proton pump inhibitor, three times per week, starting one week prior to xenograft injections. The experiment included four groups of six animals either bearing tumours consisting of OE33-GR only or OE33-GR and myofibroblasts with or without omeprazole induced hypergastrinaemia. On the first two days after injection there was a significant tumour size difference between myofibroblasts-containing tumours and cancer cell-only tumours ($p<0.001$). There was no difference between the omeprazole treated and the untreated group during the first few days. Accelerated tumour growth was observed in two animals on

omeprazole in which OE33-GR cells were injected together with myofibroblasts (figure 32). All other xenografts were stagnant or disappeared (2 omeprazole treated tumours) within 2.5 months. When comparing all omeprazole treated xenografts excluding the two animals with accelerated tumour growth to all tumours in the mock treated animals the mean tumour volume was significantly lower on days 3, 4, 20, 30, 39, 46 and 51-70 in the omeprazole group.

The thickness of gastric corpus mucosa was assessed in all animals at the end of the experiment. All animals treated with omeprazole showed gastric corpus mucosa hyperplasia, as expected, which was absent in untreated animals (figure 34).

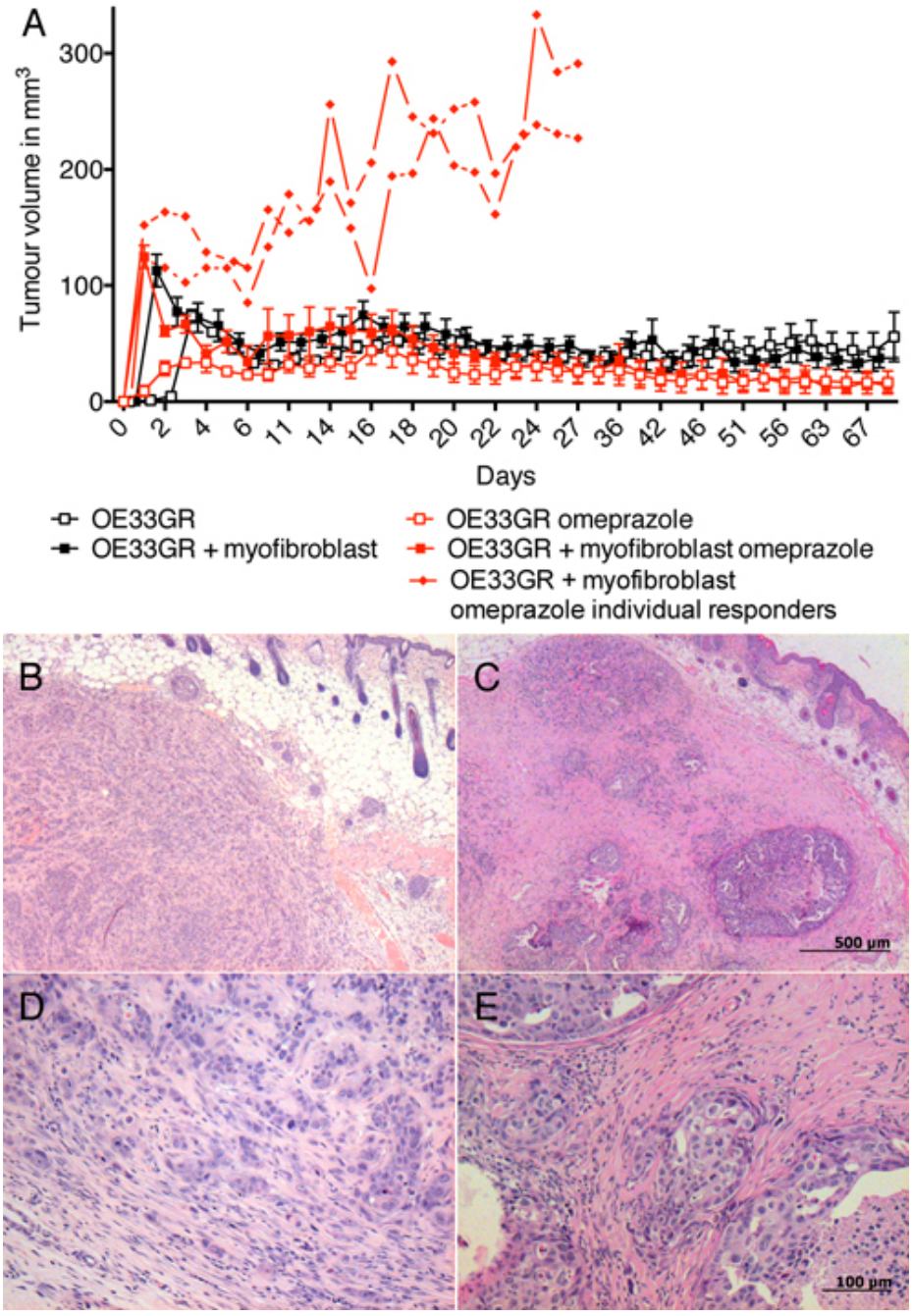

Figure 32. Effect of omeprazole-induced hypergastrinaemia on OE33-GR tumour growth. A) Mean (+/- SEM) of groups of OE33-GR cell-only tumours (empty squares), and when co-injected with myofibroblasts (filled squares). Animals (n = 6 per group) treated with omeprazole in red, sham treated in black. Two animals exhibited accelerated tumour growth ($0.6x10^6$ cancer cells with or without 241/6 NTMs $0.3x10^6$. B & D: representative photomicrographs of one of the fast growing tumours. C & E: representative photomicrographs of a control slow growing tumour.

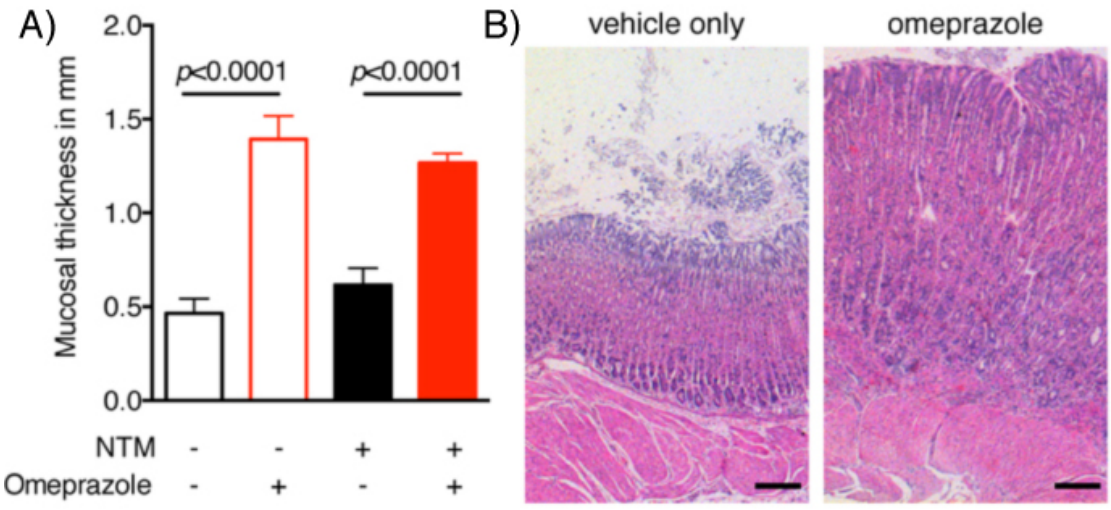

Figure 34: Omeprazole induces gastric mucosal hyperplasia in nude mice: Gastric mucosal thickness in nude mice (n = 6 per group) enrolled in the xenograft experiment with OE33-GR cells. A) mucosal thickness of omeprazole treated-mice shown in red bars and control animals in black bars. Statistical significance in t-test $p<0.0001$. B) representative photomicrographs of murine corpus mucosa of animals treated with omeprazole (right) and vehicle only (centre); scale bar = 200 μm.

8.5 Discussion

In this chapter I addressed the question of the role and fate of primary oesophageal myofibroblasts in xenografts and whether human myofibroblasts exert a systemic effect on tumour growth in xenografts. I therefore established a xenograft model with the use of primary human myofibroblasts and oesophageal cancer cell lines.

Oesophageal cancers are the fastest raising malignancies in industrialised countries and advanced tumours are still associated with high-risk surgery and poor survival rates. Myofibroblasts have been shown to play an important role in the tumour microenvironment. The effect of myofibroblasts on tumour growth per se in immunosuppressed mice has been investigated previously for various carcinomas (oral squamous cell carcinoma (222), pancreas (223), breast cancer (224), stomach (97)), but the role of primary human myofibroblasts has not yet been studied to our knowledge.

We observed rapid early tumour formation after injection of xenografts containing myofibroblasts. This early tumour formation was only very mildly established or absent when cancer cells were injected alone. The early tumour results from a predominantly pauci-cellular oedema.

Most studies document tumour measurements only 5 days after injection and seem to ignore early tumour formation. Very early tumour formation is likely to be an inflammatory process related, for example, to the release of histamine, cytokines and tumour necrosis factors. The main focus of the present study was on the role of the myofibroblasts within the first days when the injected cells are believed to integrate into the host tissue. The complement system has been reported to play an important role in stromal cell activation (225). Bulla et al. observed a C1 upregulation two days after xenograft injection in stromal cells. When we injected myofibroblasts together with cancer cells we observed a complex tumour network as can be seen at the invasion front of oesophageal carcinomas in patients. It appears that the myofibroblasts form a niche which enables the cancer cells to thrive. The observations in vivo mirror observations of mixed cell cultures where myofibroblasts stand in contact with cancer cells and migrate through the expanding cancer cells. Dvorak commented on the importance of fibrin deposition in the generation of a desmoplastic stromal reaction (226). The histological picture in day 2 mixed tumours differs significantly from animals where cancer cells alone were injected. In the latter cancer cell embedding in the host tissue was delayed by more than two days.

Additionally, xenografts which derive from combined myofibroblasts/cancer cell injections demonstrated an accelerated tumour growth. The grafting of CAMs, which can be regarded as activated myofibroblasts, accelerated tumour growth that was even more pronounced. Our findings are comparable to the results from Patel et al (227) on studies performed with primary squamous cell carcinomas of the skin. Patel et al. describe that for successful passaging of initial xenograft into a second recipient mouse, human stromal cells are required for successful xenograft formation.

Our studies on the fate of myofibroblasts co-injected together with OE21 and OE33 cancer cells into nude mice using fluorescently-labelled myofibroblasts and I-FISH revealed that all myofibroblasts primary cell lines tested disappear and are replaced by stromal cells of murine origin. Quante et al and Hutchinson et al have independently demonstrated that bone marrow derived stromal cells can migrate into tumours and differentiate into cancer associated myofibroblasts (66, 228). Morton et al. demonstrated in an elegant humanised mouse model how bone marrow derived human cells become part of the stromal tumour component in xenografted head and neck cancers (229). A similar result was also demonstrated by Terai and his colleagues who identified ‘‘fibrocytes’’ in xenografted MKN45 cancers to contribute to tumour growth and fibrosis. Terai et al also found that tumours where fibrocytes were injected together with the cancer cells demonstrated a more pronounced αSMA expression in the stromal cells (68). This underlines the findings of Kumar et al where he demonstrated that myofibroblasts attract bone marrow derived stromal cells via chemerin (95). We have observed the presence of murine stroma cells in xenografts where myofibroblasts were injected together with cancer cells. We did not address the question of the origin of the murine stromal cells. The majority of stromal cells derive from the surrounding tissue as demonstrated by Arina et al. (230).

Little is known about the fate of stromal cells in xenografts. Morton et al found persistence of human bone marrow derived stromal cells in his chimeric mouse model in late stage tumours (229). This contrasts with our finding where human myofibroblasts are not detectable in xenografts four weeks after injection. In the case of the humanised chimeric models the injection of progenitor stem cells provide an ‘unlimited’ source for cell renewal, whereas in our experimental setting where (presumably) terminally differentiated cells were injected the limiting factor could have resulted from apoptosis as observed in wound healing (231).

Our findings also stand in accordance with observations by Liu and Hornsby who injected stress (bleomycin) induced premature senescent fibroblasts

together with MDA231 breast cancer cells into immune compromised SCID mice (224). They observed a disappearance of the grafted stromal cells two weeks upon injection together with the tumour cells. In colorectal cancer xenografts grafted stromal vascular cells have been described to disappear after three weeks (232). Duda and his co-workers addressed the question about the fate of transplanted stromal cells with the use of tumour stroma derived from GFP transgenic mice. After passaging the fluorofor-expressing stromal cells into non-fluorescent mice predominantly vascular labelled cells were detectable one month after transplantation whereas myofibroblastic cells had disappeared (233).

Together the findings suggest that stromal cells play a pivotal role in the early embedding by niche formation in the xenograft setting. This might also explain why cancer cells are often difficult to grow whereas patient derived xenografts are very successfully transplantable and of great use for individualised anti cancer therapy (234). In PDX, human derived transplanted myofibroblasts persist in the transplanted tissue fragment and allow to gain deep insight on the cancer stroma interaction (235), however the stromal cells disappear after passaging (232).

Liu and Hornsby showed that myofibroblasts induce cancer cell proliferation as long as the ratio of stress-induced premature senescenced fibroblasts to cancer cells was above 1 (224). Moreover, results from our group have demonstrated that conditioned media from myofibroblasts increased cancer cell proliferation (170). In oesophageal cancers fibroblast derived Wnt2 has been shown to activate cancer cell proliferation (236).

Patients affected by cancer can demonstrate a variety of systemic manifestations anatomically distant from the primary tumour sites and malignancies can be regarded as a systemic diseases. Tumour cells can be detected in circulation as well as cellular particles such as extracellular vesicles, exosomes and microsomes and even free circulating nucleic acids (i.e. DNA and micro RNA) have been described. Little has been reported on

the role of the stromal cells on systemic effects. As mentioned above, CAMs secrete chemerin which can lead to homing of MSCs to the primary tumour site (95, 170). In xenograft experiments, CAMs injected together with MKN45 cells resulted in a suppressed growth of distant xenografts consisting of MKN45 cells only(97). In the present study, the injection of 467/1 CAMs together with OE21 cells led to an accelerated growth of contralateral OE21 only indicator tumours. The presence of CAMs therefore may be a reason why resection of the primary tumours in the metastatic setting can extend the overall survival rate (237). Pre-treatment of NTM line 241/6 with DAC as described in the previous chapter accelerated the growth of mixed tumours, but did not affect the growth of indicator tumours.

As part of the work on upper GI tumours we also asked whether the tumour stroma plays a role in gastrin-related Barrett's adenocarcinoma propagation. In the past gastrin signalling through the CCK2 receptor has been shown to exert stimulatory effects on tumour growth (238). We observed an accelerated tumour growth in 1/3 of cases when myofibroblasts were admixed to xenografts with Barrett's cancer cells expressing the CCK2 receptor (OE33GR) and these tumours were exposed to omeprazole-induced systemic hypergastrinaemia. The assessment of gastrin levels was attempted but failed for technical reasons. Gastric glandular hyperplasia which is a surrogate marker for trophic responses to prolonged hypergastrinaemia was documented in all omeprazole treated animals. The influence of gastrin on tumour development has been found to include inhibition of gastric carcinogenesis (239), while blockade of the CCK-2 receptors inhibited gastric carcinoid tumour development (240). We expected to observe an accelerated tumour growth in the omeprazole treated group in xenografts consisting of NTM+OE33-GR. Against our expectations only two animal in the NTM+OE33-GR group presented a rapid tumour growth. Omeprazole has been reported to inhibit tumour growth (241) and hypergastrinaemia itself has also been reported to decrease tumour growth (242). In all other grafted animals no substantial tumour growth was observed within three month. The low

penetrance of tumour growth in our hands might have been related to a relatively low number of cancer cells injected into these animals.

The rapid growing tumours in the omeprazole treated NTM+OE33-GR group showed centrally solid cancer cell growth with an infiltrating growth pattern in the tumour periphery. This is in contrast to the other tumours in this experiment where a prominent intra- and peri-tumoural fibrosis was evident. On H&E stained slides there was no significant morphological difference after 2.5 months between tumours in omeprazole treated animals and controls or tumours were myofibroblasts were co-injected. Clearly further experiments are needed to elucidate the mechanisms underlying these phenomena.

9 Oesophageal cancer associated myofibroblasts are epigenetically distinct

9.1 Introduction

Epigenetic regulation of gene expression has been documented in malignant cells and in cancer associated stromal cells (i.e. cancer associated fibroblasts or myofibroblasts in different cancers (109, 243). Little is known of epigenetic changes occurring in stromal cells in oesophageal cancer. We therefore compared seven pairs of CAMs and ATMs from oesophageal squamous cell carcinoma and adenocarcinoma patients using the Illumina450k methylation array. These findings were aligned with expression data of an Illumina HT expression array as well as a previously performed expression array in the laboratory.

Amongst others, ADAM metallopeptidase with thrombospondin type 1 motif 12 (ADAMTS12), paired-like homeodomain 2 (PITX2) and secreted frizzled-like protein 2 (SFRP2) were identified as potentially interesting candidates for further investigations.

ADAMTS12 is a metalloproteinase which has been shown to play an important role in tumour stroma remodelling (244, 245). SFRPs are negative regulators of the Wnt signalling pathway (246) and changes in their expression due to altered methylation have been associated with the adenoma-carcinoma progression (247). SFRP2 has also been shown to be differentially expressed in lung (108) and colon cancer associated stromal cells (244). PITX2 is a transcription factor and downstream effector of the Wnt/β-catenin signalling pathway (155, 157).

As myofibroblasts influence the tumour microenvironment, amongst other mechanisms, through their secretion of proteases and signalling peptides, the effects of modulated ADAMTS12, PITX2 and SFRP2 expression in myofibroblasts was studied. Therefore ADAMTS12, PITX2 and SFRP2 expression in myofibroblasts was modified by siRNA knock-down and plasmid overexpression. Whereas modulation of PITX2 and SFRP2 was

successful, only knock-down of ADAMTS12 was achieved and the target not further investigated. Effects of altered PITX2 and SFRP2 expression on myofibroblasts proliferation and migration as well effects via conditioned media on OE21 proliferation or on human umbilical vein cell network formation were studied.

9.2 Objectives

The specific objectives were:

- To compare the DNA methylomes and transcriptomes of CAMs and ATMs with a view to identifying DNA methylation sites that determine mRNA transcription.
- To select and validate candidates for further study where altered DNA methylation regulates protein expression in CAMs.
- To determine whether the phenotype of cells with defined methylation patterns can be changed by overexpression/siRNA knock-down of target genes.

9.3 Material and Methods

Methylation array: DNA for an Illumina 450k methylation array was isolated as described (materials and methods 5.6.1) and the array run by an external service provider (HOLOGIC®; Manchester; UK).

The methylation array was validated by pyrosequencing on CpG sites cg15482122, cg20043105, cg12967137, cg16458436, cg08318726, cg13071812, cg26620157, cg25469418, cg18229107, cg16803846 and cg14435644 as described (materials and methods 5.6.11, table 2).

Expression modulation (overexpression and knock-down) was performed for ADAMTS12, PITX2 and SFRP2 overexpressing plasmids (see materials and methods 6.2.5 table 5) or knock-down siRNA for these targets.

EdU incorporation assays (see materials and methods 5.2.6), migration assays in Boyden chambers (see materials and methods 5.2.4) and

branching morphogenesis assays (see materials and methods 5.2.12) were performed as described.

9.4 Results

9.4.1 Results of Illumina 450k methylation array

A large number of the significantly differentially methylated CpG sites were not assigned to specific gene related loci (gene promoters, gene bodies or CpG islands) and were excluded from the analysis. In a paired comparison of significantly differentially methylated CpG sites in all seven CAMs and ATM (OeAC and OeSCC) a total of 4909 CpG sites were identified as at a cut-off of 20 % CpG methylation difference between the two (figure 35). Relative hypomethylation of CAMs in relation to ATMs was more frequent, 3483 vs 1426 (71 %); of these, 101 were located in promoter sites: 79 (78.2 %) in CAMs vs 22 in ATMs, and 79 located in gene bodies: 69 (80 %) in CAMs vs 16 in ATMs; 39 were located in CpG islands: 19 (48.7 %) CAMs vs 20 in ATMs. When comparing the three pairs of adenocarcinoma CAMs with ATMs, 5303 CpG sites showed significantly changed methylation. At all sites, CAMs were more frequently hypomethylated than ATMs, 4083 (77 %) in CAMs vs 1120 in ATMs, of which 106 were located in promoter sites: 87 in CAMs (82.1 %) vs 19 in ATMs; 82 were located in gene bodies: 75 (91.5 %) in CAMs vs 7 in ATM; 27 were located in CpG islands: 17 (27 %) in CAMs vs 10 in ATMs. When comparing the four pairs of squamous cell CAMs, 16473 CpG sites showed significantly different alteration in methylation with CAMs being frequently hypomethylated in relation to their matching ATM sites: 9000 (54.6 %) vs 7473; of these 330 were located in promoter sites: 190 (57.6 %) in CAMs vs 140 in ATMs; 256 were located in gene bodies: 142 (55.5 %) in CAMs vs 114 in ATMs; 244 were located in CpG islands: 119 in CAMs (48.4 %) vs 125 in ATMs.

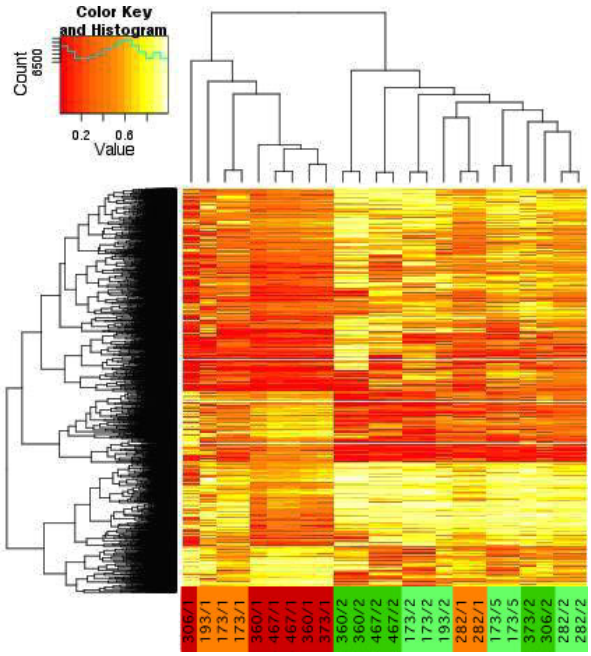

Figure 35: Illumina450k methylation array dendrogram for CAMs vs ATMs. 2D heat plot of all CpG sites comparing all CAMs (SCC CAMs in red and AC CAMs in orange, bottom) vs all ATMs (SCC ATMs in dark green, AC ATMs in light green, bottom) note segregation of CAM and ATM signatures with a single exception (282/1).

9.4.2 Validation of Illumina 450k methylation arrays

Validation of the Illumina 450k methylation array data by pyrosequencing was performed at 12 different DNA sites and showed a 91.2 % overlap (52 out of 57 pairs) of relative changes in methylation between CAMs and ATMs in the array compared with pyrosequencing. For illustration, three samples of individual pairs are shown in figure 36, and the net change of correlation for the 57 tested pairs is summarised in figure 37.

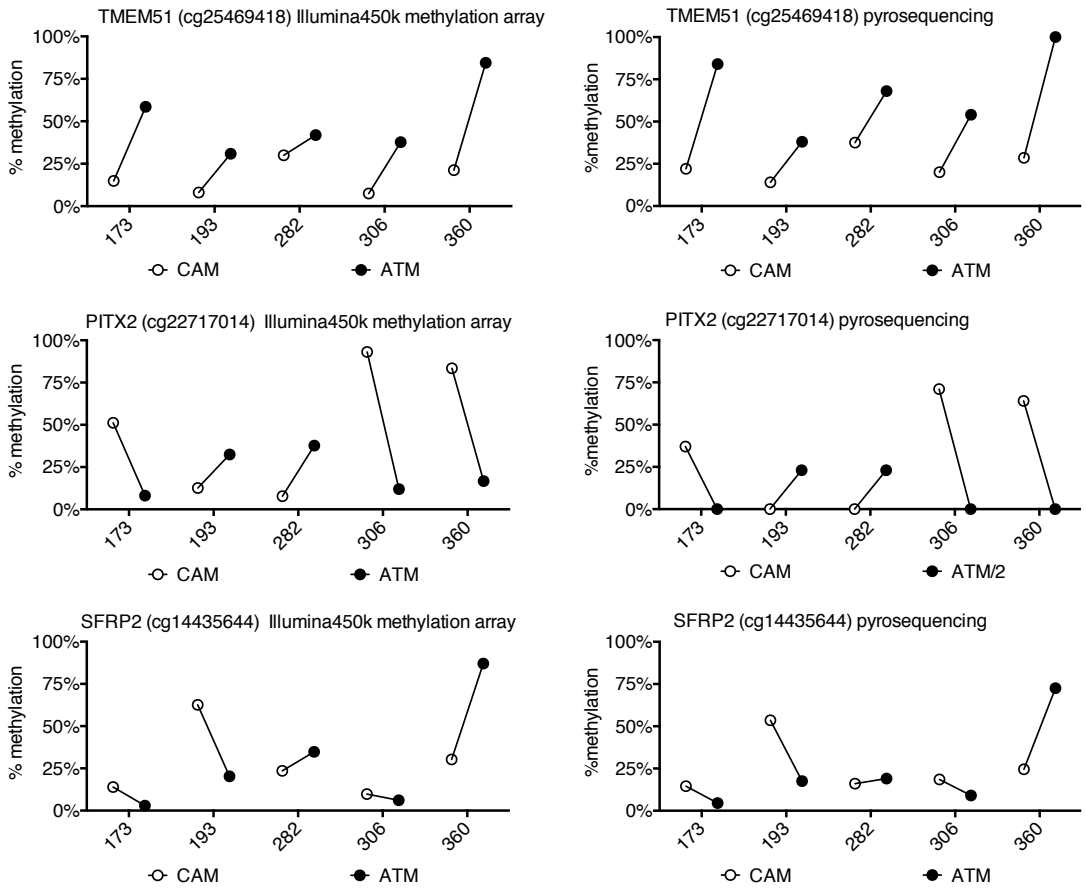

Figure 36: Validation of methylation array by pyrosequencing. Three examples of CpG sites on the array (cg25469418: TMEM51, cg22717014: PITX2, cg14435644: SFRP2). On the left side, values for three different CpG sites on the Illumina 450k methylation array in five pairs of CAM/ATM; on the right side, methylation at the same CpG sites assessed by pyrosequencing.

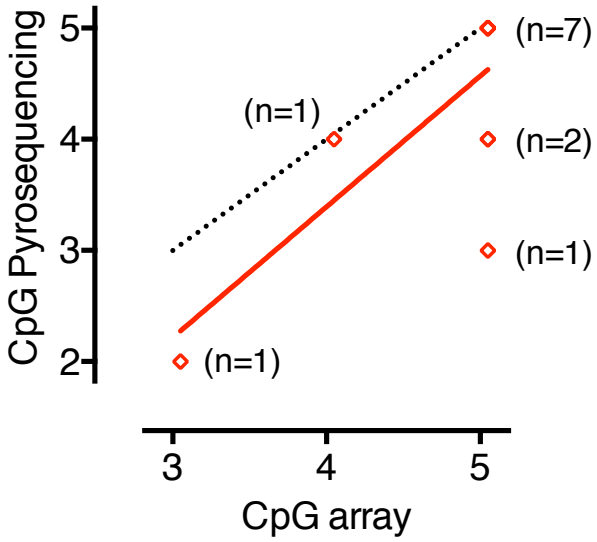

Figure 37: Summary of the validation of Illumina450k methylation array by pyrosequencing. Linear regression analysis of relative change in CpG methylation between CAMs and ATMs determined by pyrosequencing (Y-axis) compared to methylation arrays (X-axis); black dotted line shows the line of equivalence. The overlap of change between results of the methylation array and pyrosequencing between paired CAM and ATM (hypomethylated / hypermethylated / unchanged) in twelve different paired (number of pairs labelled on graph) are shown. Overlapping results were obtained between the Illumina 450k methylation array and pyrosequencing in 12 pairs of samples and in 52 of 57 amplicons (91 %). Slope for matching pyrosequencing results Y = 1.176*X - 1.255, Pearson's *r*=0.7426, statistical significance in correlation analysis *p*=0.0057.

9.4.3 Target selection

Three genes, *ADAMTS12, PITX2* and *SFRP2*, showed a significant difference between CAMs and ATMs in CpG methylation in the Illumina450k and in a previously established expression array performed by the group (Varro et al., personal communication). Methylation maps for SCC and AC CAMs and ATMs for *SFRP2* are shown in figure 38, and for *PITX2* in figure 39. Variance of expression in IlluminaHT expression array for SFRP2 and PITX2 are shown in figures 40 and 41 respectively. To further validate these targets for biological studies the success of knock-down of ADAMTS12, PITX2 and SFRP2 by siRNA in CAMs, or overexpression by plasmids containing a CMV promoter, was assessed by qPCR (figure 42). Knock-down

of all three genes by siRNA was successful in decreasing target expression by 90 %. Overexpression (over 10,000 fold) was successful for PITX2 and SFRP2, whereas an overexpression of ADAMTS12 by the plasmid construct was not detectable and as a consequence this target was not considered further.

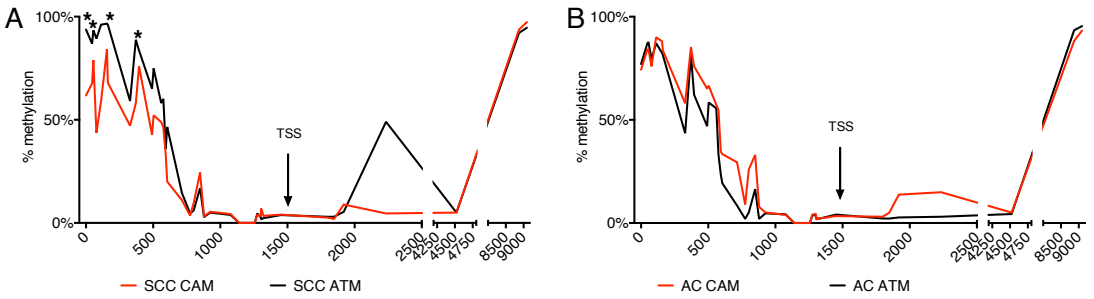

Figure 38: CpG methylation of SFRP2 in CAMs and ATMs. Using data from the Illumina450k methylation array, the mean values of individual CpG site methylation (as percentage on y-axis) are shown for *SFRP2* in SCC CAMs (red) and SCC ATMs (black)(A), and in AC CAMs and AC ATMs (B). Statistically significant altered methylation ($p<0.05$) at individual sites is marked with asterisk. X-axis represents distance in base pairs starting from the first CpG island allocated to the gene (cg04959480).

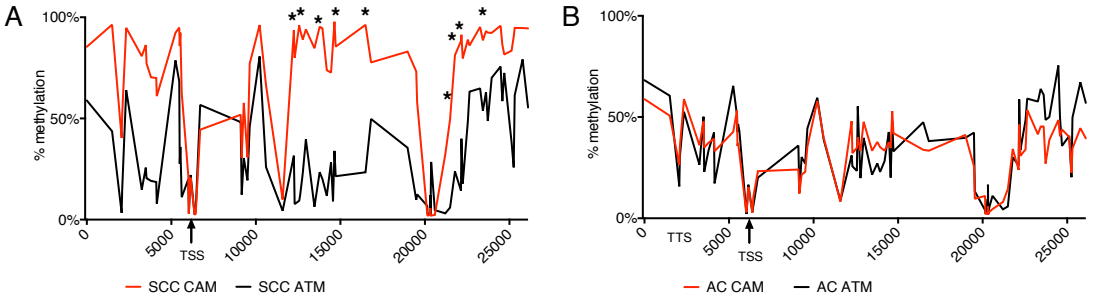

Figure 39: CpG methylation of PITX2 in CAM and ATM (Illumina450k methylation array). Using data from the Illumina450k methylation array, the mean values of individual CpG site methylation (as percentage on y-axis) are shown for *PITX2* in SCC CAMs (red) and SCC ATMs (black)(A), and in AC CAMs and AC ATMs (B). Statistically significant altered methylation ($p<0.05$) at individual sites is marked with asterisk. X-axis represents distance in base pairs starting from the first CpG island allocated to the gene (cg08326515).

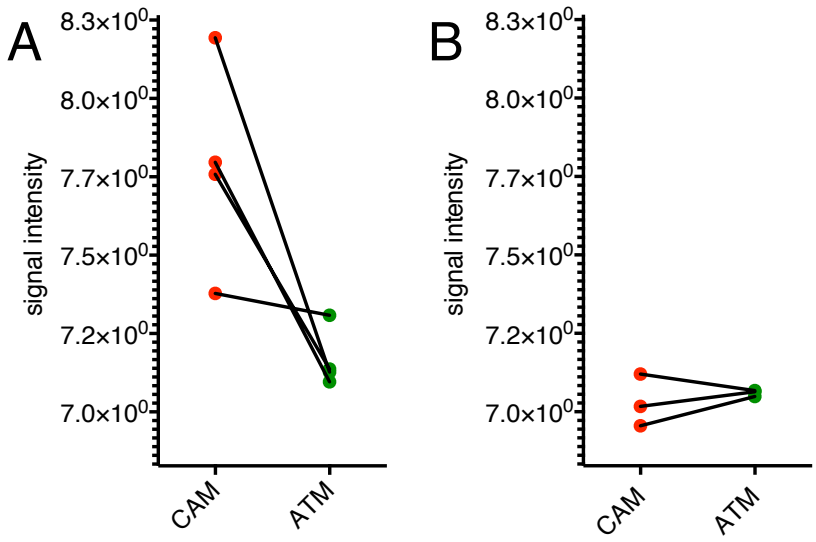

Figure 40: SFRP2 is upregulated in SCC CAMs. Illumina HT expression array signal intensity (y-axis) for SFRP2 in CAMs and ATMs (matched pairs connected by a line) in myofibroblasts from SCC patients (A) and AC patients (B).

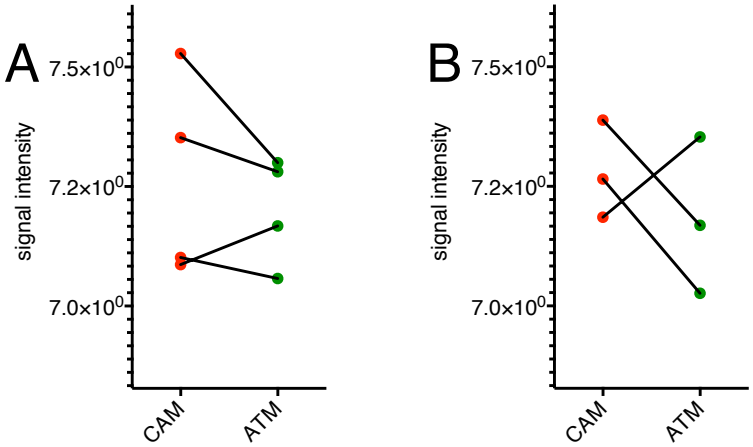

Figure 41: PITX2 expression does not vary between SCC or AC CAMs and ATMS. Illumina HT expression array signal intensity (y-axis) for SFRP2 in CAMs and ATMs (matched pairs connected by a line) in myofibroblasts from SCC patients (A) and AC patients (B).

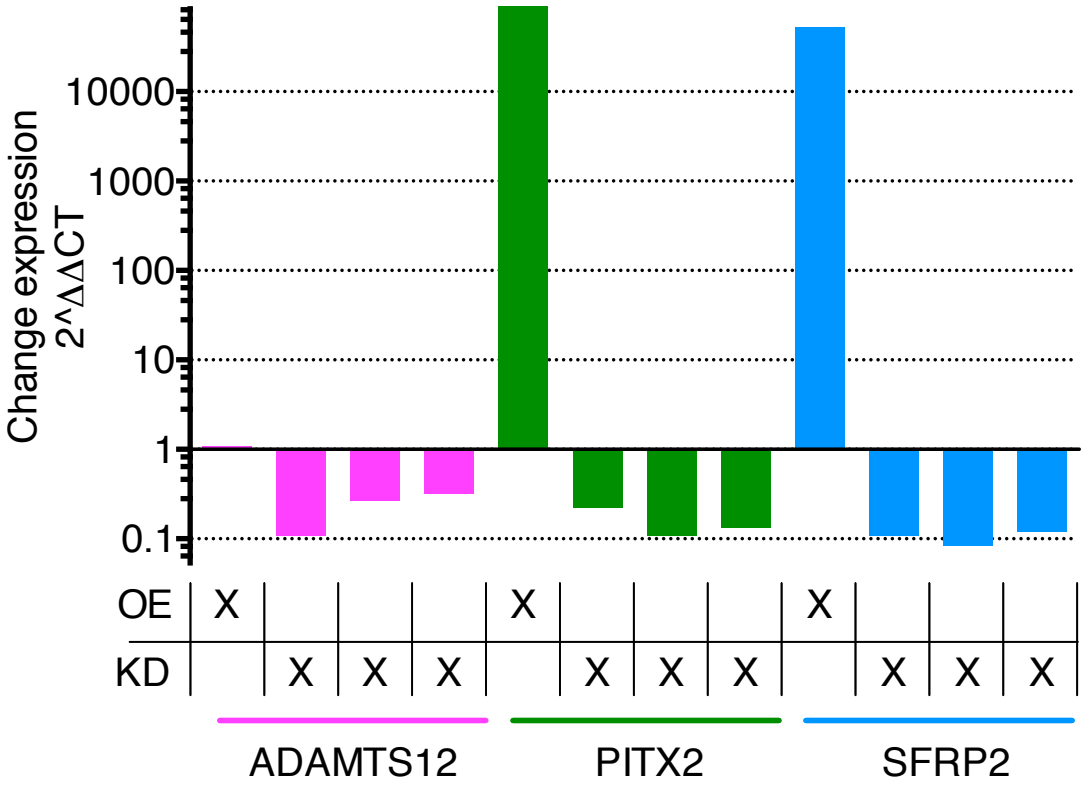

Figure 42: Overexpression and knock-down of putative targets. QPCR data showing change of expression (2^ΔΔCT) of ADAMTS12, PITX2 and SFRP2 upon plasmid overexpression (OE) or knock-down (KD) using three different siRNA constructs, in each case.

9.4.4 Effects of SFRP2 on myofibroblast proliferation

EdU incorporation by CAMs was reduced by knock-down of SFRP2 and increased in ATMs by overexpression although the results did not reach statistical significance in either case (figure 43).

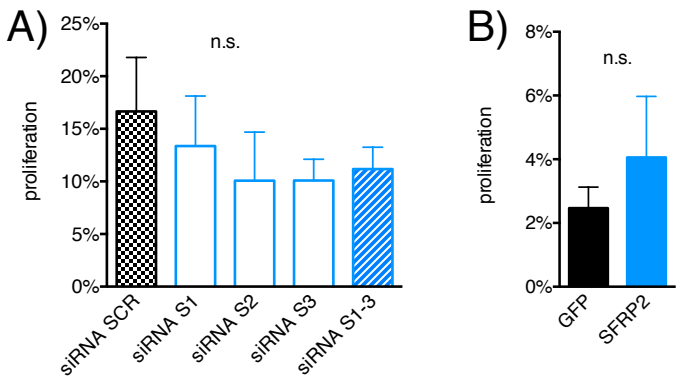

Figure 43: Effect of SFRP2 expression on myofibroblast EdU incorporation. EdU incorporation (labelled cells as a percentage of total) after A) knock-down in CAMs by three different siRNA S1, S2, S3 (for average of all S1-3) and scrambled siRNA (SCR) or B) overexpression of SFRP2 or GFP controls in ATMs.

9.4.5 Effects of SFRP2 on myofibroblast migration

Knock-down of SFRP2 in CAMs reduced migration stimulated by IGF2. When SFRP2 was overexpressed in ATMs the increased migration in response to IGF2 was also decreased (figure 44).

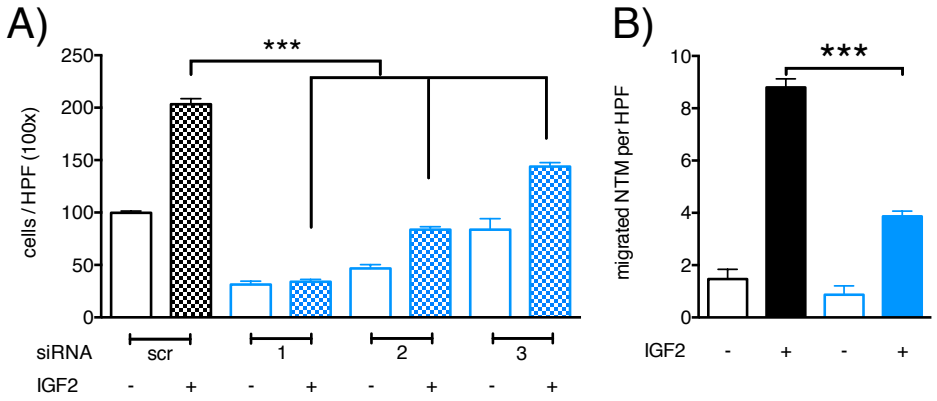

Figure 44: Effect of SFRP2 expression on myofibroblasts migration. Myofibroblast transwell migration in Boyden chamber assay after A) knock-down of SFRP2 by siRNA S1, S2, S3 or scrambled siRNA (SCR) in CAMs (p<0.0001; one way ANOVA) or B) overexpression of SFRP2 in ATMs (p<0.0001; unpaired t-test). Stimulation of migration by IGF2.

9.4.6 Effects of myofibroblast-derived SFRP2 on Oe21 proliferation

Conditioned medium from CAMs where SFRP2 was knocked down, or from ATMs where it was overexpressed, did not affect EdU incorporation in Oe21 cancer cells (figure 45).

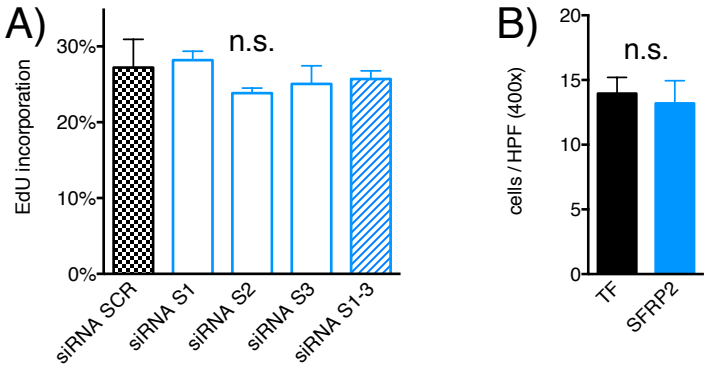

Figure 45: Effects of conditioned medium from myofibroblasts with altered SFRP2 expression on OE21 proliferation. EdU incorporation (percentage labelled cells) in OE21 cells after 24 hour exposure to A) conditioned medium from CAMs where SFRP2 was knocked down by siRNA S1, S2, S3 or SCR controls or B) overexpressed in ATMs.

9.4.7 Effects of myofibroblast-derived SFRP2 on endothelial network formation

Conditioned medium from CAMs where SFRP2 was silenced decreased network formation of HUVEC cells in a branching morphogenesis assay (figure 46). Conversely overexpression of SFRP2 in ATMs increased network formation of HUVEC cells (figure 47 & 48).

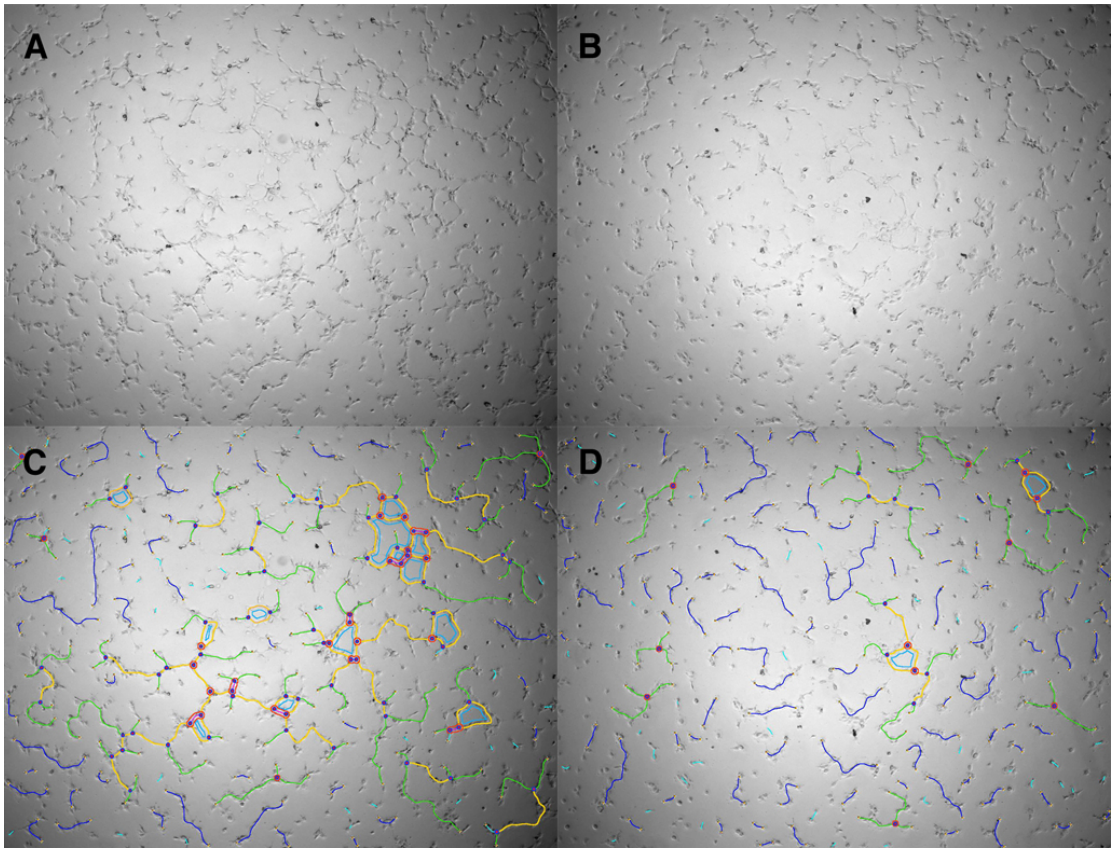

Figure 46: Branching morphogenesis in HUVEC cells exposed to CM from SFRP2 expression supressed CAMs. Photomicrographs of HUVECs grown on Matrigel exposed to serum free medium on the left side and conditioned medium from myofibroblasts after knock-down of SFRP2 by transfection with siRNA on the right side. Panels A) and B) original images; Panels C) and D) overlayed after mesh analysis by the *angiogenesis analyser* plugin from imageJ. Segments in blue or green indicate contact with a junction (red). Master segments in yellow, networks in clear blue. Master junctions in purple.

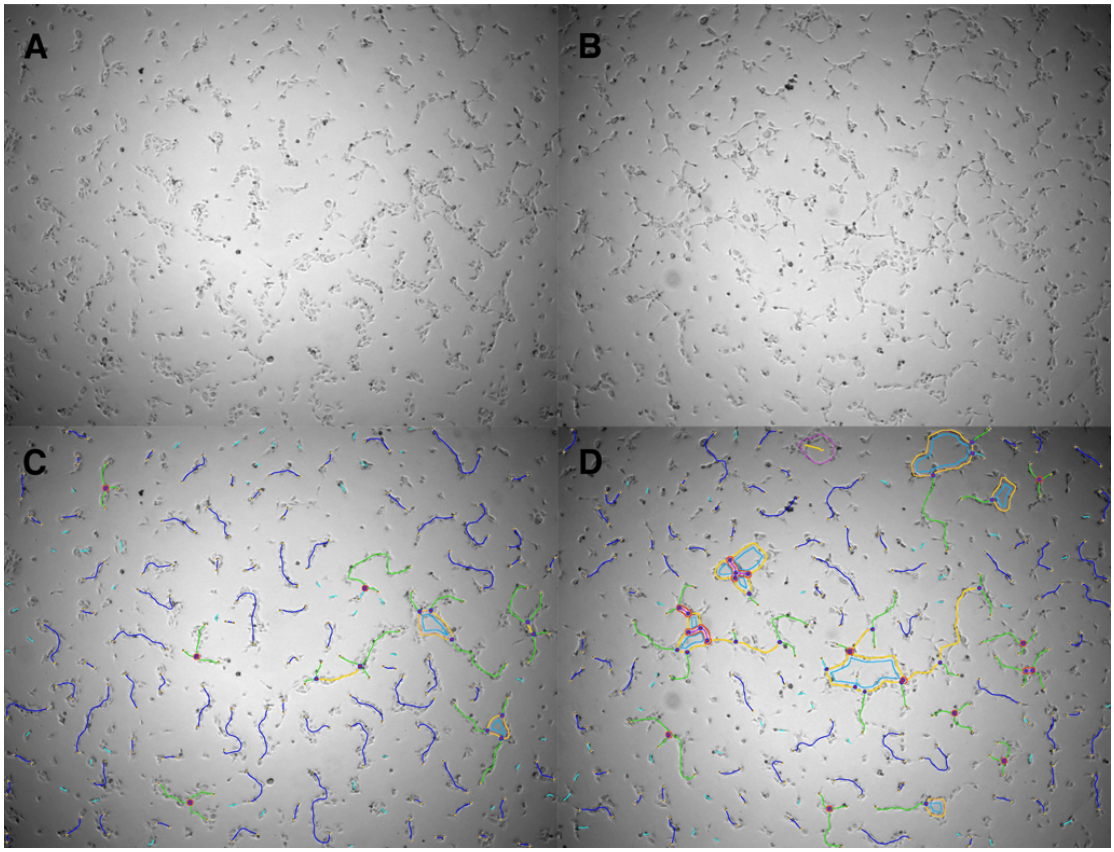

Figure 47: Branching morphogenesis in HUVEC cells exposed to CM from SFRP2 overexpressing ATMs. Photomicrographs of HUVECs grown on Matrigel exposed to serum free medium on the left side and conditioned medium from SFRP2 overexpressing myofibroblasts on the right side. Panels A) and B) original images; Panels C) and D) overlayed after mesh analysis by the *angiogenesis analyser* plugin from imageJ. Segments in blue or green indicate contact with a junction (red). Master segments in yellow, networks in clear blue. Master junctions in purple.

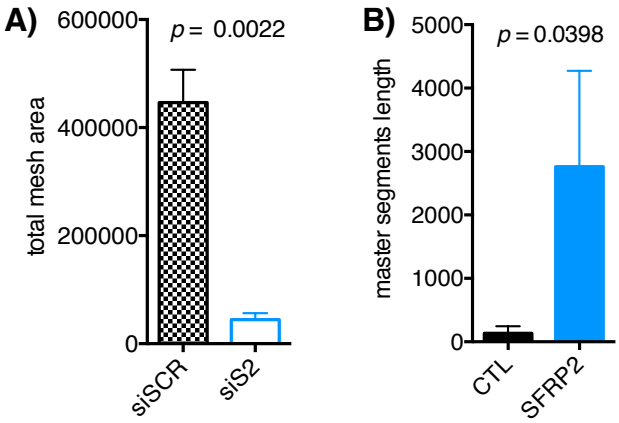

Figure 48: Effects of conditioned media from myofibroblasts with altered SFRP2 expression on angiogenesis. HUVEC total mesh area and master segment length (pixels) under exposure to conditioned medium from A) CAMs where SFRP2 was knocked down by siRNA S1 and SCR controls or B) overexpressed in ATMs. Statistical significance in paired t-tests.

9.4.8 Effects of PITX2 on myofibroblast proliferation

EdU incorporation in CAMs after transfection with siRNA against PITX2 revealed a decreased incorporation with all three siRNAs tested. When PITX2 was overexpressed in ATMs, the construct induced a loss of over 80 % of the transfected cells as compared to mock transfected controls. The remaining cells demonstrated a decreased EdU incorporation as compared to the controls (figure 49).

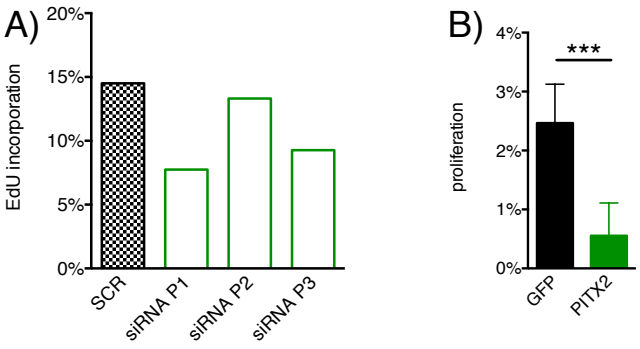

Figure 49: Effects of PITX2 expression on myofibroblasts proliferation. EdU incorporation as percentage of total cells after A) knock-down of PITX2 in CAMs by three different siRNA P1, P2, P3 and scrambled siRNA (SCR) (single value observation) or B) overexpression of PITX2 or GFP controls in ATMs ($p<0.0001$unpaired t-test).

9.4.9 Effects of PITX2 on myofibroblast migration

Knock-down of PITX2 by siRNA increased the basal migration of myofibroblasts in Boyden chamber transwell migration assays compared to controls. In response to stimulation by IGF2 there was smaller relative increase of the migration, although higher absolute migration, compared to the controls. PITX2 overexpressing cells did not show increased basal migration, and migration was decreased after IGF stimulation (figure 50).

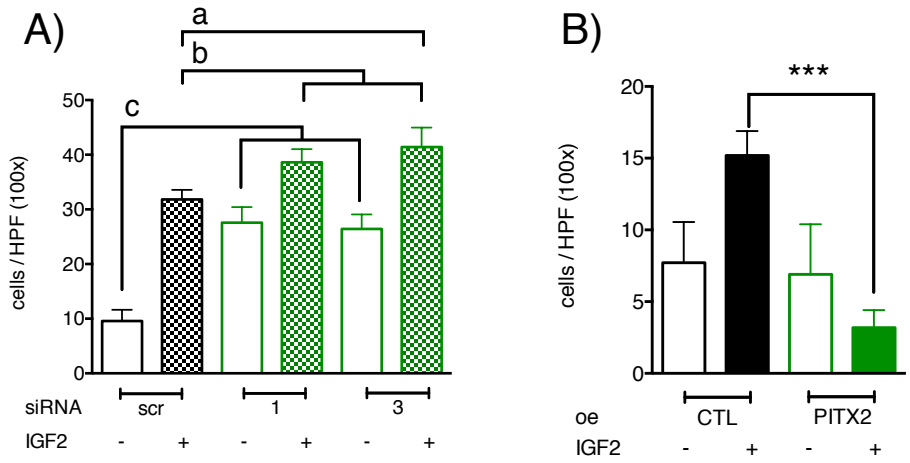

Figure 50: Effects of PITX2 expression on myofibroblasts migration. Myofibroblast transwell migration in Boyden chamber assay after A) knock-down of PITX2 by siRNA P1 and P3 or scrambled siRNA in CAMs; statistical significance a) p=0.033 (unpaired t-test), b) n.s. (one-way ANOVA), c) p=0.0001 (one-way ANOVA) or B) overexpression of PITX2 in ATMs. Stimulation of migration by IGF2; p<0.0001 (unpaired t-test).

9.4.10 Effects of myofibroblast-derived PITX2 on Oe21 proliferation

When Oe21 cells were exposed to conditioned medium harvested from CAMs where PITX2 was silenced with siRNA no difference in EdU incorporation was observed as compared to controls. Conditioned medium from PITX2 overexpressing ATMs only moderately increased EdU incorporation in Oe21 cells without reaching statistical significance as compared to controls (figure 51).

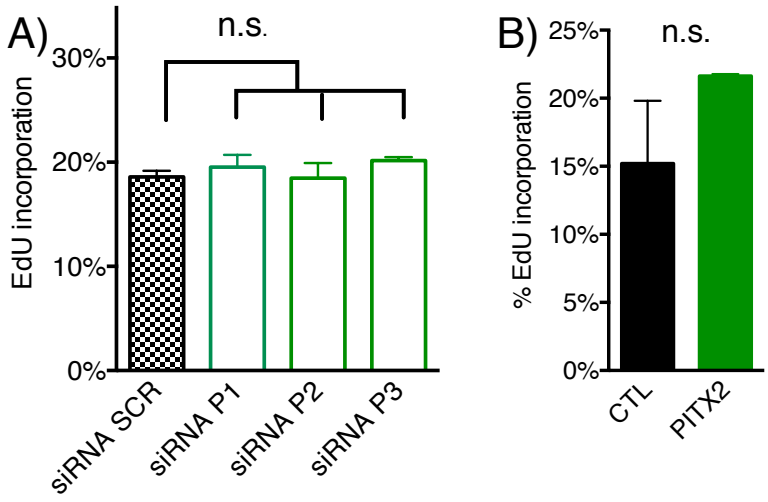

Figure 51: Effects of conditioned media from myofibroblasts with altered PITX2 expression on OE21 proliferation. EdU incorporation (percentage) in OE21 cells after 24 hour exposure to conditioned medium A) from CAMs where PITX2 as knocked down by siRNA P1, P2, P3 or scrambled controls or B) overexpressed in ATMs.

9.4.11 Effects of myofibroblasts-derived PITX2 on endothelial network formation

Conditioned medium harvested from CAMs where PITX2 was silenced with siRNA decreased network formation in branching angiogenesis assays using HUVEC cells. In contrast, network formation by HUVEC cells was increased following exposure to conditioned medium from PITX2 overexpressing ATMs although without reaching statistical significance (figure 52).

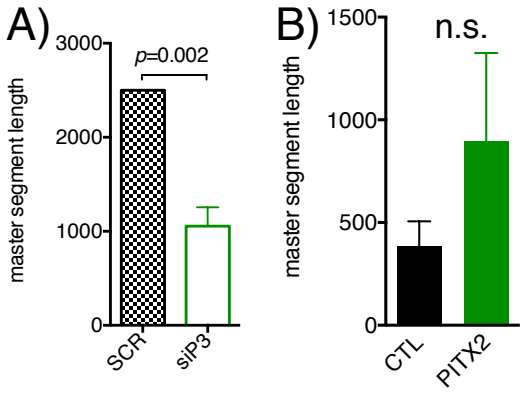

Figure 52: Effects of conditioned media from myofibroblasts with altered PITX2 expression on angiogenesis. HUVEC master segment length (pixels) under exposure to A) conditioned medium from CAMs where PITX2 as knocked down by siRNA P3 and SCR controls (A:*p*=0.078 (unpaired t-test); B) overexpressed in ATMs. Statistical significance in paired t-tests.

9.5 Discussion

The starting point for the work described in this chapter was the previous findings in our group of differences between CAMs and ATMs with regard to their secretomes and miRNA transcriptomes. A wealth of evidence suggests that transcription is epigenetically regulated and so we first assessed whether global methylation differs between ATMs and CAMs. In this chapter the results are presented of a study investigating the difference in methylation between CAMs and ATMs at a more detailed level using methylation array technology. We found over five thousand significantly different methylated sites and correlated these with the available expression data. We investigated genes from three different protein families, i.e. a metalloproteinase (ADAMTS12), a homeobox gene (PITX2) and a secreted signalling protein (SFRP2) as potential candidates for DNA methylation regulated expression by combining the results of the Illumina450k methylation array together with previous expression array data available. We successfully overexpressed and supressed the expression of PITX2 and SFRP2, whereas over expression of ADAMTS12 was unsuccessful. The main findings are that SFRP2 is hypomethylated in the promoter region of CAMs as compared to

corresponding ATMs and that SFRP2 is up-regulated in CAMs. Furthermore we found that overexpression of SFRP2 in ATM's induced angiogenesis, whereas knock-down of SFRP2 by siRNA in CAMs decreased angiogenesis, suggesting that SFRP2 secretion by myofibroblasts regulates angiogenesis in the tumour microenvironment.

The Wnt/β-catenin signalling pathway is a key element of carcinogenesis (248). SFRP family members have been attributed negative regulatory roles in the Wnt signalling cascade (249, 250). SFRP is downregulated in colorectal cancer by promoter hypermethylation which leads to an activation of Wnt/β-catenin signalling (251); moreover, reintroduction of SFRP expression leads to suppression of the Wnt signalling cascade. Silencing of SFRP family proteins in tumour stroma through promoter hypermethylation has been described for SFRP1 in colorectal cancer (140) and NSCLC (252). Also in basaloid oesophageal carcinomas, a rare entity of squamous oesophageal carcinoma SFRP expression has been shown to be epigenetically regulated (148). Moreover, altered expression of SFRP family members have been described in oesophageal adipocytes (253), although the authors did not investigate the mechanism of regulation. The present results show, for the first time, that in stromal cells too SFRP family members are epigenetically regulated. With the use of methylation array technology and PCR based technology we show that SFRP2 is hypomethylated 1450-840bp upstream of exon1 in squamous oesophageal CAMs as compared to paired ATMs.

In general, little is known on the role of stromal SFRP expression. The most interesting finding in our functional analyses was that myofibroblasts-derived SFRP2 affected angiogenesis in vitro: conditioned medium from SFRP2-overexpressing myofibroblasts stimulated vascular network formation, whereas downregulation reduced network formation. SFRP family members are known pro-angiogenetic factors (254, 255). SFRP2 is a known inhibitor of the Wnt/β-catenin-signalling cascade and has been shown to promote neovascularisation in cancers (256). CAMs have previously been shown to exhibit angiogenic potential through VEGFα secretion (257, 258). Our findings

support the idea that CAMs also exert angiogenic effects by SFRP2 secretion and that this mechanism is epigenetically activated in CAMs.

These data therefore raise the possibility that DNA methylation regulates expression of SFRP2 in myofibroblasts in oesophageal squamous cell carcinomas that is in turn associated with tumour outcome. Microvascular density in oesophageal squamous and adenocarcinomas has not been associated with tumour outcome (259), however high microvascular density was a negative predictive factor for neo-adjuvant radiotherapy response in primary oesophageal cancers (260). Whether SFRPs influence responsiveness towards radiation therapy remains to be elucidated.

PITX2 is a transcription factor and regulator of the Wnt/β-catenin signalling cascade. Overexpression of PITX2 has been associated with increased transcription of most of the Wnt-related genes which is associated with cell proliferation and migration through a transcriptional activation directed at the Wnt2 and Wnt5a promoters (155). We observed a moderate decrease of CAM proliferation upon PITX2 knock-down by siRNA. This decrease in proliferation could be explained by a decrease of a constitutively activated Wnt/β-catenin signalling axis in CAMs and a decreased TGF β stimulus as described by Basu et al (261). The overexpression of PITX2 in ATMs also decreased proliferation of transfected myofibroblasts. These data have to be interpreted with caution as overexpression of PITX2 in our experiments was associated with a substantial cell loss. Our observation that conditioned medium from PITX2 overexpressing myofibroblasts leads to an increase of OE21 proliferation mirrors the results published by Basu et al where CM from transiently transfected cells induced transcription of *CCND1* and *c-MYC*.

Interestingly downregulation of PITX2 in CAMs was associated with an increased basal migration which contradicts findings on migration of PITX2 knock-out myogenic cells in vivo (156) and findings by Basu et all where they show that PITX2 expression increases ovarian cancer motility by activation of TGF β pathway (261). Overexpression of PITX2 in myofibroblasts did, however, significantly affect cell migration.

CM from CAMs where PITX2 was knocked down suppressed angiogenesis, whereas CM from ATM where PITX2 was overexpressed increased angiogenesis. Currently there are no data available on the effect of PITX2 on angiogenesis and we can only hypothesise that a modulation of the Wnt/β-catenin signalling pathway or other PITX2 regulated genes induce angiogenesis. Recently it was reported that regulation of Wnt through FOXO1 significantly modulated vascularisation; thus downregulation of MYC by FOXO1 overexpression led to a reduction of endothelial sprouting whereas activation of MYC had the opposite effect (262). It is likely that PITX family members are direct regulators of angiogenesis through regulation of MYC.

The main findings of this chapter are (a) that the DNA methylome of oesophageal CAMs is distinctively different from their matched ATMs. (b) That some of the functional differences between CAMs and ATMs are due to altered gene transcription regulated in turn by differential DNA methylation. (c) Two genes (*PITX2* and *SFRP2*) whose products are implicated in Wnt/β-catenin signalling display altered DNA methylation and transcription in oesophageal squamous cell carcinoma but not oesophageal adenocarcinoma related myofibroblasts. Modulation of PITX2 and SFRP2 expression by knock-down and overexpression in CAMs and ATMs not only alters their individual phenotype, but also leads to alterations of other cell types in the tumour microenvironment (i.e. OE21 squamous cell carcinoma cells and HUVEC cells). Collectively, these data enhance understanding of the role of myofibroblasts in regulating the tumour microenvironment.

10 Final discussion

The work presented in this thesis shows that primary human myofibroblasts accelerate tumour growth *in vitro* and *in vivo*. (a) CAMs are shown to be epigenetically distinct from ATMs. (b) A novel model for epigenetic modification of stromal cells with the use of the DNMT inhibitor DAC is described. (c) Myofibroblasts are shown to play an important role in tumour niche formation in xenografts and (d) the tumour stroma in advanced xenografts is shown not to consist of transplanted stromal cells but rather is replaced by murine stromal cells.

The field of cancer research has now moved from a tumour-centric view to a more nuanced understanding of the role of the tumour microenvironment (53, 54). Thus it is now accepted that also non-cancerous cells in the tumour microenvironment are relevant players affecting tumour initiation, growth, metastasis and drug treatment.

Our *in vivo* experiments show that primary human cancer derived myofibroblasts are main contributors to a tumourigenic microenvironment which enables cancer cells to seed and grow as postulated by Paget (10). This is a key finding and has to our knowledge not been shown by others in this form.

It is well established that cancer cells activate stromal fibroblasts or bone marrow derived mesenchymal stromal cells mainly through TGFβ signalling to become activated myofibroblasts. Most of this evidence has been acquired from transgenic animal models or investigations on human derived FFPE tissue, but never directly from observations of primary human stromal cells in combination with cancer cells. Although efforts to mirror the in vivo situation including increasingly elaborate in vitro models such as 3-D cultures (174), chamber systems (263), spheroids (264), enteroids (265), or even *in silico* models (266) of the events occurring in the tumour microenvironment, nevertheless the fact is that xenograft models remain a pillar of cancer research. In particular, the multi-layered aspect of the tumour

microenvironment cannot be reproduced in all its complexity in vitro; moreover, systemic effects and metastatic spread of tumours inevitably requires research in entire organisms.

The present findings enhance and extend what has been assumed from earlier work – namely that activated myofibroblasts in the tumour microenvironment are able to supply the necessary components which accelerate the host cells to form a complex microenvironment that replaces the human stromal cells and in the end accelerates tumour growth. This stands in line with current models on anticancer therapies which target the tumour stroma (267).

Most xenograft studies described in the literature do not show xenograft data from the period immediately following tumour injection (229) (224) (268) (269) Thus, descriptions of tumour development in the first two days are mostly unreported, presumably because the initial swelling observed is interpreted as non-specific and related to inflammatory stimuli due to the injection. Furthermore effects related to tested substances are expected to occur at later time points. Our data confirm that myofibroblasts generate an environment hospitable for tumour cells to expand from the very beginning onwards. Already as early as two days after injection, murine non-inflammatory cells invade between the injected human myofibroblasts and cancer cells which stands in line with a recent publication on the origin of tumour stroma cells (230). One month after xenografting human myofibroblasts were not detectable and all stromal cells were of murine provenance. This also stands in line with the role of niche formation prior to the development of metastases (270, 271). It is well established that cancer associated stromal cells promote cancer cell proliferation and mobility as well as angiogenesis and microvessel density within the tumours (59, 95, 272, 273); these are associated with adverse outcome and drug resistance (274, 275). In the setting of xenografts, the effects originating from myofibroblasts seem to occur within the first two days. Myofibroblasts give cancer cells a growth advantage and accordingly lead to an accelerated tumour growth. One

practical consequence is that co-injection of stromal cells might be a suitable option to promote growth of cancer cells which are normally difficult to grow as xenografts.

The present data indicate that cancer associated myofibroblasts of the oesophagus are epigenetically distinct from matched adjacent tissue myofibroblasts. Genes encoding a transcription factor (PITX2) and a regulatory protein (SFRP2) both show altered methylation signatures and expression patterns between oesophageal cancer CAMs and ATMs and are both implicated in Wnt/β-catenin signalling. Moreover, the data show that upregulation of SFRP2 in myofibroblasts induces angiogenesis and supporting the hypothesis that epigenetic modification regulates myofibroblast derived SFRP2 expression which may play an important role in tumour neovascularisation.

CAMs are phenotypically distinct from ATMs which has been demonstrated for myofibroblasts in lung (82), stomach (60), colon (85), (83) and others. Whereas mutations, translocations and chromosomal instability are a hallmark of malignant transformation in cancer cells, such alterations were reported to occur rarely in CAFs (276). However, it is important to stress that cancer cells undergoing EMT might be identified as mutation-bearing stromal cells and thus account for a portion of the reported mutations occurring in cancer associated stromal cells (277).

Myofibroblasts have been shown to interfere with anticancer therapy by different groups (278, 279). Growth factors have been identified as a key player compromising the anticancer effect of targeted drugs such as EGFR and HER2 tyrosine kinase inhibitors and RAF GTPase inhibitors. I have shown in the previous chapters that chemical epigenetic modification of stromal cells with DAC lead to an accelerated tumour growth, suggestive that if stromal cells can be modified to promote tumour growth there should also be a way to interfere with their tumour promoting ability.

These findings underline the important role of the tumour microenvironment and myofibroblasts in particular. It also suggests that more effort in understanding the tumour stroma will be needed in order to find new anti cancer therapies.

We hypothesised that the persistence of phenotypic changes observed in CAMs are epigenetically defined. Gonda et al (73) as well as others (85, 108, 280) have shown previously that CAMs demonstrate a modified DNA methylation pattern as compared to their normal counterparts. Our finding of a global change in DNA methylation is also compatible with a previous report that CAFs show a loss of global DNA methylation and only focal gain of DNA methylation in a chemically induced gastric cancer model (109). In describing epigenetic differences between CAMs and ATMs the data therefore contribute to the rather sparse knowledge on epigenetic regulation of cancer associated stromal cells (281).

The understanding of epigenetic regulatory processes in the stromal tumour microenvironment has become important as drugs influencing epigenetic processes such as the DNA methyl transferase inhibitors 5-AzaC and 5-AzaDC and the histone-deacetylase inhibitors vorinostat and romidepsine have become available for anticancer treatment. Also miRNAs which are regarded as epigenetic regulators are being tested for anticancer treatment (282). The data indicate specific on-target results that appear promising, but even so off-target effects might lead to unwanted effects such as accelerated tumour growth as suggested by the present findings. The work in this thesis suggests that it would be appropriate to be cautious in extending the use of drugs in this class. One limitation of in vitro assays with regard to epigenomics is that cells adapt to different environments for example when growing in different organs or when cultured on plastic which may itself induce altered DNA methylation patterns (283). Using low passage cells in our experiments and strictly standardised culture conditions we attempted to minimise artificial differences in our results. The data obtained from our paired analysis between CAM with ATM using the Illumina Infinium

HumanMethylation450 (450K) BeadChip array showed that significant epigenetic differences between CAMs and ATMs persist even after few passages on plastic. However, we cannot exclude that *de novo* epigenetic changes occurred obscuring changes present before culture in vitro. In paired analyses altered DNA methylation between CAMs and ATMs were compared, and in unpaired analyses CAMs, ATMs and NTMs were compared. The data generated by the unpaired analysis did not prove to be of statistical significance. This was likely related to the relative low cohort size and the high variability between individual patients. One disadvantage of the array might be that it has been designed for use on tumour cell lines and only detects predefined methylation sites within a selected range within the genome, thus potentially over-representing these regions and under-representing others. Next-generation methylation sequencing (284) or other newer techniques (285) could now be used, however, these methods are more expensive and the data analysis is more demanding which precluded their use in the present study.

In order to investigate the biological relevance gained by the methylation array, we matched the results with pre-existing data on gene expression in these cells. Functional analysis of PITX2 and SFRP2, both of which are involved in the Wnt/β-catenin signalling pathway showed significantly altered DNA methylation in the Illumina 450k methylation array and a significantly altered gene expression in an expression array (personal communication Prof Varro). The possibility of epigenetic regulation of PITX2 and SFRP2 has not been shown in cancer associated stromal cells before.

TGF-β signalling is a key player in OESCC with dual signalling effects. In early tumour stages TGF-β signalling appears to antagonise tumour growth. Low expression levels of TGF-β were described to be associated with poor tumour differentiation and more advanced tumour stage at the time point of diagnosis (286-288). Contrary to this, in advanced tumour stages high levels of TGF-β were associated with more aggressive behaviour, presumably at least in part through the transforming effect of TGF-β on cancer associated

stromal cells, which in turn promotes tumour progression and angiogenesis (59, 95). TGF-β1 in fibroblasts leads to migration and invasion of oesophageal squamous cell cancer (289). Furthermore in both OEAC and OESCC TGF-β signalling has been shown to be associated with advanced tumour stages (289, 290).

CAFs secrete Wnt2 which also leads to cancer cell proliferation (236). The authors have also raised the question of the role of Wnt2 in EMT. They have shown that CAFs with high expression levels of Wnt2 are associated with authentic CAF phenotypes which I would argue is better described as a CAMs. I found that SFRP2, a WNT/β-catenin signal competitor, exhibits a relative loss of DNA methylation and is up-regulated in SCC CAMs. In order to assess whether altered expression of SFRP2 affects the WNT/β-catenin signal cascade, phospho β-catenin expression levels or cyclin-D1 as surrogate markers of WNT/β-catenin pathway activation could have been assessed. Surprisingly, knock-down of SFRP2 lead to a decrease in myofibroblast proliferation whereas upregulation of SFRP2 increased proliferation. A lack of negative regulators of the WNT signalling pathway would lead to a decreased proliferation and vice versa. Fibroblast-derived Wnt has been shown to be involved in activation of the WNT/β-catenin pathway in mammary glands and tumours (291, 292), pancreatic adenocarcinoma (293), non-melanotic skin tumours (294), malignant melanoma (154), gastric adenocarcinoma (87) and OESCC. The present observation showed the contrary. This raises the possibility that SFRP2 has a pro-mitotic effect in myofibroblasts, independent of the classical WNT signalling pathway. Knock-down and overexpression in myofibroblasts also lead to decreased myofibroblast migration. The effect of knock-down of SFRP2 on myofibroblasts could be explained in relation to canonical WNT signalling. In SFRP2 overexpressing cells however, competition with frizzled for the frizzled receptor might underlie the decrease in cell migration. Further experiments will be required to sustain this hypothesis.

CAFs play an important role in angiogenesis through VEGF signalling (295). In colorectal cancers, myofibroblasts and microvascular density are positively correlated with more aggressive tumour growth (296). This is of interest in the context of our observation that conditioned medium derived from cells where SFRP2 was knocked down inhibited vascular network formation, whereas conditioned medium from SFRP2 overexpressing myofibroblasts lead to an increase of vascular network formation. These findings are compatible with the published literature on the effects of other SFRP family members and their pro-angiogenic effects (154, 256). It appears that myofibroblasts which have undergone epigenetic modification might constitutively overexpress SFRP2 and thus contribute to angiogenesis in cancers.

We found that PITX2, a transcription factor which plays an important role in embryogenesis and is a downstream effector of the Wnt/β-catenin signalling was hypermethylated in squamous cell carcinoma derived CAMs. A significant difference at the transcription level however was not detected. Nevertheless when we modified PITX2 expression in myofibroblasts, we found statistically significant effects on myofibroblasts proliferation, migration and angiogenesis. These data show that the downstream target of the Wnt/β-catenin signalling directly interferes with cells involved in the tumour microenvironment. An experiment which could be performed in order to prove this hypothesis would be the assessment of PITX2 expression upon activation of the Wnt/β-catenin pathway.

The findings regarding modulation and targeting of the WNT signalling pathway underline the important role of myofibroblasts and WNT/β-catenin signalling in the tumour microenvironment. It is now important for a general understanding of tumour biology to determine how non-malignant stromal cells are epigenetically modified in ways that promote angiogenesis.

Finally, a novel model is described for epigenetic modification of cancer stroma cells: namely epigenetic modification of myofibroblasts using the DNMT inhibitor DAC. Epigenetic modification of myofibroblasts *in vitro* modifies cancer growth in vivo. We hypothesise that chemically-induced DNA

methylation leads to an activation of normally silenced genes leading to a biologically more active cell. Thus myofibroblasts treated with DAC over three days showed a mild decrease in global DNA methylation; a short treatment period with DAC also leads to persistent biological changes. In order to better understand the effects of DAC one could assess DNA methylation using array technology. DAC treatment affects mainly genes located in open nuclear euchromatin conformation where DNMT1 is active and leads to mild but persistent loss of methylation and minimally altered transcription in stromal cells (297). DAC has also been described to induce point mutations and genome rearrangements (114). DNMTs are highly expressed in proliferating cells and DAC is therefore likely to exert a stronger effect than in quiescent cells or cells with relatively low proliferation rates such as activated cancer associated stromal cells. A cell type specific, but otherwise random effect would be expected to occur when low passage myofibroblasts are treated with DAC. DAC is a Food and Drug Administration (FDA) approved cytosine analogue for the treatment of chronic myelomonocytic leukaemia and myelodysplastic syndromes. A recent in vivo study demonstrated anti-proliferative effects of DAC on pulmonary myofibroblasts which show features of CAMs (298). Orskov and his colleagues observed in patients with myelodysplastic syndromes that DAC treatment leads to a hypomethylation and overexpression of PD-1 in CD8+ tumour T-cells which might lead to immunogenic exhaustion of the anti tumour immune response (299). Little is known on other effects of this agent on other stromal cells except for growth suppression as observed here. Importantly, though, persistent changes in myofibroblasts treated with DAC were found with respect to accelerated migration, contractility and invasion. Moreover, when DAC treated myofibroblasts were injected together with oesophageal cancer cells in nude mice, there was accelerated tumour growth. The model of epigenetic targeting of stromal cells in vitro and then the study of their influence on tumour growth in vivo is novel. It allows the investigation of epigenetic modification in stromal cells on tumour growth as compared to systemic drug application which would target all cells in the tumour microenvironment. DAC

has only recently been approved by the FDA and little is known of its long term effects. Our data and those of others would suggest that DAC can potentially transform myofibroblasts into activated myofibroblasts that support tumour growth. Importantly for the future, recent publications show that targeted modification of epigenetic signatures is possible (300, 301) and this might become a powerful tool to treat human disease.

11 Prospects

Cancer epigenetics are of dual interest. First they may explain pathological mechanisms of disease the understanding of which may lead to new discoveries (with the ultimate aim of improved treatment options and better patient outcome). Therapies interfering with epigenetic mechanisms have been recently introduced in anticancer therapy. Stromal cells as shown in this work and by others undergo epigenetic modifications that can lead to tumour initiation, propagation and metastasis. Understanding the causes of this epigenetic phenotype switch could lead to new targets for treatment.

Secondly, this work may facilitate the more successful prevention of cancer related death through tumour detection at an early or pre-invasive stage. In recent years sampling of cell-free circulating DNA has become a diagnostic minimally invasive tool for prenatal diagnostics (302) and detection of early tumour relapse (303). Advances in technology that allow detection of low levels of circulating nucleic acids could be applied not only to detect tumour derived circulating DNA but also inflammatory or stromal cell derived DNA methylation signatures. Fragments of the entire human genome have also been detected in extracellular vesicles such as exosomes. Exosomes can be isolated from blood but also from less invasively accessible body fluids such as saliva and urine. It remains to be elucidated whether extracellular vesicles carry methylated DNA and whether such is easily accessible for diagnostic purpose.

12 Abbreviations

AD	anno Domini
AGS	Gastric cancer cell line
ATM	adjacent tissue myofibroblast
BC	before Christ
BM-MSC	bone marrow derived MSC
CAM	cancer associated myofibroblast
CAS	cancer associated stromal cells
CCK	cholecystokinin receptor
CM	conditioned medium
DAC	5'Aza-3'deoxy cytosine
DAPI	4′,6-Diamidin-2-phenylindol
DNA	deoxyribonucleic acid
DNMT	DNA methyl transferase
EdU	5-ethynyl-2'-deoxyuridine
EMT	epithelial to mesenchymal transition
FDA	Food and Drug Administration
FFPE	formalin-fixed and paraffin embedded
HGF	Hepatocyte growth factor
HUVEC	human umbilical vein endothelial cell
IARC	International Agency for Research on Cancer
IGF	Insulin like growth factor
LINE	long interspersed transposable elements
miR	micro RNA
MKN45	Gastric cancer cell line
MM	myofibroblast medium
MMP	matrix metalloproteinase
MSC	mesenchymal stem cells
NSCLC	non-small cell lung cancer
NTM	normal tissue myofibroblasts
OEAC	adenocarcinoma of the oesophagus
OESCC	squamous cell carcinoma of the oesophagus
PDAC	pancreatic ductal adenocarcinoma
PDGF	platelet-derived growth factor
PITX	paired like homeodomain
RNA	ribonucleic acid
SCID	severe combined immunodeficiency
SCR	scrambled
SFM	serum free medium
SFRP	secreted frizzled like protein
siRNA	small interfering RNA
SMA	smooth muscle actin

TGF	transforming growth factor-b
TIMP	tissue inhibitor of metalloproteinase
VEGF	vascular endothelial growth factor
WHO	World Health Organisation

13 References

1. D.J.Th. W. The history of oncology. Houton: Springer Uitgeverij; 2009.
2. Leake CD. The Old Egyptian Medical Papyri Kansas USA: LAWRENCE, UNIVERSITY OF KANSAS PRESS; 1952 1952.
3. Dran H-FL. Consultations sur la pluspart des maladies qui sont du ressort de la chirurgie1765.
4. Morgagni G. De sedibus, et causis morborum per anatomen indagatis libri quinque1761.
5. Home SE. A short tract on the formation of tumours, and the peculiarities that are met within the structure of those who have become cancersous, with their mode of treatment. London: Longman, Rees, Orme, Brown, and Green; Paternoster-Row; 1830.
6. Müller J. Ueber den feinern Bau und die Formen der krankhaften Geschwülste1838.
7. Roguin A. Rene Theophile Hyacinthe Laennec (1781-1826): the man behind the stethoscope. Clin Med Res. 2006;4(3):230-5.
8. Hannover A. Das Epithelioma eine egentümliche Geschwulst, die man im allgemeinen bisher als Krebs angesehen hat. Leibzig: Leopold Voss; 1843.
9. Virchow R. Die Cellularpathologie in ihrer Begründung auf physiologische und pathologische Gewebelehre. 1 ed: Hirschwald, Berlin; 1858
10. Paget S. The distribution of secondary growths in cancer of the breast. 1889. Cancer metastasis reviews. 1889;8(2):98-101.
11. Shimkin MB. Arthur Nathan Hanau: a further note on the history of transplantation of tumors. Cancer. 1960;13:221.
12. Watson JD, Crick FH. Molecular structure of nucleic acids; a structure for deoxyribose nucleic acid. Nature. 1953;171(4356):737-8.
13. Dietel M. Boveri at 100: the life and times of Theodor Boveri. J Pathol. 2014;234(2):135-7.
14. Joe Hin Tjio AL. The chromosome number of man. Hereditas. 1956(42):1–6.
15. Nowell PC. Discovery of the Philadelphia chromosome: a personal perspective. J Clin Invest. 2007;117(8):2033-5.
16. de Klein A, van Kessel AG, Grosveld G, Bartram CR, Hagemeijer A, Bootsma D, et al. A cellular oncogene is translocated to the Philadelphia chromosome in chronic myelocytic leukaemia. Nature. 1982;300(5894):765-7.
17. Heisterkamp N, Stephenson JR, Groffen J, Hansen PF, de Klein A, Bartram CR, et al. Localization of the c-ab1 oncogene adjacent to a translocation break point in chronic myelocytic leukaemia. Nature. 1983;306(5940):239-42.

18. Southern EM. Detection of specific sequences among DNA fragments separated by gel electrophoresis. Journal of molecular biology. 1975;98(3):503-17.
19. Alwine JC, Kemp DJ, Stark GR. Method for detection of specific RNAs in agarose gels by transfer to diazobenzyloxymethyl-paper and hybridization with DNA probes. Proc Natl Acad Sci U S A. 1977;74(12):5350-4.
20. Burnette WN. "Western blotting": electrophoretic transfer of proteins from sodium dodecyl sulfate--polyacrylamide gels to unmodified nitrocellulose and radiographic detection with antibody and radioiodinated protein A. Analytical biochemistry. 1981;112(2):195-203.
21. Coons AH, Kaplan MH. Localization of antigen in tissue cells; improvements in a method for the detection of antigen by means of fluorescent antibody. The Journal of experimental medicine. 1950;91(1):1-13.
22. Nakane PK, Pierce GB, Jr. Enzyme-labeled antibodies: preparation and application for the localization of antigens. The journal of histochemistry and cytochemistry : official journal of the Histochemistry Society. 1966;14(12):929-31.
23. Mason DY, Sammons R. Alkaline phosphatase and peroxidase for double immunoenzymatic labelling of cellular constituents. Journal of clinical pathology. 1978;31(5):454-60.
24. Kleppe K, Ohtsuka E, Kleppe R, Molineux I, Khorana HG. Studies on polynucleotides. XCVI. Repair replications of short synthetic DNA's as catalyzed by DNA polymerases. Journal of molecular biology. 1971;56(2):341-61.
25. Mullis K, Faloona F, Scharf S, Saiki R, Horn G, Erlich H. Specific enzymatic amplification of DNA in vitro: the polymerase chain reaction. Cold Spring Harbor symposia on quantitative biology. 1986;51 Pt 1:263-73.
26. Mullis KB, Faloona FA. Specific synthesis of DNA in vitro via a polymerase-catalyzed chain reaction. Methods in enzymology. 1987;155:335-50.
27. Sanger F, Nicklen S, Coulson AR. DNA sequencing with chain-terminating inhibitors. Proc Natl Acad Sci U S A. 1977;74(12):5463-7.
28. Gregory SG, Barlow KF, McLay KE, Kaul R, Swarbreck D, Dunham A, et al. The DNA sequence and biological annotation of human chromosome 1. Nature. 2006;441(7091):315-21.
29. Langer-Safer PR, Levine M, Ward DC. Immunological method for mapping genes on Drosophila polytene chromosomes. Proc Natl Acad Sci U S A. 1982;79(14):4381-5.
30. Dietel M, Johrens K, Laffert M, Hummel M, Blaker H, Muller BM, et al. Predictive molecular pathology and its role in targeted cancer therapy: a review focussing on clinical relevance. Cancer gene therapy. 2013;20(4):211-21.
31. Dietel M, Johrens K, Laffert MV, Hummel M, Blaker H, Pfitzner BM, et al. A 2015 update on predictive molecular pathology and its role in targeted

cancer therapy: a review focussing on clinical relevance. Cancer gene therapy. 2015;22(9):417-30.
32. Cristofanilli M, Budd GT, Ellis MJ, Stopeck A, Matera J, Miller MC, et al. Circulating tumor cells, disease progression, and survival in metastatic breast cancer. The New England journal of medicine. 2004;351(8):781-91.
33. Cheng F, Su L, Qian C. Circulating tumor DNA: a promising biomarker in the liquid biopsy of cancer. Oncotarget. 2016.
34. Kinoshita T, Yip KW, Spence T, Liu FF. MicroRNAs in extracellular vesicles: potential cancer biomarkers. Journal of human genetics. 2016.
35. Kohler G, Milstein C. Continuous cultures of fused cells secreting antibody of predefined specificity. Nature. 1975;256(5517):495-7.
36. Montgomery MK, Xu S, Fire A. RNA as a target of double-stranded RNA-mediated genetic interference in Caenorhabditis elegans. Proc Natl Acad Sci U S A. 1998;95(26):15502-7.
37. Fire A, Xu S, Montgomery MK, Kostas SA, Driver SE, Mello CC. Potent and specific genetic interference by double-stranded RNA in Caenorhabditis elegans. Nature. 1998;391(6669):806-11.
38. Horvath P, Barrangou R. CRISPR/Cas, the immune system of bacteria and archaea. Science. 2010;327(5962):167-70.
39. McCarty PJ, Million RR. History of radiation oncology. The Journal of the Florida Medical Association. 1995;82(11):745-8.
40. Krumbhaar EB, Krumbhaar HD. The Blood and Bone Marrow in Yelloe Cross Gas (Mustard Gas) Poisoning: Changes produced in the Bone Marrow of Fatal Cases. The Journal of medical research. 1919;40(3):497-508 3.
41. Ritchie M. Alfred Gilman; 1908 - 1984. National Academies Press. 1996.
42. Farber S, Diamond LK. Temporary remissions in acute leukemia in children produced by folic acid antagonist, 4-aminopteroyl-glutamic acid. The New England journal of medicine. 1948;238(23):787-93.
43. Reports of Societies. British Medical Journal. 1896;1849(1):1386–8.
44. Haddow A, Watkinson JM, Paterson E, Koller PC. Influence of Synthetic Oestrogens on Advanced Malignant Disease. Br Med J. 1944;2(4368):393-8.
45. Savage DG, Antman KH. Imatinib mesylate--a new oral targeted therapy. The New England journal of medicine. 2002;346(9):683-93.
46. Shen J, Valero V, Buchholz TA, Singletary SE, Ames FC, Ross MI, et al. Effective local control and long-term survival in patients with T4 locally advanced breast cancer treated with breast conservation therapy. Annals of surgical oncology. 2004;11(9):854-60.
47. Yared MA, Middleton LP, Meric F, Cristofanilli M, Sahin AA. Expression of c-kit proto-oncogene product in breast tissue. The breast journal. 2004;10(4):323-7.
48. Juttermann R, Li E, Jaenisch R. Toxicity of 5-aza-2'-deoxycytidine to mammalian cells is mediated primarily by covalent trapping of DNA methyltransferase rather than DNA demethylation. Proc Natl Acad Sci U S A. 1994;91(25):11797-801.

49. Sorm F, Vesely J. Effect of 5-aza-2'-deoxycytidine against leukemic and hemopoietic tissues in AKR mice. Neoplasma. 1968;15(4):339-43.
50. Verma M, Banerjee HN. Epigenetic inhibitors. Methods Mol Biol. 2015;1238:469-85.
51. Vesalius A. De Humani Corporis Fabrica. Basel: Johannes Oporinus; 1543.
52. Baillie M. The morbid anatomy of some of the most important parts of the human body London: Barber & Southwick; 1793.
53. Hanahan D, Weinberg RA. The hallmarks of cancer. Cell. 2000;100(1):57-70.
54. Hanahan D, Weinberg RA. Hallmarks of cancer: the next generation. Cell. 2011;144(5):646-74.
55. McLare E. Deaths Registered in England and Wales in 2010, by Cause. 2011 28 October 2011.
56. Hinz B, Phan SH, Thannickal VJ, Galli A, Bochaton-Piallat ML, Gabbiani G. The myofibroblast: one function, multiple origins. The American journal of pathology. 2007;170(6):1807-16.
57. Hanahan D, Coussens LM. Accessories to the crime: functions of cells recruited to the tumor microenvironment. Cancer Cell. 2012;21(3):309-22.
58. Serini G, Bochaton-Piallat ML, Ropraz P, Geinoz A, Borsi L, Zardi L, et al. The fibronectin domain ED-A is crucial for myofibroblastic phenotype induction by transforming growth factor-beta1. The Journal of cell biology. 1998;142(3):873-81.
59. Noma K, Smalley KS, Lioni M, Naomoto Y, Tanaka N, El-Deiry W, et al. The essential role of fibroblasts in esophageal squamous cell carcinoma-induced angiogenesis. Gastroenterology. 2008;134(7):1981-93.
60. Fuyuhiro Y, Yashiro M, Noda S, Kashiwagi S, Matsuoka J, Doi Y, et al. Upregulation of cancer-associated myofibroblasts by TGF-beta from scirrhous gastric carcinoma cells. Br J Cancer. 2011;105(7):996-1001.
61. Cadamuro M, Nardo G, Indraccolo S, Dall'olmo L, Sambado L, Moserle L, et al. Platelet-derived growth factor-D and Rho GTPases regulate recruitment of cancer-associated fibroblasts in cholangiocarcinoma. Hepatology. 2013;58(3):1042-53.
62. Heldin CH. Targeting the PDGF signaling pathway in tumor treatment. Cell Commun Signal. 2013;11:97.
63. Lewis MP, Lygoe KA, Nystrom ML, Anderson WP, Speight PM, Marshall JF, et al. Tumour-derived TGF-beta1 modulates myofibroblast differentiation and promotes HGF/SF-dependent invasion of squamous carcinoma cells. Br J Cancer. 2004;90(4):822-32.
64. Semba S, Kodama Y, Ohnuma K, Mizuuchi E, Masuda R, Yashiro M, et al. Direct cancer-stromal interaction increases fibroblast proliferation and enhances invasive properties of scirrhous-type gastric carcinoma cells. Br J Cancer. 2009;101(8):1365-73.
65. Bucala R, Spiegel LA, Chesney J, Hogan M, Cerami A. Circulating fibrocytes define a new leukocyte subpopulation that mediates tissue repair. Molecular medicine. 1994;1(1):71-81.

66. Quante M, Tu SP, Tomita H, Gonda T, Wang SS, Takashi S, et al. Bone marrow-derived myofibroblasts contribute to the mesenchymal stem cell niche and promote tumor growth. Cancer Cell. 2011;19(2):257-72.
67. Johann PD, Muller I. Multipotent Mesenchymal Stromal Cells: Possible Culprits in Solid Tumors? Stem cells international. 2015;2015:914632.
68. Terai S, Fushida S, Tsukada T, Kinoshita J, Oyama K, Okamoto K, et al. Bone marrow derived "fibrocytes" contribute to tumor proliferation and fibrosis in gastric cancer. Gastric cancer : official journal of the International Gastric Cancer Association and the Japanese Gastric Cancer Association. 2015;18(2):306-13.
69. Gascard P, Tlsty TD. Carcinoma-associated fibroblasts: orchestrating the composition of malignancy. Genes Dev. 2016;30(9):1002-19.
70. Garin-Chesa P, Old LJ, Rettig WJ. Cell surface glycoprotein of reactive stromal fibroblasts as a potential antibody target in human epithelial cancers. Proc Natl Acad Sci U S A. 1990;87(18):7235-9.
71. De Wever O, Demetter P, Mareel M, Bracke M. Stromal myofibroblasts are drivers of invasive cancer growth. Int J Cancer. 2008;123(10):2229-38.
72. Varro A. Stromal Cells and Tumor Microenvironment. In: Wang TC, editor. Biology of Gastric Cancers2008.
73. Gonda TA, Varro A, Wang TC, Tycko B. Molecular biology of cancer-associated fibroblasts: can these cells be targeted in anti-cancer therapy? Semin Cell Dev Biol. 2010;21(1):2-10.
74. Ohtani H, Sasano N. Stromal cell changes in human colorectal adenomas and carcinomas. An ultrastructural study of fibroblasts, myofibroblasts, and smooth muscle cells. Virchows Archiv A, Pathological anatomy and histopathology. 1983;401(2):209-22.
75. Lund LR, Riccio A, Andreasen PA, Nielsen LS, Kristensen P, Laiho M, et al. Transforming growth factor-beta is a strong and fast acting positive regulator of the level of type-1 plasminogen activator inhibitor mRNA in WI-38 human lung fibroblasts. EMBO J. 1987;6(5):1281-6.
76. Hakelius M, Koskela A, Ivarsson M, Grenman R, Rubin K, Gerdin B, et al. Keratinocytes and head and neck squamous cell carcinoma cells regulate urokinase-type plasminogen activator and plasminogen activator inhibitor-1 in fibroblasts. Anticancer research. 2013;33(8):3113-8.
77. Hawinkels LJ, Paauwe M, Verspaget HW, Wiercinska E, van der Zon JM, van der Ploeg K, et al. Interaction with colon cancer cells hyperactivates TGF-beta signaling in cancer-associated fibroblasts. Oncogene. 2014;33(1):97-107.
78. Desmouliere A, Geinoz A, Gabbiani F, Gabbiani G. Transforming growth factor-beta 1 induces alpha-smooth muscle actin expression in granulation tissue myofibroblasts and in quiescent and growing cultured fibroblasts. The Journal of cell biology. 1993;122(1):103-11.
79. Ronnov-Jessen L, Petersen OW. Induction of alpha-smooth muscle actin by transforming growth factor-beta 1 in quiescent human breast gland fibroblasts. Implications for myofibroblast generation in breast

neoplasia. Laboratory investigation; a journal of technical methods and pathology. 1993;68(6):696-707.
80. Kosmehl H, Berndt A, Strassburger S, Borsi L, Rousselle P, Mandel U, et al. Distribution of laminin and fibronectin isoforms in oral mucosa and oral squamous cell carcinoma. Br J Cancer. 1999;81(6):1071-9.
81. Holmberg C, Ghesquiere B, Impens F, Gevaert K, Kumar JD, Cash N, et al. Mapping proteolytic processing in the secretome of gastric cancer-associated myofibroblasts reveals activation of MMP-1, MMP-2, and MMP-3. Journal of proteome research. 2013;12(7):3413-22.
82. Navab R, Strumpf D, Bandarchi B, Zhu CQ, Pintilie M, Ramnarine VR, et al. Prognostic gene-expression signature of carcinoma-associated fibroblasts in non-small cell lung cancer. Proc Natl Acad Sci U S A. 2011;108(17):7160-5.
83. Tchou J, Kossenkov AV, Chang L, Satija C, Herlyn M, Showe LC, et al. Human breast cancer associated fibroblasts exhibit subtype specific gene expression profiles. BMC Med Genomics. 2012;5:39.
84. Underwood TJ, Hayden AL, Derouet M, Garcia E, Noble F, White MJ, et al. Cancer-associated fibroblasts predict poor outcome and promote periostin-dependent invasion in oesophageal adenocarcinoma. J Pathol. 2015;235(3):466-77.
85. Mrazek AA, Carmical JR, Wood TG, Hellmich MR, Eltorky M, Bohanon FJ, et al. Colorectal Cancer-Associated Fibroblasts are Genotypically Distinct. Current cancer therapy reviews. 2014;10(2):97-218.
86. Higuchi Y, Kojima M, Ishii G, Aoyagi K, Sasaki H, Ochiai A. Gastrointestinal Fibroblasts Have Specialized, Diverse Transcriptional Phenotypes: A Comprehensive Gene Expression Analysis of Human Fibroblasts. PLoS One. 2015;10(6):e0129241.
87. Wang L, Steele I, Kumar JD, Dimaline R, Jithesh PV, Tiszlavicz L, et al. Distinct miRNA profiles in normal and gastric cancer myofibroblasts and significance in Wnt signalling. American journal of physiology Gastrointestinal and liver physiology. 2016:ajpgi 00443 2015.
88. Orimo A, Gupta PB, Sgroi DC, Arenzana-Seisdedos F, Delaunay T, Naeem R, et al. Stromal fibroblasts present in invasive human breast carcinomas promote tumor growth and angiogenesis through elevated SDF-1/CXCL12 secretion. Cell. 2005;121(3):335-48.
89. Lau EY, Lo J, Cheng BY, Ma MK, Lee JM, Ng JK, et al. Cancer-Associated Fibroblasts Regulate Tumor-Initiating Cell Plasticity in Hepatocellular Carcinoma through c-Met/FRA1/HEY1 Signaling. Cell Rep. 2016;15(6):1175-89.
90. Hwang RF, Moore T, Arumugam T, Ramachandran V, Amos KD, Rivera A, et al. Cancer-associated stromal fibroblasts promote pancreatic tumor progression. Cancer Res. 2008;68(3):918-26.
91. Leali D, Dell'Era P, Stabile H, Sennino B, Chambers AF, Naldini A, et al. Osteopontin (Eta-1) and fibroblast growth factor-2 cross-talk in angiogenesis. Journal of immunology. 2003;171(2):1085-93.
92. Anderberg C, Li H, Fredriksson L, Andrae J, Betsholtz C, Li X, et al. Paracrine signaling by platelet-derived growth factor-CC promotes tumor

growth by recruitment of cancer-associated fibroblasts. Cancer Res. 2009;69(1):369-78.
93. Vong S, Kalluri R. The role of stromal myofibroblast and extracellular matrix in tumor angiogenesis. Genes & cancer. 2011;2(12):1139-45.
94. Holmberg C, Quante M, Steele I, Kumar JD, Balabanova S, Duval C, et al. Release of TGFbetaig-h3 by gastric myofibroblasts slows tumor growth and is decreased with cancer progression. Carcinogenesis. 2012;33(8):1553-62.
95. Kumar JD, Holmberg C, Kandola S, Steele I, Hegyi P, Tiszlavicz L, et al. Increased expression of chemerin in squamous esophageal cancer myofibroblasts and role in recruitment of mesenchymal stromal cells. PLoS One. 2014;9(7):e104877.
96. Paunescu V, Bojin FM, Tatu CA, Gavriliuc OI, Rosca A, Gruia AT, et al. Tumour-associated fibroblasts and mesenchymal stem cells: more similarities than differences. Journal of cellular and molecular medicine. 2011;15(3):635-46.
97. Kandola Sa, Varro Ads, Dockray Gds. The role of extracellular proteases in stromal-epithelial interactions in gastric cancer [Thesis (Ph.D.)]: University of Liverpool; 2014.
98. Schneiderhan W, Diaz F, Fundel M, Zhou S, Siech M, Hasel C, et al. Pancreatic stellate cells are an important source of MMP-2 in human pancreatic cancer and accelerate tumor progression in a murine xenograft model and CAM assay. Journal of cell science. 2007;120(Pt 3):512-9.
99. Wu H, Zhang Y. Reversing DNA methylation: mechanisms, genomics, and biological functions. Cell. 2014;156(1-2):45-68.
100. Du J, Johnson LM, Jacobsen SE, Patel DJ. DNA methylation pathways and their crosstalk with histone methylation. Nature reviews Molecular cell biology. 2015;16(9):519-32.
101. Feinberg AP. Epigenetic stochasticity, nuclear structure and cancer: the implications for medicine. Journal of internal medicine. 2014;276(1):5-11.
102. Holoch D, Moazed D. RNA-mediated epigenetic regulation of gene expression. Nature reviews Genetics. 2015;16(2):71-84.
103. Blackledge NP, Rose NR, Klose RJ. Targeting Polycomb systems to regulate gene expression: modifications to a complex story. Nature reviews Molecular cell biology. 2015;16(11):643-9.
104. Halfmann R, Lindquist S. Epigenetics in the extreme: prions and the inheritance of environmentally acquired traits. Science. 2010;330(6004):629-32.
105. Berdasco M, Esteller M. Aberrant epigenetic landscape in cancer: how cellular identity goes awry. Developmental cell. 2010;19(5):698-711.
106. Daskalos A, Nikolaidis G, Xinarianos G, Savvari P, Cassidy A, Zakopoulou R, et al. Hypomethylation of retrotransposable elements correlates with genomic instability in non-small cell lung cancer. Int J Cancer. 2009;124(1):81-7.
107. Pogribny IP, Beland FA. DNA hypomethylation in the origin and pathogenesis of human diseases. Cellular and molecular life sciences : CMLS. 2009;66(14):2249-61.

108. Vizoso M, Puig M, Carmona FJ, Maqueda M, Velasquez A, Gomez A, et al. Aberrant DNA methylation in Non Small Cell Lung Cancer associated fibroblasts. Carcinogenesis. 2015.
109. Jiang L, Gonda TA, Gamble MV, Salas M, Seshan V, Tu S, et al. Global hypomethylation of genomic DNA in cancer-associated myofibroblasts. Cancer Res. 2008;68(23):9900-8.
110. Yu J, Walter K, Omura N, Hong SM, Young A, Li A, et al. Unlike pancreatic cancer cells pancreatic cancer associated fibroblasts display minimal gene induction after 5-aza-2'-deoxycytidine. PLoS One. 2012;7(9):e43456.
111. Chen ZX, Riggs AD. DNA methylation and demethylation in mammals. J Biol Chem. 2011;286(21):18347-53.
112. Griffiths EA, Gore SD. Epigenetic therapies in MDS and AML. Advances in experimental medicine and biology. 2013;754:253-83.
113. Liang G, Gonzales FA, Jones PA, Orntoft TF, Thykjaer T. Analysis of gene induction in human fibroblasts and bladder cancer cells exposed to the methylation inhibitor 5-aza-2'-deoxycytidine. Cancer Res. 2002;62(4):961-6.
114. Maslov AY, Lee M, Gundry M, Gravina S, Strogonova N, Tazearslan C, et al. 5-aza-2'-deoxycytidine-induced genome rearrangements are mediated by DNMT1. Oncogene. 2012;31(50):5172-9.
115. Soria C, Estermann FE, Espantman KC, O'Shea CC. Heterochromatin silencing of p53 target genes by a small viral protein. Nature. 2010;466(7310):1076-81.
116. Zhu Q, Pao GM, Huynh AM, Suh H, Tonnu N, Nederlof PM, et al. BRCA1 tumour suppression occurs via heterochromatin-mediated silencing. Nature. 2011;477(7363):179-84.
117. Yu W, Gius D, Onyango P, Muldoon-Jacobs K, Karp J, Feinberg AP, et al. Epigenetic silencing of tumour suppressor gene p15 by its antisense RNA. Nature. 2008;451(7175):202-6.
118. Martin V, Ribieras S, Song-Wang XG, Lasne Y, Frappart L, Rio MC, et al. Involvement of DNA methylation in the control of the expression of an estrogen-induced breast-cancer-associated protein (pS2) in human breast cancers. Journal of cellular biochemistry. 1997;65(1):95-106.
119. Watt PM, Kumar R, Kees UR. Promoter demethylation accompanies reactivation of the HOX11 proto-oncogene in leukemia. Genes, chromosomes & cancer. 2000;29(4):371-7.
120. Merlo A, Herman JG, Mao L, Lee DJ, Gabrielson E, Burger PC, et al. 5' CpG island methylation is associated with transcriptional silencing of the tumour suppressor p16/CDKN2/MTS1 in human cancers. Nature medicine. 1995;1(7):686-92.
121. Veigl ML, Kasturi L, Olechnowicz J, Ma AH, Lutterbaugh JD, Periyasamy S, et al. Biallelic inactivation of hMLH1 by epigenetic gene silencing, a novel mechanism causing human MSI cancers. Proc Natl Acad Sci U S A. 1998;95(15):8698-702.
122. Hu M, Yao J, Cai L, Bachman KE, van den Brule F, Velculescu V, et al. Distinct epigenetic changes in the stromal cells of breast cancers. Nat Genet. 2005;37(8):899-905.

123. Banerjee J, Mishra R, Li X, Jackson RS, 2nd, Sharma A, Bhowmick NA. A reciprocal role of prostate cancer on stromal DNA damage. Oncogene. 2014;33(41):4924-31.
124. Li P, Shan JX, Chen XH, Zhang D, Su LP, Huang XY, et al. Epigenetic silencing of microRNA-149 in cancer-associated fibroblasts mediates prostaglandin E2/interleukin-6 signaling in the tumor microenvironment. Cell research. 2015;25(5):588-603.
125. Kurashige J, Mima K, Sawada G, Takahashi Y, Eguchi H, Sugimachi K, et al. Epigenetic modulation and repression of miR-200b by cancer-associated fibroblasts contribute to cancer invasion and peritoneal dissemination in gastric cancer. Carcinogenesis. 2015;36(1):133-41.
126. Bosman FT, World Health Organization., International Agency for Research on Cancer. WHO classification of tumours of the digestive system. Lyon: IARC Press; 2010. 417 p. p.
127. Pennathur A, Gibson MK, Jobe BA, Luketich JD. Oesophageal carcinoma. Lancet. 2013;381(9864):400-12.
128. Napier KJ, Scheerer M, Misra S. Esophageal cancer: A Review of epidemiology, pathogenesis, staging workup and treatment modalities. World journal of gastrointestinal oncology. 2014;6(5):112-20.
129. Prabhu A, Obi KO, Rubenstein JH. Systematic review with meta-analysis: race-specific effects of alcohol and tobacco on the risk of oesophageal squamous cell carcinoma. Aliment Pharmacol Ther. 2013;38(10):1145-55.
130. Reid BJ, Paulson TG, Li X. Genetic Insights in Barrett's Esophagus and Esophageal Adenocarcinoma. Gastroenterology. 2015;149(5):1142-52 e3.
131. Hayakawa Y, Sethi N, Sepulveda AR, Bass AJ, Wang TC. Oesophageal adenocarcinoma and gastric cancer: should we mind the gap? Nature reviews Cancer. 2016;16(5):305-18.
132. Kapoor H, Lohani KR, Lee TH, Agrawal DK, Mittal SK. Animal Models of Barrett's Esophagus and Esophageal Adenocarcinoma-Past, Present, and Future. Clin Transl Sci. 2015;8(6):841-7.
133. Tetreault MP. Esophageal Cancer: Insights From Mouse Models. Cancer Growth Metastasis. 2015;8(Suppl 1):37-46.
134. Ito R, Takahashi T, Katano I, Ito M. Current advances in humanized mouse models. Cellular & molecular immunology. 2012;9(3):208-14.
135. MacDonald BT, Tamai K, He X. Wnt/beta-catenin signaling: components, mechanisms, and diseases. Developmental cell. 2009;17(1):9-26.
136. Song X, Wang S, Li L. New insights into the regulation of Axin function in canonical Wnt signaling pathway. Protein & cell. 2014;5(3):186-93.
137. Mayr T, Deutsch U, Kuhl M, Drexler HC, Lottspeich F, Deutzmann R, et al. Fritz: a secreted frizzled-related protein that inhibits Wnt activity. Mechanisms of development. 1997;63(1):109-25.
138. Leyns L, Bouwmeester T, Kim SH, Piccolo S, De Robertis EM. Frzb-1 is a secreted antagonist of Wnt signaling expressed in the Spemann organizer. Cell. 1997;88(6):747-56.

139. Wang S, Krinks M, Lin K, Luyten FP, Moos M, Jr. Frzb, a secreted protein expressed in the Spemann organizer, binds and inhibits Wnt-8. Cell. 1997;88(6):757-66.
140. Valcz G, Patai AV, Kalmar A, Peterfia B, Furi I, Wichmann B, et al. Myofibroblast-derived SFRP1 as potential inhibitor of colorectal carcinoma field effect. PLoS One. 2014;9(11):e106143.
141. Leimeister C, Bach A, Gessler M. Developmental expression patterns of mouse sFRP genes encoding members of the secreted frizzled related protein family. Mechanisms of development. 1998;75(1-2):29-42.
142. Voorham QJ, Janssen J, Tijssen M, Snellenberg S, Mongera S, van Grieken NC, et al. Promoter methylation of Wnt-antagonists in polypoid and nonpolypoid colorectal adenomas. BMC cancer. 2013;13:603.
143. Silva AL, Dawson SN, Arends MJ, Guttula K, Hall N, Cameron EA, et al. Boosting Wnt activity during colorectal cancer progression through selective hypermethylation of Wnt signaling antagonists. BMC cancer. 2014;14:891.
144. Urakami S, Shiina H, Enokida H, Kawakami T, Kawamoto K, Hirata H, et al. Combination analysis of hypermethylated Wnt-antagonist family genes as a novel epigenetic biomarker panel for bladder cancer detection. Clin Cancer Res. 2006;12(7 Pt 1):2109-16.
145. Urakami S, Shiina H, Enokida H, Hirata H, Kawamoto K, Kawakami T, et al. Wnt antagonist family genes as biomarkers for diagnosis, staging, and prognosis of renal cell carcinoma using tumor and serum DNA. Clin Cancer Res. 2006;12(23):6989-97.
146. Marsit CJ, McClean MD, Furniss CS, Kelsey KT. Epigenetic inactivation of the SFRP genes is associated with drinking, smoking and HPV in head and neck squamous cell carcinoma. Int J Cancer. 2006;119(8):1761-6.
147. Nojima M, Suzuki H, Toyota M, Watanabe Y, Maruyama R, Sasaki S, et al. Frequent epigenetic inactivation of SFRP genes and constitutive activation of Wnt signaling in gastric cancer. Oncogene. 2007;26(32):4699-713.
148. Saito T, Mitomi H, Imamhasan A, Hayashi T, Mitani K, Takahashi M, et al. Downregulation of sFRP-2 by epigenetic silencing activates the beta-catenin/Wnt signaling pathway in esophageal basaloid squamous cell carcinoma. Virchows Archiv : an international journal of pathology. 2014;464(2):135-43.
149. Qi J, Zhu YQ, Luo J, Tao WH. Hypermethylation and expression regulation of secreted frizzled-related protein genes in colorectal tumor. World J Gastroenterol. 2006;12(44):7113-7.
150. Oberwalder M, Zitt M, Wontner C, Fiegl H, Goebel G, Zitt M, et al. SFRP2 methylation in fecal DNA--a marker for colorectal polyps. International journal of colorectal disease. 2008;23(1):15-9.
151. Kohno H, Amatya VJ, Takeshima Y, Kushitani K, Hattori N, Kohno N, et al. Aberrant promoter methylation of WIF-1 and SFRP1, 2, 4 genes in mesothelioma. Oncology reports. 2010;24(2):423-31.
152. Kalmar A, Peterfia B, Hollosi P, Galamb O, Spisak S, Wichmann B, et al. DNA hypermethylation and decreased mRNA expression of MAL,

PRIMA1, PTGDR and SFRP1 in colorectal adenoma and cancer. BMC cancer. 2015;15:736.
153. Sui C, Ma J, Chen Q, Yang Y. The variation trends of SFRP2 methylation of tissue, feces, and blood detection in colorectal cancer development. European journal of cancer prevention : the official journal of the European Cancer Prevention Organisation. 2015.
154. Kaur A, Webster MR, Marchbank K, Behera R, Ndoye A, Kugel CH, 3rd, et al. sFRP2 in the aged microenvironment drives melanoma metastasis and therapy resistance. Nature. 2016;532(7598):250-4.
155. Basu M, Roy SS. Wnt/beta-catenin pathway is regulated by PITX2 homeodomain protein and thus contributes to the proliferation of human ovarian adenocarcinoma cell, SKOV-3. J Biol Chem. 2013;288(6):4355-67.
156. Campbell AL, Shih HP, Xu J, Gross MK, Kioussi C. Regulation of motility of myogenic cells in filling limb muscle anlagen by Pitx2. PLoS One. 2012;7(4):e35822.
157. Kioussi C, Briata P, Baek SH, Rose DW, Hamblet NS, Herman T, et al. Identification of a Wnt/Dvl/beta-Catenin --> Pitx2 pathway mediating cell-type-specific proliferation during development. Cell. 2002;111(5):673-85.
158. Liu W, Selever J, Lu MF, Martin JF. Genetic dissection of Pitx2 in craniofacial development uncovers new functions in branchial arch morphogenesis, late aspects of tooth morphogenesis and cell migration. Development. 2003;130(25):6375-85.
159. Liu Y, Huang Y, Fan J, Zhu GZ. PITX2 associates with PTIP-containing histone H3 lysine 4 methyltransferase complex. Biochemical and biophysical research communications. 2014;444(4):634-7.
160. Reis LM, Tyler RC, Volkmann Kloss BA, Schilter KF, Levin AV, Lowry RB, et al. PITX2 and FOXC1 spectrum of mutations in ocular syndromes. European journal of human genetics : EJHG. 2012;20(12):1224-33.
161. Strand SH, Orntoft TF, Sorensen KD. Prognostic DNA methylation markers for prostate cancer. International journal of molecular sciences. 2014;15(9):16544-76.
162. Carol Tullo CoHMsSOaQsPoAoP. Human Tissue Act. 2004.
163. II E. Animals (Scientific Procedures) Act 1986. 2013.
164. Rockett JC, Larkin K, Darnton SJ, Morris AG, Matthews HR. Five newly established oesophageal carcinoma cell lines: phenotypic and immunological characterization. Br J Cancer. 1997;75(2):258-63.
165. Wu KC, Jackson LM, Galvin AM, Gray T, Hawkey CJ, Mahida YR. Phenotypic and functional characterisation of myofibroblasts, macrophages, and lymphocytes migrating out of the human gastric lamina propria following the loss of epithelial cells. Gut. 1999;44(3):323-30.
166. McCaig C, Duval C, Hemers E, Steele I, Pritchard DM, Przemeck S, et al. The role of matrix metalloproteinase-7 in redefining the gastric microenvironment in response to Helicobacter pylori. Gastroenterology. 2006;130(6):1754-63.

167. Balabanova S, Holmberg C, Steele I, Ebrahimi B, Rainbow L, Burdyga T, et al. The neuroendocrine phenotype of gastric myofibroblasts and its loss with cancer progression. Carcinogenesis. 2014;35(8):1798-806.

168. Kemeny LV, Schnur A, Czepan M, Rakonczay Z, Jr., Gal E, Lonovics J, et al. Na+/Ca2+ exchangers regulate the migration and proliferation of human gastric myofibroblasts. American journal of physiology Gastrointestinal and liver physiology. 2013;305(8):G552-63.
169. Kumar JD, Steele I, Moore AR, Murugesan SV, Rakonczay Z, Venglovecz V, et al. Gastrin stimulates MMP-1 expression in gastric epithelial cells: putative role in gastric epithelial cell migration. American journal of physiology Gastrointestinal and liver physiology. 2015;309(2):G78-86.
170. Kumar JD, Varro A, Dockray G. Novel stromal cell signalling systems in oesophageal cancer [Thesis (Ph.D.)]: Institute of Translational Medicine,University of Liverpool; 2013.
171. Boyden S. The chemotactic effect of mixtures of antibody and antigen on polymorphonuclear leucocytes. The Journal of experimental medicine. 1962;115:453-66.
172. Rostovtsev VV, Green LG, Fokin VV, Sharpless KB. A stepwise huisgen cycloaddition process: copper(I)-catalyzed regioselective "ligation" of azides and terminal alkynes. Angewandte Chemie. 2002;41(14):2596-9.
173. Salic A, Mitchison TJ. A chemical method for fast and sensitive detection of DNA synthesis in vivo. Proc Natl Acad Sci U S A. 2008;105(7):2415-20.
174. Smola H, Thiekotter G, Fusenig NE. Mutual induction of growth factor gene expression by epidermal-dermal cell interaction. The Journal of cell biology. 1993;122(2):417-29.
175. Nystrom ML, Thomas GJ, Stone M, Mackenzie IC, Hart IR, Marshall JF. Development of a quantitative method to analyse tumour cell invasion in organotypic culture. J Pathol. 2005;205(4):468-75.
176. Bantly AD, Gray BD, Breslin E, Weinstein EG, Muirhead KA, Ohlsson-Wilhelm BM, et al. CellVue Claret, a new far-red dye, facilitates polychromatic assessment of immune cell proliferation. Immunological investigations. 2007;36(5-6):581-605.
177. Wallace PK, Tario JD, Jr., Fisher JL, Wallace SS, Ernstoff MS, Muirhead KA. Tracking antigen-driven responses by flow cytometry: monitoring proliferation by dye dilution. Cytometry Part A : the journal of the International Society for Analytical Cytology. 2008;73(11):1019-34.
178. Lawley TJ, Kubota Y. Induction of morphologic differentiation of endothelial cells in culture. The Journal of investigative dermatology. 1989;93(2 Suppl):59S-61S.
179. Bishop ET, Bell GT, Bloor S, Broom IJ, Hendry NF, Wheatley DN. An in vitro model of angiogenesis: basic features. Angiogenesis. 1999;3(4):335-44.
180. Donovan D, Brown NJ, Bishop ET, Lewis CE. Comparison of three in vitro human 'angiogenesis' assays with capillaries formed in vivo. Angiogenesis. 2001;4(2):113-21.

181. Carpentier G. Angiogenesis Analyzer. 2012.
182. Neumann E, Schaefer-Ridder M, Wang Y, Hofschneider PH. Gene transfer into mouse lyoma cells by electroporation in high electric fields. EMBO J. 1982;1(7):841-5.
183. Rygaard J, Povlsen CO. Heterotransplantation of a human malignant tumour to "Nude" mice. Acta pathologica et microbiologica Scandinavica. 1969;77(4):758-60.
184. Noble PJ, Wilde G, White MR, Pennington SR, Dockray GJ, Varro A. Stimulation of gastrin-CCKB receptor promotes migration of gastric AGS cells via multiple paracrine pathways. American journal of physiology Gastrointestinal and liver physiology. 2003;284(1):G75-84.
185. Imbeaud S, Graudens E, Boulanger V, Barlet X, Zaborski P, Eveno E, et al. Towards standardization of RNA quality assessment using user-independent classifiers of microcapillary electrophoresis traces. Nucleic acids research. 2005;33(6):e56.
186. Schroeder A, Mueller O, Stocker S, Salowsky R, Leiber M, Gassmann M, et al. The RIN: an RNA integrity number for assigning integrity values to RNA measurements. BMC molecular biology. 2006;7:3.
187. Frommer M, McDonald LE, Millar DS, Collis CM, Watt F, Grigg GW, et al. A genomic sequencing protocol that yields a positive display of 5-methylcytosine residues in individual DNA strands. Proc Natl Acad Sci U S A. 1992;89(5):1827-31.
188. Garner DL, Johnson LA, Yue ST, Roth BL, Haugland RP. Dual DNA staining assessment of bovine sperm viability using SYBR-14 and propidium iodide. Journal of andrology. 1994;15(6):620-9.
189. Singer VL, Lawlor TE, Yue S. Comparison of SYBR Green I nucleic acid gel stain mutagenicity and ethidium bromide mutagenicity in the Salmonella/mammalian microsome reverse mutation assay (Ames test). Mutat Res. 1999;439(1):37-47.
190. Livak KJ, Schmittgen TD. Analysis of relative gene expression data using real-time quantitative PCR and the 2(-Delta Delta C(T)) Method. Methods. 2001;25(4):402-8.
191. Ronaghi M, Karamohamed S, Pettersson B, Uhlen M, Nyren P. Real-time DNA sequencing using detection of pyrophosphate release. Analytical biochemistry. 1996;242(1):84-9.
192. Ronaghi M, Uhlen M, Nyren P. A sequencing method based on real-time pyrophosphate. Science. 1998;281(5375):363, 5.
193. Sanger F, Coulson AR. A rapid method for determining sequences in DNA by primed synthesis with DNA polymerase. Journal of molecular biology. 1975;94(3):441-8.
194. Assenov Y, Muller F, Lutsik P, Walter J, Lengauer T, Bock C. Comprehensive analysis of DNA methylation data with RnBeads. Nature methods. 2014;11(11):1138-40.
195. Du P, Kibbe WA, Lin SM. lumi: a pipeline for processing Illumina microarray. Bioinformatics. 2008;24(13):1547-8.
196. Ritchie ME, Phipson B, Wu D, Hu Y, Law CW, Shi W, et al. limma powers differential expression analyses for RNA-sequencing and microarray studies. Nucleic acids research. 2015;43(7):e47.

197. Mossman D, Kim KT, Scott RJ. Demethylation by 5-aza-2'-deoxycytidine in colorectal cancer cells targets genomic DNA whilst promoter CpG island methylation persists. BMC cancer. 2010;10:366.
198. Wijermans PW, Krulder JW, Huijgens PC, Neve P. Continuous infusion of low-dose 5-Aza-2'-deoxycytidine in elderly patients with high-risk myelodysplastic syndrome. Leukemia. 1997;11(1):1-5.
199. Cheishvili D, Boureau L, Szyf M. DNA demethylation and invasive cancer: implications for therapeutics. British journal of pharmacology. 2015;172(11):2705-15.
200. Bird AP. CpG-rich islands and the function of DNA methylation. Nature. 1986;321(6067):209-13.
201. Jiang BH, Liu LZ. PI3K/PTEN signaling in angiogenesis and tumorigenesis. Advances in cancer research. 2009;102:19-65.
202. Herman JG, Umar A, Polyak K, Graff JR, Ahuja N, Issa JP, et al. Incidence and functional consequences of hMLH1 promoter hypermethylation in colorectal carcinoma. Proc Natl Acad Sci U S A. 1998;95(12):6870-5.
203. Aaltonen LA, Peltomaki P, Leach FS, Sistonen P, Pylkkanen L, Mecklin JP, et al. Clues to the pathogenesis of familial colorectal cancer. Science. 1993;260(5109):812-6.
204. Simpkins SB, Bocker T, Swisher EM, Mutch DG, Gersell DJ, Kovatich AJ, et al. MLH1 promoter methylation and gene silencing is the primary cause of microsatellite instability in sporadic endometrial cancers. Human molecular genetics. 1999;8(4):661-6.
205. Klump B, Hsieh CJ, Holzmann K, Gregor M, Porschen R. Hypermethylation of the CDKN2/p16 promoter during neoplastic progression in Barrett's esophagus. Gastroenterology. 1998;115(6):1381-6.
206. Carethers JM, Chauhan DP, Fink D, Nebel S, Bresalier RS, Howell SB, et al. Mismatch repair proficiency and in vitro response to 5-fluorouracil. Gastroenterology. 1999;117(1):123-31.
207. Li Y, Yang Y, Lu Y, Herman JG, Brock MV, Zhao P, et al. Predictive value of CHFR and MLH1 methylation in human gastric cancer. Gastric cancer : official journal of the International Gastric Cancer Association and the Japanese Gastric Cancer Association. 2015;18(2):280-7.
208. Plumb JA, Strathdee G, Sludden J, Kaye SB, Brown R. Reversal of drug resistance in human tumor xenografts by 2'-deoxy-5-azacytidine-induced demethylation of the hMLH1 gene promoter. Cancer Res. 2000;60(21):6039-44.
209. Ehrlich M. DNA methylation in cancer: too much, but also too little. Oncogene. 2002;21(35):5400-13.
210. Shakya R, Gonda T, Quante M, Salas M, Kim S, Brooks J, et al. Hypomethylating therapy in an aggressive stroma-rich model of pancreatic carcinoma. Cancer Res. 2013;73(2):885-96.
211. Holliday R. Strong effects of 5-azacytidine on the in vitro lifespan of human diploid fibroblasts. Experimental cell research. 1986;166(2):543-52.

212. Rasanen K, Vaheri A. Proliferation and motility of HaCaT keratinocyte derivatives is enhanced by fibroblast nemosis. Experimental cell research. 2010;316(10):1739-47.
213. Vaheri A, Enzerink A, Rasanen K, Salmenpera P. Nemosis, a novel way of fibroblast activation, in inflammation and cancer. Experimental cell research. 2009;315(10):1633-8.
214. Kankuri E, Cholujova D, Comajova M, Vaheri A, Bizik J. Induction of hepatocyte growth factor/scatter factor by fibroblast clustering directly promotes tumor cell invasiveness. Cancer Res. 2005;65(21):9914-22.
215. Fujita H, Ohuchida K, Mizumoto K, Nakata K, Yu J, Kayashima T, et al. alpha-Smooth Muscle Actin Expressing Stroma Promotes an Aggressive Tumor Biology in Pancreatic Ductal Adenocarcinoma. Pancreas. 2010.
216. Abercrombie M, Heaysman JE, Pegrum SM. The locomotion of fibroblasts in culture. I. Movements of the leading edge. Experimental cell research. 1970;59(3):393-8.
217. Bard JB, Hay ED. The behavior of fibroblasts from the developing avian cornea. Morphology and movement in situ and in vitro. The Journal of cell biology. 1975;67(2PT.1):400-18.
218. Lo A, Wang LS, Scholler J, Monslow J, Avery D, Newick K, et al. Tumor-Promoting Desmoplasia Is Disrupted by Depleting FAP-Expressing Stromal Cells. Cancer Res. 2015.
219. Maykel J, Liu JH, Li H, Shultz LD, Greiner DL, Houghton J. NOD-scidIl2rg (tm1Wjl) and NOD-Rag1 (null) Il2rg (tm1Wjl) : a model for stromal cell-tumor cell interaction for human colon cancer. Digestive diseases and sciences. 2014;59(6):1169-79.
220. Varro A, Noble PJ, Wroblewski LE, Bishop L, Dockray GJ. Gastrin-cholecystokinin(B) receptor expression in AGS cells is associated with direct inhibition and indirect stimulation of cell proliferation via paracrine activation of the epidermal growth factor receptor. Gut. 2002;50(6):827-33.
221. Steigedal TS, Prestvik WS, Selvik LK, Fjeldbo CS, Bruland T, Laegreid A, et al. Gastrin-induced proliferation involves MEK partner 1 (MP1). In vitro cellular & developmental biology Animal. 2013;49(3):162-9.
222. Kellermann MG, Sobral LM, da Silva SD, Zecchin KG, Graner E, Lopes MA, et al. Mutual paracrine effects of oral squamous cell carcinoma cells and normal oral fibroblasts: induction of fibroblast to myofibroblast transdifferentiation and modulation of tumor cell proliferation. Oral Oncol. 2008;44(5):509-17.
223. Schafer H, Geismann C, Heneweer C, Egberts JH, Korniienko O, Kiefel H, et al. Myofibroblast-induced tumorigenicity of pancreatic ductal epithelial cells is L1CAM dependent. Carcinogenesis. 2012;33(1):84-93.
224. Liu D, Hornsby PJ. Senescent human fibroblasts increase the early growth of xenograft tumors via matrix metalloproteinase secretion. Cancer Res. 2007;67(7):3117-26.
225. Bulla R, Tripodo C, Rami D, Ling GS, Agostinis C, Guarnotta C, et al. C1q acts in the tumour microenvironment as a cancer-promoting factor independently of complement activation. Nature communications. 2016;7:10346.

226. Dvorak HF. Tumors: wounds that do not heal. Similarities between tumor stroma generation and wound healing. The New England journal of medicine. 1986;315(26):1650-9.
227. Patel GK, Yee CL, Yuspa SH, Vogel JC. A humanized stromal bed is required for engraftment of isolated human primary squamous cell carcinoma cells in immunocompromised mice. The Journal of investigative dermatology. 2012;132(2):284-90.
228. Hutchinson L, Stenstrom B, Chen D, Piperdi B, Levey S, Lyle S, et al. Human Barrett's adenocarcinoma of the esophagus, associated myofibroblasts, and endothelium can arise from bone marrow-derived cells after allogeneic stem cell transplant. Stem cells and development. 2011;20(1):11-7.
229. Morton JJ, Bird G, Keysar SB, Astling DP, Lyons TR, Anderson RT, et al. XactMice: humanizing mouse bone marrow enables microenvironment reconstitution in a patient-derived xenograft model of head and neck cancer. Oncogene. 2015.
230. Arina A, Idel C, Hyjek EM, Alegre ML, Wang Y, Bindokas VP, et al. Tumor-associated fibroblasts predominantly come from local and not circulating precursors. Proc Natl Acad Sci U S A. 2016;113(27):7551-6.
231. Desmouliere A, Redard M, Darby I, Gabbiani G. Apoptosis mediates the decrease in cellularity during the transition between granulation tissue and scar. The American journal of pathology. 1995;146(1):56-66.
232. Hylander BL, Punt N, Tang H, Hillman J, Vaughan M, Bshara W, et al. Origin of the vasculature supporting growth of primary patient tumor xenografts. Journal of translational medicine. 2013;11:110.
233. Duda DG, Fukumura D, Munn LL, Booth MF, Brown EB, Huang P, et al. Differential transplantability of tumor-associated stromal cells. Cancer Res. 2004;64(17):5920-4.
234. Cassidy JW, Caldas C, Bruna A. Maintaining Tumor Heterogeneity in Patient-Derived Tumor Xenografts. Cancer Res. 2015;75(15):2963-8.
235. Bradford JR, Wappett M, Beran G, Logie A, Delpuech O, Brown H, et al. Whole transcriptome profiling of patient-derived xenograft models as a tool to identify both tumor and stromal specific biomarkers. Oncotarget. 2016;7(15):20773-87.
236. Fu L, Zhang C, Zhang LY, Dong SS, Lu LH, Chen J, et al. Wnt2 secreted by tumour fibroblasts promotes tumour progression in oesophageal cancer by activation of the Wnt/beta-catenin signalling pathway. Gut. 2011;60(12):1635-43.
237. Verberne CJ, de Bock GH, Pijl ME, Baas PC, Siesling S, Wiggers T. Palliative resection of the primary tumour in stage IV rectal cancer. Colorectal Dis. 2012;14(3):314-9.
238. Dockray GJ, Moore A, Varro A, Pritchard DM. Gastrin receptor pharmacology. Current gastroenterology reports. 2012;14(6):453-9.
239. Tomita H, Takaishi S, Menheniott TR, Yang X, Shibata W, Jin G, et al. Inhibition of gastric carcinogenesis by the hormone gastrin is mediated by suppression of TFF1 epigenetic silencing. Gastroenterology. 2011;140(3):879-91.

240. Kidd M, Siddique ZL, Drozdov I, Gustafsson BI, Camp RL, Black JW, et al. The CCK(2) receptor antagonist, YF476, inhibits Mastomys ECL cell hyperplasia and gastric carcinoid tumor development. Regulatory peptides. 2010;162(1-3):52-60.
241. Jin UH, Lee SO, Pfent C, Safe S. The aryl hydrocarbon receptor ligand omeprazole inhibits breast cancer cell invasion and metastasis. BMC cancer. 2014;14:498.
242. Muerkoster S, Isberner A, Arlt A, Witt M, Reimann B, Blaszczuk E, et al. Gastrin suppresses growth of CCK2 receptor expressing colon cancer cells by inducing apoptosis in vitro and in vivo. Gastroenterology. 2005;129(3):952-68.
243. Mingzhou Guo WY. Epigenetics of Gastric Cancer. In: Verma M, editor. Cancer epigenetics. New York: Springer; 2014. p. 783-99.
244. Moncada-Pazos A, Obaya AJ, Fraga MF, Viloria CG, Capella G, Gausachs M, et al. The ADAMTS12 metalloprotease gene is epigenetically silenced in tumor cells and transcriptionally activated in the stroma during progression of colon cancer. Journal of cell science. 2009;122(Pt 16):2906-13.
245. Wang D, Zhu T, Zhang FB, He C. Expression of ADAMTS12 in colorectal cancer-associated stroma prevents cancer development and is a good prognostic indicator of colorectal cancer. Digestive diseases and sciences. 2011;56(11):3281-7.
246. Surana R, Sikka S, Cai W, Shin EM, Warrier SR, Tan HJ, et al. Secreted frizzled related proteins: Implications in cancers. Biochim Biophys Acta. 2014;1845(1):53-65.
247. Ibrahim AE, Arends MJ, Silva AL, Wyllie AH, Greger L, Ito Y, et al. Sequential DNA methylation changes are associated with DNMT3B overexpression in colorectal neoplastic progression. Gut. 2011;60(4):499-508.
248. Anastas JN, Moon RT. WNT signalling pathways as therapeutic targets in cancer. Nature reviews Cancer. 2013;13(1):11-26.
249. Rattner A, Hsieh JC, Smallwood PM, Gilbert DJ, Copeland NG, Jenkins NA, et al. A family of secreted proteins contains homology to the cysteine-rich ligand-binding domain of frizzled receptors. Proc Natl Acad Sci U S A. 1997;94(7):2859-63.
250. Heller RS, Dichmann DS, Jensen J, Miller C, Wong G, Madsen OD, et al. Expression patterns of Wnts, Frizzleds, sFRPs, and misexpression in transgenic mice suggesting a role for Wnts in pancreas and foregut pattern formation. Developmental dynamics : an official publication of the American Association of Anatomists. 2002;225(3):260-70.
251. Suzuki H, Watkins DN, Jair KW, Schuebel KE, Markowitz SD, Chen WD, et al. Epigenetic inactivation of SFRP genes allows constitutive WNT signaling in colorectal cancer. Nat Genet. 2004;36(4):417-22.
252. Oehrle B, Burgstaller G, Irmler M, Dehmel S, Grun J, Hwang T, et al. Validated prediction of pro-invasive growth factors using a transcriptome-wide invasion signature derived from a complex 3D invasion assay. Scientific reports. 2015;5:12673.

253. Ehrlund A, Mejhert N, Lorente-Cebrian S, Astrom G, Dahlman I, Laurencikiene J, et al. Characterization of the Wnt inhibitors secreted frizzled-related proteins (SFRPs) in human adipose tissue. The Journal of clinical endocrinology and metabolism. 2013;98(3):E503-8.
254. Ishikawa T, Tamai Y, Zorn AM, Yoshida H, Seldin MF, Nishikawa S, et al. Mouse Wnt receptor gene Fzd5 is essential for yolk sac and placental angiogenesis. Development. 2001;128(1):25-33.
255. Dufourcq P, Couffinhal T, Ezan J, Barandon L, Moreau C, Daret D, et al. FrzA, a secreted frizzled related protein, induced angiogenic response. Circulation. 2002;106(24):3097-103.
256. Courtwright A, Siamakpour-Reihani S, Arbiser JL, Banet N, Hilliard E, Fried L, et al. Secreted frizzle-related protein 2 stimulates angiogenesis via a calcineurin/NFAT signaling pathway. Cancer Res. 2009;69(11):4621-8.
257. Grunewald M, Avraham I, Dor Y, Bachar-Lustig E, Itin A, Jung S, et al. VEGF-induced adult neovascularization: recruitment, retention, and role of accessory cells. Cell. 2006;124(1):175-89.
258. Shao J, Sheng GG, Mifflin RC, Powell DW, Sheng H. Roles of myofibroblasts in prostaglandin E2-stimulated intestinal epithelial proliferation and angiogenesis. Cancer Res. 2006;66(2):846-55.
259. Dutta S, Going JJ, Crumley AB, Mohammed Z, Orange C, Edwards J, et al. The relationship between tumour necrosis, tumour proliferation, local and systemic inflammation, microvessel density and survival in patients undergoing potentially curative resection of oesophageal adenocarcinoma. Br J Cancer. 2012;106(4):702-10.
260. Imdahl A, Bognar G, Schulte-Monting J, Schoffel U, Farthmann EH, Ihling C. Predictive factors for response to neoadjuvant therapy in patients with oesophageal cancer. European journal of cardio-thoracic surgery : official journal of the European Association for Cardio-thoracic Surgery. 2002;21(4):657-63.
261. Basu M, Bhattacharya R, Ray U, Mukhopadhyay S, Chatterjee U, Roy SS. Invasion of ovarian cancer cells is induced byPITX2-mediated activation of TGF-beta and Activin-A. Molecular cancer. 2015;14:162.
262. Wilhelm K, Happel K, Eelen G, Schoors S, Oellerich MF, Lim R, et al. FOXO1 couples metabolic activity and growth state in the vascular endothelium. Nature. 2016;529(7585):216-20.
263. Kumar JD, Kandola S, Tiszlavicz L, Reisz Z, Dockray GJ, Varro A. The role of chemerin and ChemR23 in stimulating the invasion of squamous oesophageal cancer cells. Br J Cancer. 2016;114(10):1152-9.
264. Salmenpera P, Karhemo PR, Rasanen K, Laakkonen P, Vaheri A. Fibroblast spheroids as a model to study sustained fibroblast quiescence and their crosstalk with tumor cells. Experimental cell research. 2016;345(1):17-24.
265. Zachos NC, Kovbasnjuk O, Foulke-Abel J, In J, Blutt SE, de Jonge HR, et al. Human Enteroids/Colonoids and Intestinal Organoids Functionally Recapitulate Normal Intestinal Physiology and Pathophysiology. J Biol Chem. 2016;291(8):3759-66.

266. Kam Y, Rejniak KA, Anderson AR. Cellular modeling of cancer invasion: integration of in silico and in vitro approaches. Journal of cellular physiology. 2012;227(2):431-8.
267. Gerber DE, Gupta P, Dellinger MT, Toombs J, Valencia I, Peyton M, et al. The effects of targeting stromal and tumor cell platelet-derived growth factor receptor (PDGFR) in non-small cell lung cancer (NSCLC). J Clin Oncol. 2011;29(15_suppl):10533.
268. Zhao WM, Wang L, Park H, Chhim S, Tanphanich M, Yashiro M, et al. Monoclonal antibodies to fibroblast growth factor receptor 2 effectively inhibit growth of gastric tumor xenografts. Clin Cancer Res. 2010;16(23):5750-8.
269. Wang W, Kryczek I, Dostal L, Lin H, Tan L, Zhao L, et al. Effector T Cells Abrogate Stroma-Mediated Chemoresistance in Ovarian Cancer. Cell. 2016;165(5):1092-105.
270. Nielsen SR, Quaranta V, Linford A, Emeagi P, Rainer C, Santos A, et al. Macrophage-secreted granulin supports pancreatic cancer metastasis by inducing liver fibrosis. Nature cell biology. 2016;18(5):549-60.
271. Liu J, Mi J, Zhou BP. Metabolic rewiring in cancer-associated fibroblasts provides a niche for oncogenesis and metastatic dissemination. Molecular & cellular oncology. 2016;3(1):e1056331.
272. Zhang C, Fu L, Fu J, Hu L, Yang H, Rong TH, et al. Fibroblast growth factor receptor 2-positive fibroblasts provide a suitable microenvironment for tumor development and progression in esophageal carcinoma. Clin Cancer Res. 2009;15(12):4017-27.
273. Ha SY, Yeo SY, Xuan YH, Kim SH. The prognostic significance of cancer-associated fibroblasts in esophageal squamous cell carcinoma. PLoS One. 2014;9(6):e99955.
274. Paraiso KH, Smalley KS. Fibroblast-mediated drug resistance in cancer. Biochemical pharmacology. 2013;85(8):1033-41.
275. Lin EW, Karakasheva TA, Hicks PD, Bass AJ, Rustgi AK. The tumor microenvironment in esophageal cancer. Oncogene. 2016;35(41):5337-49.
276. Qiu W, Hu M, Sridhar A, Opeskin K, Fox S, Shipitsin M, et al. No evidence of clonal somatic genetic alterations in cancer-associated fibroblasts from human breast and ovarian carcinomas. Nat Genet. 2008;40(5):650-5.
277. Celesti G, Di Caro G, Bianchi P, Grizzi F, Basso G, Marchesi F, et al. Presence of Twist1-positive neoplastic cells in the stroma of chromosome-unstable colorectal tumors. Gastroenterology. 2013;145(3):647-57 e15.
278. Junttila MR, de Sauvage FJ. Influence of tumour micro-environment heterogeneity on therapeutic response. Nature. 2013;501(7467):346-54.
279. Onion D, Argent RH, Reece-Smith AM, Craze ML, Pineda RG, Clarke PA, et al. 3-Dimensional Patient-Derived Lung Cancer Assays Reveal Resistance to Standards-of-Care Promoted by Stromal Cells but Sensitivity to Histone Deacetylase Inhibitors. Molecular cancer therapeutics. 2016;15(4):753-63.

280. Xiao Q, Zhou D, Rucki AA, Williams J, Zhou J, Mo G, et al. Cancer-Associated Fibroblasts in Pancreatic Cancer Are Reprogrammed by Tumor-Induced Alterations in Genomic DNA Methylation. Cancer Res. 2016;76(18):5395-404.
281. Marks DL, Olson RL, Fernandez-Zapico ME. Epigenetic control of the tumor microenvironment. Epigenomics. 2016.
282. Merhautova J, Demlova R, Slaby O. MicroRNA-Based Therapy in Animal Models of Selected Gastrointestinal Cancers. Front Pharmacol. 2016;7:329.
283. Nestor CE, Ottaviano R, Reddington J, Sproul D, Reinhardt D, Dunican D, et al. Tissue type is a major modifier of the 5-hydroxymethylcytosine content of human genes. Genome research. 2012;22(3):467-77.
284. Bhat S, Mallya S, Varghese VK, Jayaram P, Chakrabarty S, Joshi KS, et al. DNA methylation detection at single base resolution using targeted next generation bisulfite sequencing and cross validation using capillary sequencing. Gene. 2016;594(2):259-67.
285. Yong WS, Hsu FM, Chen PY. Profiling genome-wide DNA methylation. Epigenetics & chromatin. 2016;9:26.
286. Fukuchi M, Masuda N, Miyazaki T, Nakajima M, Osawa H, Kato H, et al. Decreased Smad4 expression in the transforming growth factor-beta signaling pathway during progression of esophageal squamous cell carcinoma. Cancer. 2002;95(4):737-43.
287. Wu L, Herman JG, Brock MV, Wu K, Mao G, Yan W, et al. Silencing DACH1 promotes esophageal cancer growth by inhibiting TGF-beta signaling. PLoS One. 2014;9(4):e95509.
288. Cheng H, Chen C, Liu LU, Zhan NA, Li B. Expression of Smad4, TGF-betaRII, and p21waf1 in esophageal squamous cell carcinoma tissue. Oncology letters. 2015;9(6):2847-53.
289. Ozawa D, Yokobori T, Sohda M, Sakai M, Hara K, Honjo H, et al. TGFBI Expression in Cancer Stromal Cells is Associated with Poor Prognosis and Hematogenous Recurrence in Esophageal Squamous Cell Carcinoma. Annals of surgical oncology. 2016;23(1):282-9.
290. von Rahden BH, Stein HJ, Feith M, Puhringer F, Theisen J, Siewert JR, et al. Overexpression of TGF-beta1 in esophageal (Barrett's) adenocarcinoma is associated with advanced stage of disease and poor prognosis. Molecular carcinogenesis. 2006;45(10):786-94.
291. Jue SF, Bradley RS, Rudnicki JA, Varmus HE, Brown AM. The mouse Wnt-1 gene can act via a paracrine mechanism in transformation of mammary epithelial cells. Molecular and cellular biology. 1992;12(1):321-8.
292. Avgustinova A, Iravani M, Robertson D, Fearns A, Gao Q, Klingbeil P, et al. Tumour cell-derived Wnt7a recruits and activates fibroblasts to promote tumour aggressiveness. Nature communications. 2016;7:10305.
293. Pilarsky C, Ammerpohl O, Sipos B, Dahl E, Hartmann A, Wellmann A, et al. Activation of Wnt signalling in stroma from pancreatic cancer identified by gene expression profiling. Journal of cellular and molecular medicine. 2008;12(6B):2823-35.

294. Pourreyron C, Reilly L, Proby C, Panteleyev A, Fleming C, McLean K, et al. Wnt5a is strongly expressed at the leading edge in non-melanoma skin cancer, forming active gradients, while canonical Wnt signalling is repressed. PLoS One. 2012;7(2):e31827.
295. Vempati P, Popel AS, Mac Gabhann F. Extracellular regulation of VEGF: isoforms, proteolysis, and vascular patterning. Cytokine & growth factor reviews. 2014;25(1):1-19.
296. Janevska VB. Pathology: North Sydney : Modern Medicine, 1969-; 2014.
297. Ramos MP, Wijetunga NA, McLellan AS, Suzuki M, Greally JM. DNA demethylation by 5-aza-2'-deoxycytidine is imprinted, targeted to euchromatin, and has limited transcriptional consequences. Epigenetics & chromatin. 2015;8:11.
298. Zhao S, Cao M, Wu H, Hu Y, Xue X. 5-aza-2'-deoxycytidine Inhibits the Proliferation of Lung Fibroblasts in Neonatal Rats Exposed to Hyperoxia. Pediatrics and neonatology. 2016.
299. Orskov AD, Treppendahl MB, Skovbo A, Holm MS, Friis LS, Hokland M, et al. Hypomethylation and up-regulation of PD-1 in T cells by azacytidine in MDS/AML patients: A rationale for combined targeting of PD-1 and DNA methylation. Oncotarget. 2015;6(11):9612-26.
300. Vojta A, Dobrinic P, Tadic V, Bockor L, Korac P, Julg B, et al. Repurposing the CRISPR-Cas9 system for targeted DNA methylation. Nucleic acids research. 2016;44(12):5615-28.
301. Liu XS, Wu H, Ji X, Stelzer Y, Wu X, Czauderna S, et al. Editing DNA Methylation in the Mammalian Genome. Cell. 2016;167(1):233-47 e17.
302. Norton ME, Jacobsson B, Swamy GK, Laurent LC, Ranzini AC, Brar H, et al. Cell-free DNA analysis for noninvasive examination of trisomy. The New England journal of medicine. 2015;372(17):1589-97.
303. Newman AM, Bratman SV, To J, Wynne JF, Eclov NC, Modlin LA, et al. An ultrasensitive method for quantitating circulating tumor DNA with broad patient coverage. Nature medicine. 2014;20(5):548-54.